

**CYCLIC RESPONSE OF OAK STREET BRIDGE BENTS**

by

**MARKUS SEETHALER**

B.A.Sc., The University of Toronto, 1989

A THESIS SUBMITTED IN PARTIAL FULFILLMENT OF  
THE REQUIREMENTS FOR THE DEGREE OF  
MASTER OF APPLIED SCIENCE

in

THE FACULTY OF GRADUATE STUDIES  
DEPARTMENT OF CIVIL ENGINEERING

We accept this thesis as conforming  
to the required standard

THE UNIVERSITY OF BRITISH COLUMBIA

APRIL, 1995

© Markus F. Seethaler, 1995

In presenting this thesis in partial fulfilment of the requirements for an advanced degree at the University of British Columbia, I agree that the Library shall make it freely available for reference and study. I further agree that permission for extensive copying of this thesis for scholarly purposes may be granted by the head of my department or by his or her representatives. It is understood that copying or publication of this thesis for financial gain shall not be allowed without my written permission.

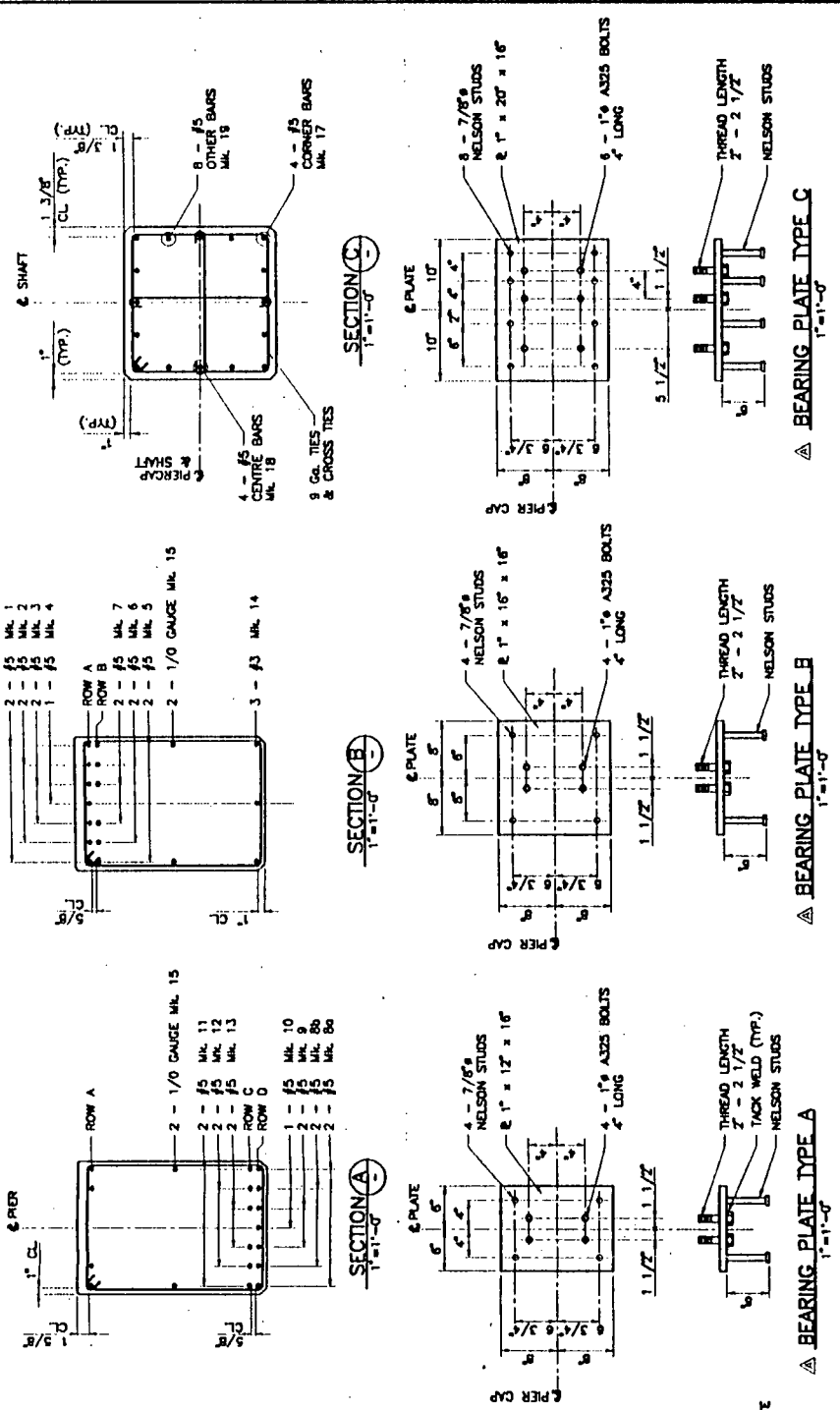
Department of CIVIL ENGINEERING

The University of British Columbia  
Vancouver, Canada

Date 23 . APR '95

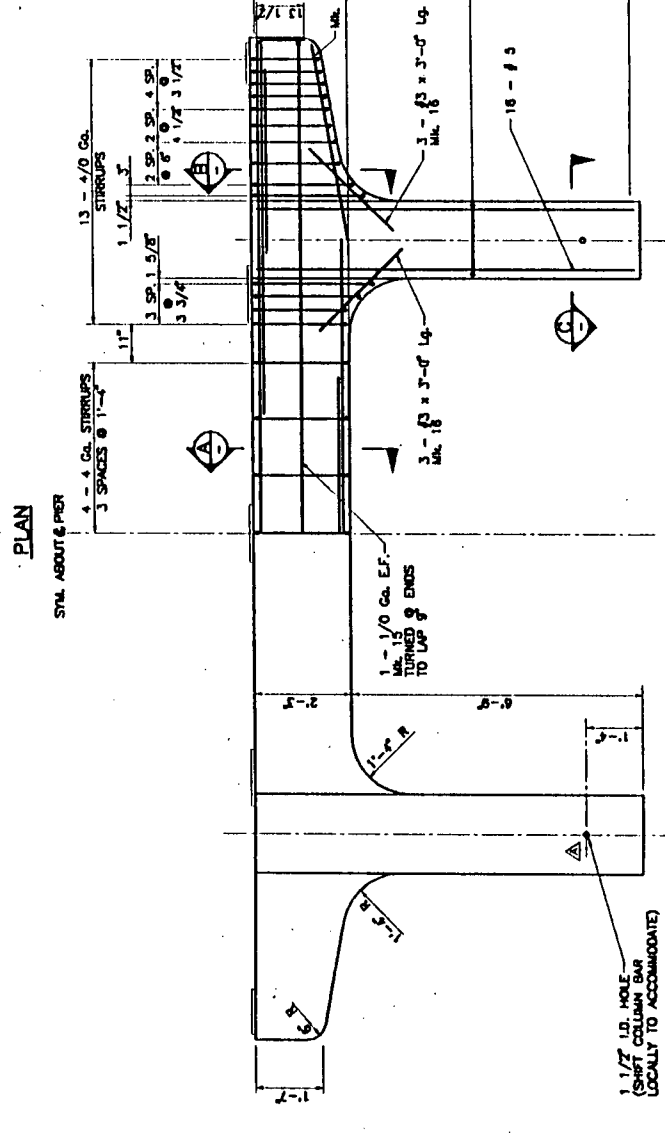
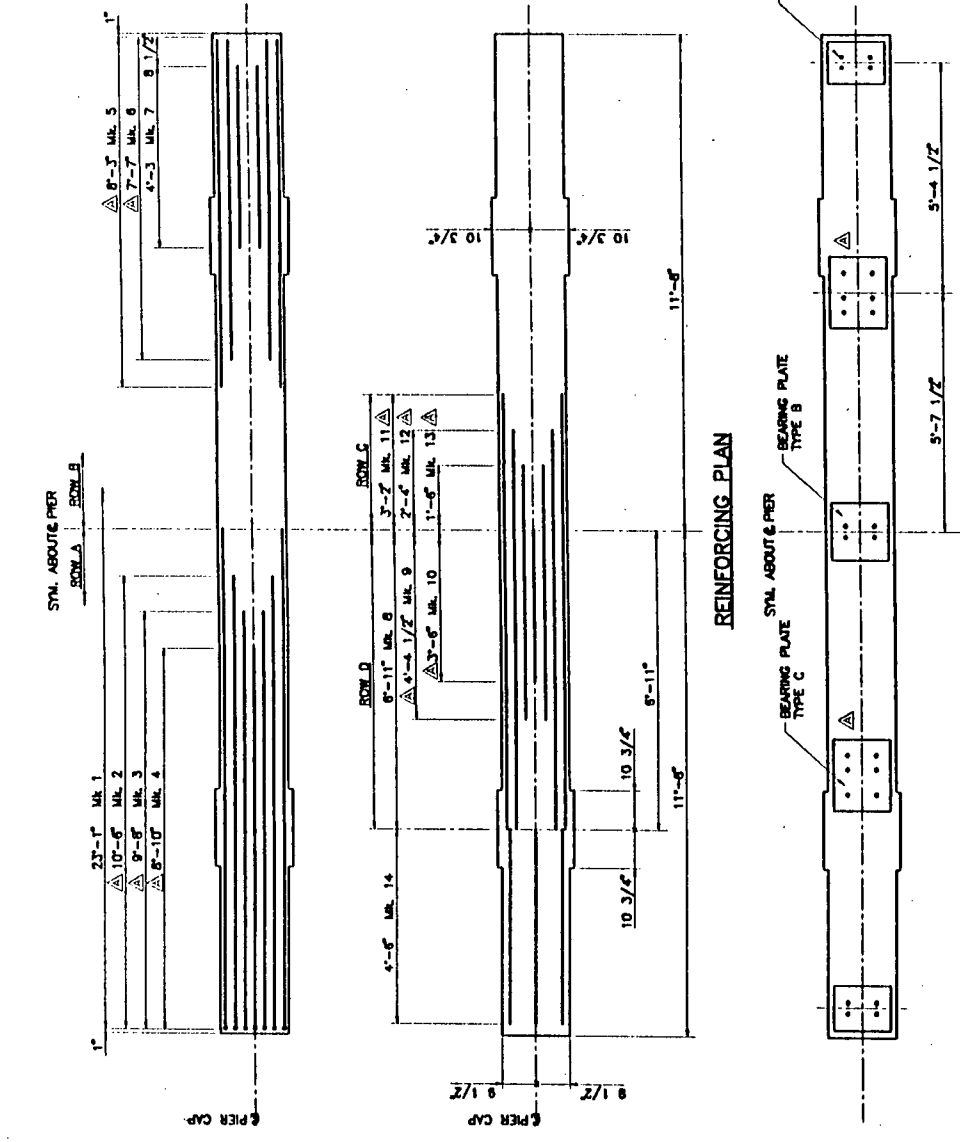






**NOTES:**

1. CONCRETE COVERS SHOWN ARE TO MAIN REINFORCING BARS.
2. FOR PROTOTYPE PIER DETAILS REPRESENTED BY THIS MODEL SEE DRAWING Q117-01.
3. MODEL IS 0.45 SCALE.
4. MATERIAL PROPERTIES MEASURED FROM DESTRUCTIVE TESTING ARE:  
 $f'_c = 46$  KSI & 58 KSI (COLUMN BARS TESTED S46 & N217)  
 $f_y = 46$  KSI & 58 KSI  
 MATERIAL PROPERTIES ORIGINALLY SPECIFIED ARE:  
 $f'_c = 3$  KSI  
 $f_y = 40$  KSI
5. ORIGINAL CONCRETE MIX SPECIFICATIONS CALLED FOR:  
 $f'_c = 3$  KSI  
 $f_y = 40$  KSI  
 $w/c = 0.55$   
 $slump = 7" - 5"$   
 $max. agg. = 1 1/4"$   
 $CEMENT FACTOR = 480-525 lb/yd^3$
6. AVERAGE CONCRETE TARGET STRENGTH TO BE 6 KSI - NOT 6 KSI "MINIMUM".
7. MAXIMUM AGGREGATE SIZE TO BE 1/2". CONCRETE SHALL NOT BE AIR ENTRAINED.
8. MAIN BARS TO BE GRADE 40 TO ASTM SPECIFICATION A615 (IMPERIAL VERSION), WITH MAXIMUM  $f_y$  OF 55 KSI.
9. STIRRUPS AND TIES SHALL BE ANNEALED WIRE WITH  $f_y$  NOT GREATER THAN 50 KSI.
10. REBAR QUANTITIES ON THESE DRAWINGS ARE DESIGNED ASSUMING UNIFORM REBAR SPACING. REBAR SHALL BE PLACED AS SHOWN, AND NO MAJOR ADJUSTMENTS TO REINFORCEMENT VOLUME MAY BE NECESSARY TO ADJUST FOR MEASURED YIELD STRENGTH OF REBAR AS SUPPLIED.
11. REBAR BEND DETAILS SHALL BE AS FOLLOWS:  
 - TIES AROUND #5 MAIN BARS TO HAVE HOOK INSIDE DIAMETERS OF 3/4".  
 - 13# & 18# HOOKS TO HAVE HOOK EXTENSIONS OF 6 BAR DIAMETERS, BUT NOT LESS THAN 1" BEYOND THE CENTRE OF THE BEND DIAMETER.
12. BEARING PLATES TO CONFORM TO CSA SPECIFICATION C40.21 300W AND TO BE EMBEDDED 1/2" INTO CONCRETE.



**Province of British Columbia**  
**MINISTRY OF TRANSPORTATION AND HIGHWAYS**  
 BRIDGE ENGINEERING BRANCH

**CRIPPEN INTERNATIONAL LTD.**  
 300 - 101 WEST GARDEN STREET / WASHINGTON, D.C. / CANADA M8 8T1  
 TEL: (301) 461-3000 / TELEFAX: (301) 461-3175

SCALE 1/2" = 1'-0" U/N

DESIGNED: J.W.K. DATE: FEB. 83  
 CHECKED: [ ] DATE: [ ]  
 DRAWN: R.G. DATE: FEB. 83

PROVIDED UNDER THE DIRECTION OF [ ]  
 APPROVED FOR CONSTRUCTION [ ]  
 SUPERVISOR OF BRIDGE CONSTRUCTION [ ]  
 CONSULTANT [ ]  
 DATE [ ]  
 FILE NO. [ ]  
 REVISION NO. [ ]  
 DRAWING NO. Q117-11

**SEISMIC RETROFIT**  
**CONCRETE PIER PROOF TESTS**  
**OAK STREET BRIDGE - PIER S28 MODEL**

REVISIONS

A 3/5/83 BEARING PLATE & REBAR LENGTHS REISED OK

CANCEL PRINTS BEARING PREVIOUS LETTER

## ABSTRACT

The Ministry of Transportation and Highways (MOTH) of British Columbia has initiated an upgrade program for its bridges. Among them is Oak Street Bridge, which spans the Fraser River between Vancouver and Richmond.

The Ministry of Transportation and Highways of British Columbia decided to supplement the seismic assessment of the Oak Street Bridge by large scale tests of the bridge bents at the structures laboratories of the University of British Columbia. The proposed tests consists of slow cyclic loading through increasing displacements. The test series consists of five specimens of the Oak Street Bridge, with various retrofits and an as built version, and one as built specimen representing the Queensborough Bridge. A test setup to conduct the tests was designed and installed in the UBC structures laboratory.

Predictions of the response of the prototype and the test specimen were conducted to establish a testing regime and loading sequence for the slow cyclic testing program. Various analysis methods were used to assess the seismic performance of the as built bridge bent. The first test, an as built model of the Oak Street Bridge bent, supplied the data of the experimental response to compare to the analytical predictions, and gave some further insight into the failure modes, and established the ultimate strengths.

The severe deficiencies in shear reinforcement in the cap beam of the bents made an accurate prediction of the response of the bridge bent very difficult. The experimental investigation resulted in much improved understanding of the seismic performance of this very typical structural component of many bridge approaches in the Lower Mainland of British Columbia.

## TABLE OF CONTENTS

	Page
ABSTRACT	ii
TABLE OF CONTENTS .....	iii
LIST OF FIGURES.....	vii
LIST OF TABLES .....	x
ACKNOWLEDGMENTS .....	xii
CHAPTER 1 INTRODUCTION .....	1
1.1 Background.....	1
1.2 Objectives .....	5
1.3 Scope.....	6
CHAPTER 2 SEISMIC DESIGN.....	8
2.1 Introduction .....	8
2.2 Response of Structures to Earthquakes.....	8
2.3 Analysis Tools.....	10
2.4 Philosophy of Seismic Design .....	12
2.5 Concept of Ductility .....	13
2.6 Capacity Design .....	16
2.7 Reinforced Concrete Analysis.....	17
CHAPTER 3 SEISMIC ASSESSMENT OF THE PROTOTYPE.....	19
3.1 Introduction .....	19
3.2 Description of the Bridge Bent .....	19
3.3 Seismic Assessment according to AASHO 1961 .....	21
3.4 Assessment according to ATC-6.....	23
3.5 Assessment of Member Capacities .....	26

3.5.1 Cap beam.....	27
3.5.2 Columns.....	29
3.5.3 Joint Shear Strength.....	31
3.5.4 Conclusion.....	33
3.6 Push-Over Analysis of the Prototype (Flexural Behaviour).....	34
3.7 Modified Compression Field Theory Analysis.....	41
3.8 Conclusions.....	44
<b>CHAPTER 4 DYNAMIC ANALYSIS OF THE PROTOTYPE.....</b>	<b>45</b>
4.1 Introduction.....	45
4.2. DRAIN-2DX.....	45
4.3 Spectral Analysis of the Prototype.....	46
4.4 Nonlinear Time Step Analysis of the Prototype.....	49
4.4.1 Earthquake Records.....	49
4.4.2 DRAIN-2DX Results.....	50
<b>CHAPTER 5 PREDICTION OF THE MODEL SPECIMEN BEHAVIOUR.....</b>	<b>53</b>
5.1 Introduction.....	53
5.2 The Test Model.....	53
5.3 Elastic Demand Calculations.....	54
5.4 Flexural Analysis.....	59
5.5. Push Over Analysis of the Test Model.....	62
5.6 Shear Capacity.....	64
5.7 Modified Compression Field Theory.....	67
<b>CHAPTER 6 TEST SETUP.....</b>	<b>71</b>
6.1 Introduction.....	71
6.2 Material Properties of the Test Specimen.....	71

6.3 The Loading Frame .....	72
6.3.1 Reaction Frame .....	72
6.3.2 Dead Load System .....	74
6.3.3 Load Distribution System .....	74
6.3.4 Bearing Assembly .....	74
6.4 Data Acquisition .....	76
6.4.1 Data Acquisition System Components .....	76
6.4.2 External Instrumentation .....	77
6.4.3 Internal Instrumentation .....	78
6.5 Data Processing .....	80
6.6 Load Application (Load History) .....	81
<b>CHAPTER 7 INTERPRETATION OF TEST RESULTS .....</b>	<b>84</b>
7.1 Introduction .....	84
7.2 Event Table .....	85
7.3 Load - Deflection Curves .....	88
7.4 Strain gauge results .....	93
7.5 Comments on the Response of the Test Specimen .....	96
<b>CHAPTER 8 CONCLUSIONS .....</b>	<b>98</b>
8.1 Introduction .....	98
8.2 Analytical Predictions .....	98
8.3 Test Setup .....	100
8.4 Test Results .....	101
8.5 Conclusions .....	102

BIBLIOGRAPHY .....	104
APPENDIX A STRUCTURAL DRAWINGS .....	108
APPENDIX B PHOTOGRAPHS OF THE FIRST TEST .....	112
APPENDIX C DP - PROGRAM .....	118
C.1 The DP Program.....	118
C.2 User Guide .....	127

## LIST OF FIGURES

Figure	Page
<b>Fig. 2.1</b> Accelerogram from the Santa Cruz Mountains (Loma Prieta) Earthquake, Oct. 17, 1989, Corralitos-Eureka Canyon Rd. ....	9
<b>Fig. 2.2</b> Response Spectrum of the Santa Cruz Mountains (Loma Prieta) Earthquake, Oct. 17, 1989, Corralitos-Eureka Canyon Rd. ....	10
<b>Fig. 2.3</b> Ductility of a single degree of freedom system. ....	14
<b>Fig. 2.4</b> Influence of period change on ductile force reduction. ....	15
<b>Fig. 2.5</b> Relationship between ductility and force reduction factor. ....	16
<b>Fig. 3.1</b> Oak Street Bridge bent S28. ....	20
<b>Fig. 3.2</b> Loading EQ + DL (AASHO 1961). ....	22
<b>Fig. 3.3</b> Shear force diagram (kips) for the EQ + DL (AASHO 1961). ....	22
<b>Fig. 3.4</b> Bending moment diagram (kip-ft) for the EQ + DL (AASHO 1961). ....	23
<b>Fig. 3.5</b> Loading (ATC-6). ....	24
<b>Fig. 3.6</b> Shear force diagram (kips) for the DL + EQ (ATC-6). ....	25
<b>Fig. 3.7</b> Bending moment diagram (kip-ft) for the DL + EQ (ATC-6). ....	25
<b>Fig. 3.8</b> Cap beam sections. ....	28
<b>Fig. 3.9</b> Force demands for the beam column joints (kips). ....	32
<b>Fig. 3.10</b> Model of the yield surfaces for columns (DRAIN-2DX). ....	36
<b>Fig. 3.11</b> Model for MS-V1 (racking truss). ....	37
<b>Fig. 3.12</b> Model for MS-V2 and MS-V3 (triangular truss). ....	37
<b>Fig. 3.13</b> Model for Klohn-Crippen (stiff cantilevers). ....	38
<b>Fig. 3.14</b> MS-V2 Model. ....	38

<b>Fig. 3.15</b> Comparison of base shear vs. deflection for the MS and K-C analyses .....	41
<b>Fig. 3.16</b> Flexure and shear response of the bent. ....	44
<b>Fig. 4.1</b> Spectrum for Oak Street Bridge bent S31. ....	46
<b>Fig. 4.2</b> Model for the spectral analysis (weights are in kips.).....	47
<b>Fig. 4.3</b> Spectral analysis results including the dead load and the flexural capacities (bending moments in kip-ft).....	48
<b>Fig. 4.4</b> Modified spectra .....	50
<b>Fig. 4.5</b> Relative displacement history (Griffith Park Observatory record).....	51
<b>Fig. 4.6</b> Relative displacement history (3838 Lankershim Blvd. record).....	51
<b>Fig. 4.7</b> Relative displacement history (234 Figueroa Street record).....	52
<b>Fig. 5.1</b> Cap beam sections. ....	55
<b>Fig. 5.2</b> Computer model for elastic demand calculations (forces in kips).....	56
<b>Fig. 5.3</b> Shear force diagram for the dead load (forces in kips).....	57
<b>Fig. 5.4</b> Bending moment diagram for dead load (moments in kip-ft).....	57
<b>Fig. 5.5</b> Shear force diagram for the lateral load of 100 kips (forces in kips).....	58
<b>Fig. 5.6</b> Bending moment diagram for a lateral load of 100 kips (moments in kip-ft).....	58
<b>Fig. 5.7</b> Bending moment reduction due to shear cracks for negative moment.....	60
<b>Fig. 5.8</b> Flexural capacity/demand for the cap beam (push to the right).....	61
<b>Fig. 5.9</b> Push over analysis results.....	63
<b>Fig. 5.10</b> Shear analysis for the cap beam at a lateral load of 35 kips.....	67
<b>Fig. 5.11</b> Sections for the RESPONSE analysis.....	68
<b>Fig. 6.1</b> Test setup.....	73
<b>Fig. 6.2</b> Bearing assembly.....	75
<b>Fig. 6.3</b> External instrumentation locations.....	77
<b>Fig. 6.4</b> Internal deformation measurement.....	79

<b>Fig. 6.5</b> Arrangement of internal gauges. ....	79
<b>Fig. 6.6</b> Filtering on a sample of data. ....	81
<b>Fig. 6.7</b> General test responses. ....	82
<b>Fig. 7.1</b> Load deflection curve up to sequence H. ....	90
<b>Fig. 7.2</b> Load deflection for OSB1. ....	91
<b>Fig. 7.3</b> Load deflection envelope for OSB1. ....	92
<b>Fig. 7.4</b> Strain gauge reading, top reinforcement at south end, negative moment. ....	93
<b>Fig. 7.5</b> Strain gauge reading, top reinforcement at north end, negative moment. ....	94
<b>Fig 7.6</b> Bending moments in the cap beam at the south end of specimen. ....	94
<b>Fig. 7.7</b> Bending moments in the cap beam at the north end of specimen. ....	95
<b>Fig 7.8</b> Bending moments in the cap beam at base shear 33 kips. ....	96

## LIST OF TABLES

Table	Page
<b>Table 3.1</b> Sectional flexure parameters of the cap beam.....	27
<b>Table 3.2</b> Sectional shear parameters of the cap beam. ....	28
<b>Table 3.3</b> Sectional capacities of the cap beam. ....	29
<b>Table 3.4</b> Sectional flexural capacities of the columns.....	30
<b>Table 3.5</b> Sectional shear parameters of the columns. ....	31
<b>Table 3.6</b> Joint shear demands.....	32
<b>Table 3.7</b> Joint shears (kips).....	33
<b>Table 3.8</b> Comparison of the cross sectional properties. ....	35
<b>Table 3.9</b> Nodal coordinates of the computer model.....	39
<b>Table 3.10</b> Sequence of hinge formation and corresponding base shear.....	40
<b>Table 3.11</b> Elastic demand constants and ratios. ....	42
<b>Table 3.12</b> RESPONSE Analysis Results. ....	43
<b>Table 4.1</b> Natural periods for bent S28.....	47
<b>Table 4.2</b> Earthquake records for the Oak Street Bridge.....	49
<b>Table 4.3</b> Scaling factors.....	50
<b>Table 5.1</b> Sectional properties. ....	55
<b>Table 5.2</b> Computer model node coordinates.....	56
<b>Table 5.3.</b> Moment capacities of cap beam. ....	60
<b>Table 5.4</b> Column capacity iterations.....	62
<b>Table 5.5</b> DRAIN-2DX cross sectional parameters for the test model.....	62
<b>Table 5.6</b> Cross sectional parameters.....	65

**Table 5.7** Shear capacities ..... 65

**Table 5.8** Reinforcement in the analysis sections..... 68

**Table 5.9** Elastic demand constants and ratios. .... 69

**Table 5.10** RESPONSE results. .... 69

**Table 6.1** Target loading sequence for the first test..... 83

**Table 7.1** The Event Table. .... 86

**Table 7. 2** Loading history. .... 88

## ACKNOWLEDGMENTS

The author is very grateful to his supervisors Dr. Robert Sexsmith and Dr. Donald Anderson for their guidance, suggestions, and encouragement through this research. Gratitude is expressed to Dr. Perry Adebar for giving some insight into the complicated matter of reinforced concrete and finally reading this thesis.

The advice and assistance of Mr. Don Kennedy and Mr. Dan Jennings from Klohn-Crippen Consultants is grateful appreciated. Funding for this project was provided by the Ministry of Transportation and Highways of British Columbia, with partial support from the Natural Sciences and Engineering Research Council of Canada through an NSERC scholarship and NSERC research grant funding.

The cooperation of Mr. Fabio Manarin from APS and Mr. Jerry Boychuk from Inlet Metal and Machining is grateful appreciated. Appreciation is also extended to Mr. Howard Nichol and Mr. Paul Symons for their helpful participation and assistance during the experimental investigation.

The author is in debt to his friends and families for their support through this part of his life as a graduate student at the University of British Columbia.

# CHAPTER 1

## INTRODUCTION

### 1.1 Background

Severe earthquakes in recent years in California (San Fernando 1971, Loma Prieta 1989, and Northridge 1994) have brought attention to the vulnerability of the infrastructure on the west coast of continental North America to seismic attack. The Ministry of Transportation and Highways (MOTH) of British Columbia has conducted a general seismic assessment of its major bridges in the Lower Mainland and uncovered serious deficiencies in the reinforced concrete bents typical for the approach spans of many bridges, especially those built prior to about 1975. It has been realized that there remains much to be learned about the behavior of existing structures exposed to seismic lateral loads.

The magnitude 6.6 San Fernando earthquake in 1971, with failures of essential public service buildings and numerous bridges, was instrumental in prompting local authorities to fundamentally revise their design criteria. Pioneer work was done by CALTRANS, the California Transportation Authority, in respect to highway bridges by quickly devising and implementing new design guidelines by 1973. These provisions were then essentially adopted by the American Association of State Highway and Transportation Officials (AASHTO) in 1975 for national use with adaptations for varying seismicity for different regions of the country. The Applied Technology Council initiated a program to formalize comprehensively the seismic design guidelines in 1979, resulting in a draft model code (ATC-6 1983). It was then incorporated into AASHTO's design guidelines as an option (AASHTO 1983). After the 1989 Loma Prieta earthquake the

ATC launched an extensive revision of ATC-6 in 1991 and is expected to complete ATC-32 by 1994.

There are essentially four different areas of seismic consideration for structures. One is the assessment of damages in actual earthquakes and monitoring of structures during earthquakes with sets of strong motion accelerometers. Since 1970 a comprehensive network of seismographs has been installed in critical regions, particular in California, and this effort is fairly well documented. The second issue is the evaluation and assessment of existing structures towards their vulnerability to seismic attack and the associated probabilities of the seismicity and failure of the structure. This leads to risk analysis and prioritization of upgrading efforts. The third point is a fundamental understanding of the various components of structure and the overall structural response to strong ground motion. A reasonable prediction of failure mechanisms and ultimate strengths of the structure are key elements to assess the response of existing structures and the possible upgrades of said structures in an effort to ascertain desired performance levels. This leads to the fourth point, the development of retrofit methods. These areas overlap a great deal and are interrelated. The first two are generally carried out by local and national building authorities, which own the structures. The latter two are dealt with by professional consultants and partially by research institutions.

The seismic design of new structures and the assessment of existing structures generally follow simplified code approaches, which is adequate for the majority of structures. For the important structures such as emergency facilities, schools, and structures that are critical parts of the infrastructure, such as bridges, more detailed analyses and design guidelines are called for. One of the important aspects is the earthquake forces and related design spectra. Many parameters influence site specific response spectra and a lot of research effort has been spent to establish procedures to

obtain reasonable seismic loadings (see Seed and Dickenson (1993) and Byrne (1993)). Another aspect is the analysis approach. For most cases a simplified modal analysis is sufficient; for very irregular structures however a nonlinear dynamic analysis of the complete structure seems to be the only way to assess the seismic response with any confidence; see Filippou (1992) and Powell (1992). For regular structures, and most fall into that category, it is sufficient to determine strength and ductilities. For poorly detailed concrete structures this can become quite difficult. Despite many decades of concrete research, there does not yet exist a comprehensive understanding of reinforced concrete, in particular the interaction between shear and flexure. Consequently extensive experimental work has been conducted and is still underway (Schultz (1990)).

Most of the experimental testing has concentrated around the behavior of poorly confined concrete columns and the anchorage of the columns into the footings. Also quite a few tests have been done on 'outrigger joints' for California's typical double decker highway structures. Relatively little has been done on testing for strength and ductility of older style, two column bridge bents, which are typical for bridge approaches found in the Lower Mainland of British Columbia.

Various retrofit schemes have been developed over the years. The most widely applied one is the use of support restrainers. Earthquakes impose much larger displacements than the bearings of older bridges were designed for. In the 1971 San Fernando earthquake bridges falling off their supports was one of the main failures. Another quite successful retrofit scheme is the use of steel jackets for columns to increase the concrete confinement. This improves not only the overall strength of the column but also adds to the shear capacity and the ductility of the columns. See Chai, Priestley, and Seible (1991).

Various other retrofit schemes are very specific to the individual structure. The design of retrofits in general is not governed by an increase in strength but by an improvement in ductility. In many cases the increase in shear capacity without increasing the flexural capacity shifts the brittle failure mode to a flexural one and ensures a ductile behavior. A few of the earlier retrofit designs implemented after the Loma Prieta earthquake proved to be quite ineffective. A number of unknowns in the seismic assessment of existing structures and in the design of retrofit schemes can only be quantified through experimental testing.

In preliminary studies specific shortcomings in the reinforcing details of the Oak Street Bridge approach bents were noted by consultants retained by MOTH (Crippen International (1993), now Klohn-Crippen). In the midsection of the cap beam only #4 ties at a spacing of 36" are provided for shear reinforcement. This amount of transverse reinforcement falls far short of today's minimum shear reinforcement requirements. The top and bottom flexural reinforcement in the cap beam curtails rapidly following a bending moment diagram based predominately on gravity loading. Very light bottom reinforcement, four #11's, is brought into the columns and terminated at the centre of the column. Heavy transverse reinforcement in the region of the architectural fillet at the beam column interface provides enough anchorage against bottom bar pull out. The #3 column ties at 12" provide inadequate shear reinforcement, particular for shorter columns, and are insufficient for confinement and restraint of the main column bars by today's standards. These deficiencies are typical for older structures as shown by Priestley and Calvi (1991) and Mitchell, Tinawi, and Sexsmith (1991).

The Ministry of Transportation and Highways engaged Klohn-Crippen as consultants for the assessment and design of the retrofit of the Oak Street Bridge. Considering the large number of bridge bents built in a similar fashion, the severity of the

anticipated failure modes, and the unknowns in this relatively young field of structural behaviour, the MOTH then decided to augment the consultants studies with large scale tests in order to improve confidence in the retrofit options. They contracted with the University of British Columbia (UBC) to carry out the experimental program.

## **1.2 Objectives**

The main objectives of the test project carried out for the Ministry of Transportation and Highways were to determine the seismic response of a two column bridge bent of a typical reinforced concrete approach span of the Oak Street Bridge, to experimentally determine the critical failure modes and quantify the ultimate strengths and ductilities of the as-built bridge bent, to demonstrate the effectiveness of retrofit schemes to be implemented, and to prove that the design criteria established provide acceptable margins of safety.

The objectives of this thesis were:

1. To design a suitable test setup to apply slow cyclic loads to large scale models of the Oak Street Bridge bents. Bent S28 of the Oak Street Bridge was chosen as the prototype. A 0.45 scale was later adopted. The test setup was required to provide test loadings suitable for as-built and retrofit tests.
2. To use a variety of predictive models to predict performance of the prototype and the as-built model.
3. To establish a program of data acquisition suitable to carry out the tests and acquire data on important displacements and strains.
4. To carry out the test on the as-built model.
5. Interpret results of the model test.

### 1.3 Scope

This thesis covers the initial stages of a large testing series conducted by the Ministry of Transportation and Highways at the UBC structure laboratory. This testing program itself consists of five specimens of a representative 0.45 scale bridge bent of the Oak Street Bridge and one specimen of the Queensborough Bridge, which has identical dimensions but a slightly different layout of the reinforcement. The development of the test program, the analysis of the bridge bent, the design of the test setup, and the test of the first, an as-built specimen, are the principal topics of this thesis. The remaining tests of the other specimens, which will be retrofitted to some extent, will be the subject of other reports.

An analytical investigation was carried out to determine the seismic performance of the prototype and the test model, comprising of a seismic assessment of the prototype including a dynamic analysis and a static analysis to predict the behavior of the test model.

The seismic assessment of the prototype considered the design criteria of AASHTO 1961 and ATC-6. Sectional analysis of the various elements of the bent established the likely failure modes. The sequence of flexural hinging was established by a push over analysis. A shear analysis explored the brittle failure modes. A spectral and a dynamic time step analyses were performed on the prototype to establish the expected displacement demands.

The static analysis of the test model addresses flexure and shear interaction to predict a plausible mode of failure of the test. A push over analysis and a quasi static analysis using the loading history of the test are performed to provide a basis for a comparison of the test results.

The design of the test setup simulated the actual support and loading conditions as closely as possible. The main mass of the bridge is located at the centre of mass of the bridge deck, which is located 5' above the cap beam. A loading system was devised to introduce a realistic loading path into the test specimens. The vertical dead load was applied on the five bearing points of the bridge deck. The supports simulated an inflection point of the columns and therefore had to provide freedom of rotation but restrain any possible uplift from the overturning moments.

The raw data as recorded was quite noisy. A filtering process was devised to eliminate any ambient noise and the signals were then converted into physical dimensions.

## **CHAPTER 2**

### **SEISMIC DESIGN**

#### **2.1 Introduction**

The relatively new field of seismic assessment and design is undergoing some rapid developments. Since the origin of the lateral force input into the structures is a random excitation, all analysis and design approaches are in the realm of probability and risk evaluation. Past earthquakes and geological features determine the site specific seismicity which then lead to a set of design criteria; in many cases the design criteria do not include forces but a design spectrum. The modern philosophy of seismic design is based on a limit states approach. This and the concept of ductility are the underlying principles of the capacity design method, which is gaining wide acceptance as a rational approach to deal with the inherent uncertainties. The most common building material, however, reinforced concrete is the least understood. In particular, the shear capacity of lightly reinforced concrete sections in plastic hinge regions is not well understood at all. This only adds to the difficulties to understand the seismic behavior of concrete structures.

#### **2.2 Response of Structures to Earthquakes**

Earthquakes are caused by relative movements of the earth's tectonic plates. There are a few parameters to describe the magnitude of an earthquake. The most common measure of magnitude, one often cited by the media, is the Richter scale. It is a measure of the energy released by the earthquake by the maximum trace deformation of a standard seismograph at a certain distance. The effect on a structure depends on the distance from the epicentre. Earthquakes of Richter magnitude less than M5 generally do not cause any

damage. In the range between M5 and M6 only areas close to the epicenter are affected. Earthquakes above M7 are considered major and affect a large area.

A common descriptor of an earthquake is the accelerogram, which is a record of the accelerations induced by the earthquake to a particular point on the ground (see Fig. 2.1). These records vary dramatically for the same event depending on the location relative to the epicenter and the local site conditions, i.e. soft soil, rock, etc.

A further concept to describe an earthquake is the response spectra. It gives an indication of the frequency content of the ground shaking. Consider a single degree of freedom system (SDOF) with one particular natural frequency and damping value. When excited by the earthquake, it will respond with a maximum acceleration. Repeating the process with SDOF with varying natural frequencies will lead to an array of maximum responses to the corresponding frequencies see Clough and Penzien (1975). The response spectrum for the earthquake record shown in Fig. 2.1 is given in Fig. 2.2.

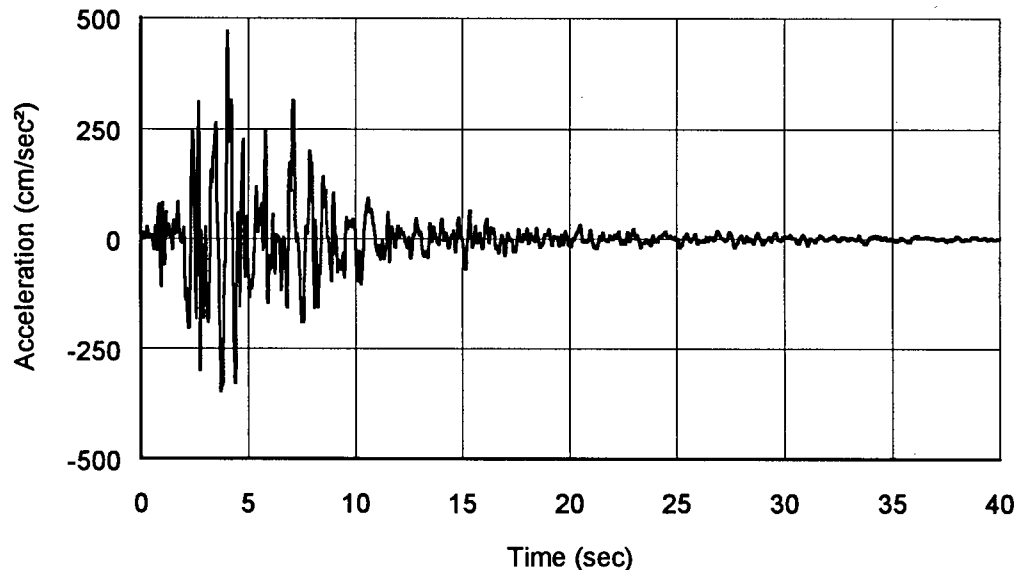


**Fig. 2.1** Accelerogram from the Santa Cruz Mountains (Loma Prieta) Earthquake, Oct. 17, 1989, Corralitos-Eureka Canyon Rd.

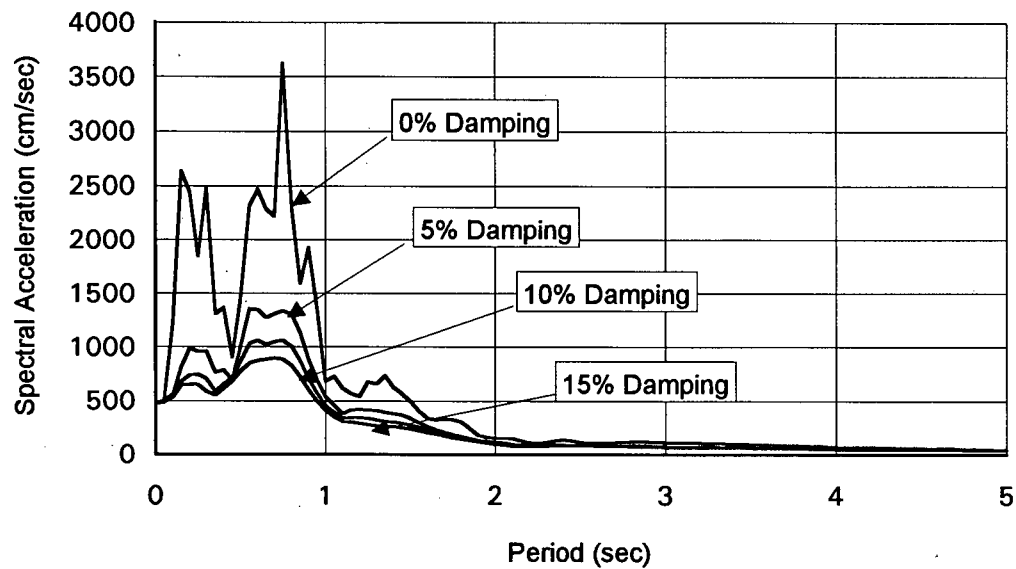


**Fig. 2.2** Response Spectrum of the Santa Cruz Mountains (Loma Prieta) Earthquake, Oct. 17, 1989, Corralitos-Eureka Canyon Rd.

Most earthquakes show a similar pattern with a maximum spectral response acceleration at a period of 0.2 to 0.3 sec on rock or firm soil. Damping, which for most structures lies between 5 and 10 % of critical damping, will reduce the maximum spectral response as shown in Fig. 2.2.

### 2.3 Analysis Tools

There are principally three approaches towards an analysis for seismic loading. They are described here briefly in their order of complexity.

*a) Quasi-Static Load* : The simplest but the most widely used method is the so called quasi static load method. A lateral load which simulates the dynamic loads from an earthquake is applied statically. Most building codes give a relatively simple procedure to

obtain these equivalent seismic loads, which are based on the seismicity of the region, the local soil conditions, type of structure and risk level.

*b) Dynamic Modal Analysis* : The natural frequencies and mode shapes are determined for the structure, most commonly by a modal analysis. Typically for a 2D model only the first three to five natural frequencies have the biggest effect on the seismic behavior; the upper modes of vibrations are generally ignored. The soil consultants usually provide a series of applicable, very site specific response spectra. Otherwise some design spectra have to be chosen, which could be adopted from various design codes. The spectral accelerations for each natural frequency are applied to all the nodal masses of the structural model. This in turn constitutes a whole array of external forces which then are evaluated like a static load case. Different methods of combining the modal responses have been used; the most common one is the SRSS (square root of sum of squares). Another frequently used method is the CQC (complete quadratic combination).

*c) Dynamic Time Step Analysis* : The most general dynamic analysis method is the numerical step by step integration of the coupled differential equations of motion that describe the structure when subjected to a time history of displacement (or acceleration) at the supports.

This method can account for the nonlinear response of the structure during the earthquake and gives the time history of the response, not just the maximum values as given by the above two methods. However the results are strongly dependent on the chosen input history. Since all seismic events are random occurrences, an exact future earthquake record cannot be predicted. Any useful results from this type of analysis have to be obtained by a series of analyses of different input records. Considering the

computational effort to the end results, this type of analysis finds very little application in practice.

## 2.4 Philosophy of Seismic Design

Modern philosophy on seismic design postulates an acceptable level of public safety. Structures are to be designed to resist moderate earthquakes without significant damage and to prevent collapse during major earthquakes. In principle, structures can be designed to withstand major earthquakes without any damage. This would, however, be uneconomical and unwarranted for the small probability for such an event; see Commentary J in the Supplement of the NBC (1990).

A modern concept of structural design is the limit state, which was developed to introduce a more rational approach and to incorporate risk evaluation into the design equations. Basically three limit states can be identified for seismic design to signify the levels of anticipated damage corresponding to the intensity and magnitude of the ground shaking, as shown by Paulay and Priestley (1992):

*a) Serviceability Limit State* : For relatively frequent occurring earthquakes the structure should suffer no damage to the structural and non structural components. The recommended return period of the ground shaking for office buildings is about 50 years. For hospitals, fire stations, and telecommunication systems a much longer return period is required since these facilities have to be functional during and after emergency situations.

*b) Damage Control Limit State* : For ground shaking beyond the level of serviceability limit state, damage is permissible to structural components but should still be repairable. The level of ground accelerations that initiate this state should have a low probability during the expected life of the building.

*c) Survival Limit State* : The structure will be severely damaged, even beyond the point of an economical repair. But a total collapse i.e. the loss of human life should be prevented. The structural system has to be able to undergo very large lateral deformations. The integrity of the structure should be preserved to maintain the support of gravity loads after the maximum credible ground shaking at the particular site.

For bridges similar criteria govern the design process. In addition to the intrinsic considerations of the structure, bridges are part of an infrastructure, a more global life line system. Local civil defense plans depend on certain key elements of that system to be operational after disastrous earthquakes to ensure accessibility to emergency facilities such as hospitals, fire stations, etc. Also the economic loss due to extended closures of major traffic arteries warrants special considerations.

## 2.5 Concept of Ductility

In seismic design it is not feasible to design a structure to behave purely elastically. This would be prohibitively expensive. Since the probability of large earthquakes is rather small, it is only necessary to be able to resist small to moderate earthquakes with little to no structural damage. For severe events it is imperative to be able to prevent total collapse. It is therefore desired that a structure performs to a limited level elastically and be able to undergo large plastic deformations for extreme situations. This limits the force on the structure and its elements. Ductility ( $\mu$ ) is the relationship between the yield and ultimate deformation ( $\Delta$ ). Refer to Fig. 2.3.

$$\mu_{\Delta} = \frac{\Delta_m}{\Delta_y} \quad (2.1)$$

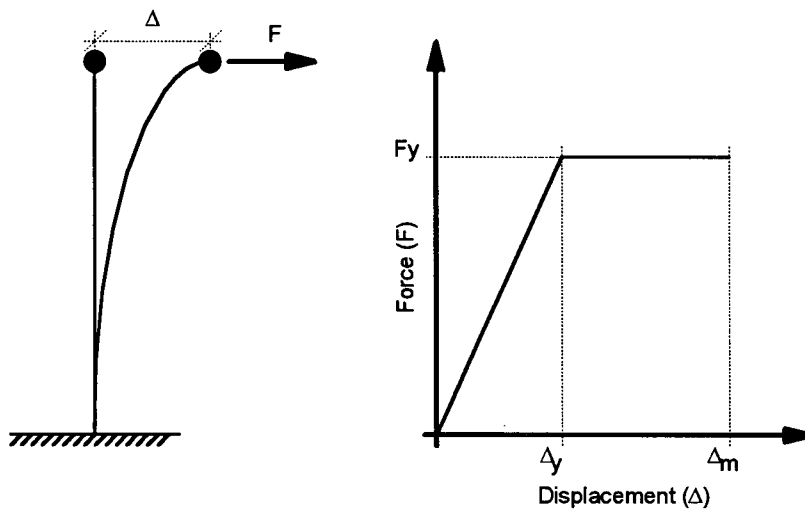


Fig. 2.3 Ductility of a single degree of freedom system.

The ductility of an element of a structure and consequently the displacement ductility of the whole structure is an essential measure of the performance of the structure under seismic attack. From a design point of view one is interested in how much the maximum seismic forces are reduced due to the ductility. Design codes introduced a force reduction factor  $R$ :

$$R = \frac{F_e}{F_y} \quad (2.2)$$

where  $F_e$  is the maximum elastic seismic force and  $F_y$  is the seismic design yield force.

Ductility in a structure is largely dependent on the detailing of structural components. Consequently when a ductile framing system is chosen the structure can be designed for lower force levels. There is a trade off for more expensive structural detailing and lower strength requirements. It is the task of the designer to find an optimum.

When an inelastic dynamic analysis is performed, it has been observed that for structures with natural periods larger than the period at peak elastic response  $T_m$  (see Fig.

2.4) the maximum displacement is similar to that of an elastic system with the same initial stiffness but unlimited strength (see Fig. 2.5a). This phenomenon is called the *equal displacement principle*. This implies that the maximum force  $F_y$  is approximately equal to the elastic force  $F_e$  divided by the ductility.

$$F_y = F_e / \mu \quad (2.3)$$

therefore

$$R = \mu \quad (2.4)$$

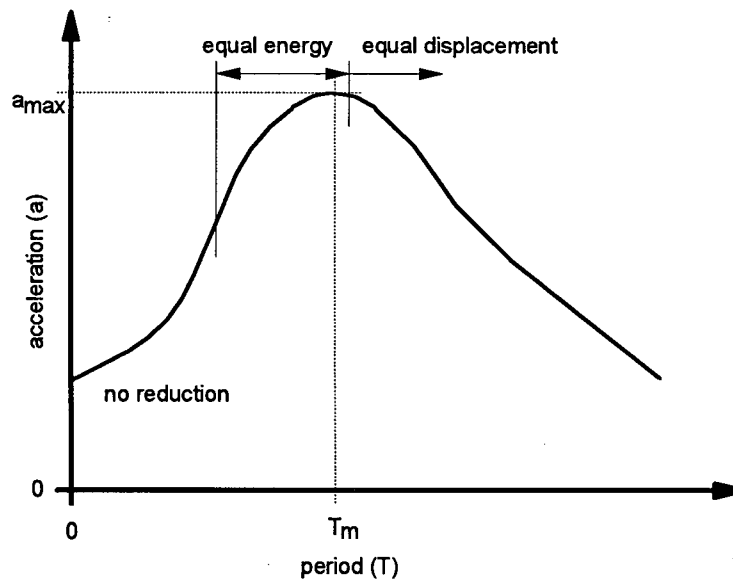


Fig. 2.4 Influence of period change on ductile force reduction.

For shorter period structures, where the natural period is less than  $T_m$  (see Fig 2.4), this has proven to be non conservative; the displacement ductility demand is greater than the force reduction factor. In this case it was found that the area under the inelastic force-deflection curve can be equated with the area under the elastic one (see Fig. 2.5b). Since the area under the force deflection curve represents the total energy absorbed this concept

is called *equal energy principle*. The relationship between ductility and force reduction can be expressed as

$$\mu = \frac{R^2 + 1}{2} \quad (2.5)$$

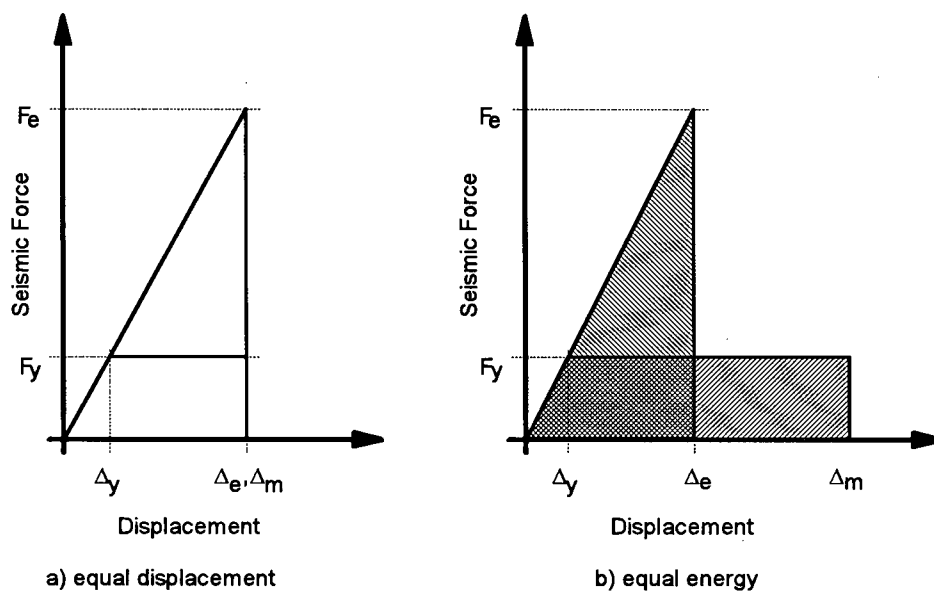


Fig. 2.5 Relationship between ductility and force reduction factor.

Summarizing the above:

for long period structures ( $T > T_m$ ):  $R \cong \mu_\Delta$

for short period structures ( $T < T_m$ ):  $R = \sqrt{2\mu_\Delta - 1}$

## 2.6 Capacity Design

The capacity design philosophy was developed in New Zealand (Paulay, Park, and Priestley (1978)). A failure mechanism for the primary lateral force resisting system is chosen by introducing regions of plastic hinging. These plastic hinges are designed and detailed to maintain their strength and integrity while undergoing inelastic flexural action.

All the other components of the structural system are then designed to exhibit elastic behaviour. In other words the designer chooses, if the structure should yield, *how* it will yield, and has therefore control over the critical points in the design.

To insure that the critical regions do display ductile behaviour, the actual capacity, rather than safe or nominal capacity, is required, thus an over strength, the inherent strength beyond that corresponding to the specified material properties, has to be taken into consideration. A general procedure was outlined by Paulay and Priestley (1992):

1. A kinematically admissible displacement mechanism is chosen.
2. The mechanism selected should be such that the necessary displacement ductility can be accommodated with the smallest rotational demands in the hinges.
3. Once a suitable mechanism is selected, the regions of plastic hinging are identified and can be designed and detailed.
4. The strength, including overstrength of the hinge regions, is estimated.
5. The strength required by all the other components should be in excess of the over strength demand of the plastic hinges.

## **2.7 Reinforced Concrete Analysis**

Since reinforced concrete is a non-homogeneous material the modeling of such generally eludes a closed form solution. There is a formidable list of behavior patterns such as shear aggregate interlock, shrinkage, creep, redistribution, crack propagation, bond slip, etc. which are extremely difficult to accurately capture in an analytical model. Due to the complexity of the problem, many researchers have felt that a finite element approach would provide appropriate models. The simplest approach is to assume a smeared cracked model for the concrete and formulate constitutive relationships based on this model (e.g. Hu and Schnobrich (1990)). A further refinement is to implement the

compression field theory as the constitutive relationships, (e.g. Steven et al (1991)) and Vecchio and Selby (1991)). A different approach is to separate the concrete and the reinforcement into different layers and develop an interaction between the various material based elements (Choi and Kwak (1990)). The above approaches address only single structural elements and are mostly restricted to monotonic loading. They lack application to overall structures. A more global approach for analyzing complete structures is the use of subassemblages of the structure into the various structural elements. Critical regions such as joints are modeled as 3D finite elements, whereas columns and beams are modeled as 2D layered fibre elements. This allows for a dynamic analysis of larger structures and gives results for the global behaviour of the structure (Filippou and Fenves (1990)). All this research is still at an early stage. Most approaches address just one or two typical reinforced concrete behaviour patterns such as tension stiffening or strain softening. At this point the interaction between flexural and shear behavior has created a new concern. This is particularly significant for concrete sections with light shear reinforcing, which are found in older structures. When they were designed, the concrete contribution to the shear capacity was assumed to be much higher than currently accepted.

In recent years research has been directed towards the refinement of the modeling to explain the experimental findings. Many of these efforts have proven to be excessively complex to perform with little or no improvement to the analytical results. In practice simpler methods are applied, such as the ACI/ASCE design formulae and capacity demand calculations of the sections, to analyze concrete structures. This sets the stage for this research work on the Oak Street Bridge bents, which show severely deficient shear reinforcements in the cap beam.

## CHAPTER 3

### SEISMIC ASSESSMENT OF THE PROTOTYPE

#### 3.1 Introduction

As a first step to assess the seismic performance of Oak Street Bridge the seismic behavior of the prototype bridge bent was evaluated. Bent S28 was chosen to represent a typical concrete approach bent. A comparison between the code requirements of AASHTO (1961), which was the applicable design specification at that time, and the current standards for seismic bridge design, shows a substantial increase in lateral force demands. Sectional analysis, which follows the work by Priestley and Seible (1991), determines the local capacities. The hinging sequence based on flexural capacities, is established by a pushover analysis. Using the forces from the pushover analysis potential shear failures are investigated. This study is a rational approach for a seismic assessment and indicates the deficiencies in the local sectional capacities and in the global response of bridge bent S28.

#### 3.2 Description of the Bridge Bent

Klohn-Crippen chose a pier similar to S28 to represent an average bridge bent of the Oak Street Bridge as a prototype for the proposed tests. Pier S28 is a first interior support for a typical four span bridge segment and attracts therefore the largest component of the dead load of the bridge deck. The physical properties and load assumptions cited herein are applicable throughout the remainder of this thesis.

The dimensions of the prototype bent are shown in Fig. 3.1; for more details refer to drawing Q117-1 by Klohn-Crippen (see Appendix A). The columns are 4 feet by 4 feet. The cap beam measures 3'-6" in width and 5'-0" in depth and has a length of 51'-8" with 10'-6" cantilevers on either side which taper to a depth of 3'-6".

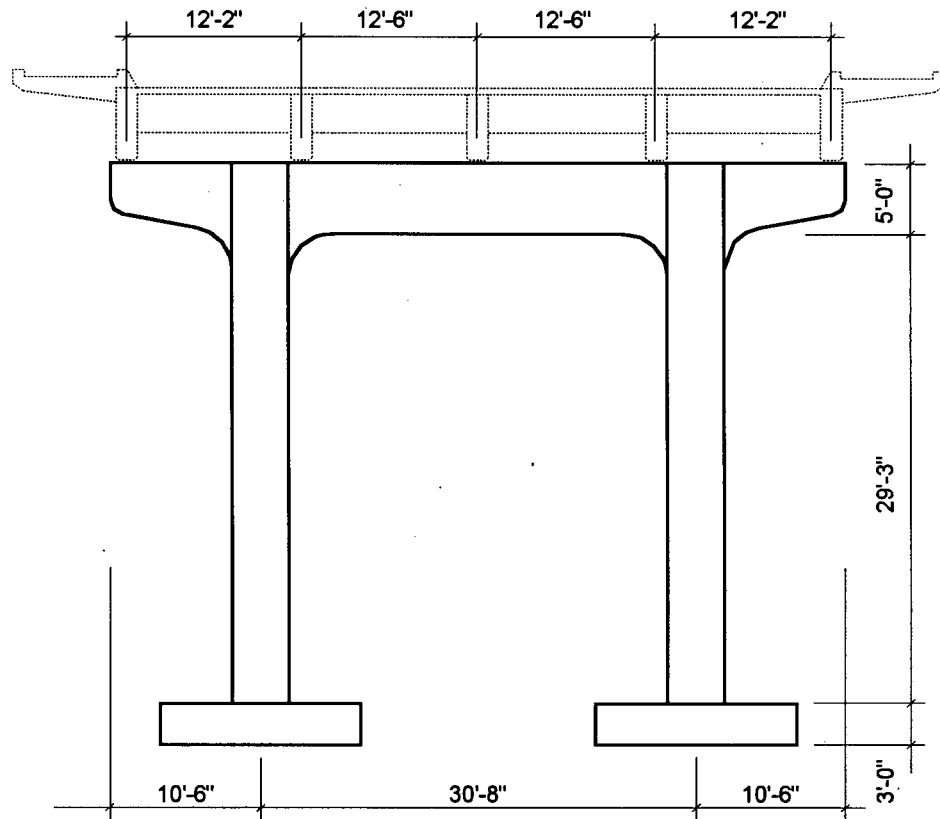


**Fig. 3.1** Oak Street Bridge bent S28.

The bridge was built in the late 1950's and the concrete has gained strength over the years. Klohn-Crippen took a number of core samples and estimated the concrete strength at 6000 psi, which is double the specified 3000 psi. Samples of the rebar indicated an actual yield strength of 50 ksi compared to the specified Grade 40 steel. The parameters used in the structural models were based on these measured material properties. The Young's modulus for the concrete was set at 4650 ksi ( $60000\sqrt{f'_c}$ ).  $\sqrt{f'_c}$  in this thesis is based on  $f'_c$  in psi units, and is taken as psi.

The self weight of the concrete bridge bent of pier S28 with 30 feet columns is about 285 kips. The superstructure, i.e. the bridge deck, constitutes most of the mass and some conservative estimates by Klohn-Crippen put the weight at 900 kips, which is introduced into the structure at the five bearing points on the bridge bent. The main earthquake base shear is applied at the center of gravity of the bridge deck structure, which is located according to Klohn-Crippens calculations 5 feet above the top of the cap beam.

### **3.3 Seismic Assessment according to AASHO 1961**

When the Oak Street bridge was designed, the applicable code was the *Design Specifications for Highway Bridges* (DSHB) by the Department of Public Works of British Columbia, which drew heavily on AASHO provisions. At that time earthquakes had been recognized to be part of possible lateral force, but estimated force levels were very low. The code required a lateral load of 6% of the total dead load, albeit at working stress levels.

The dead and earthquake loads are shown in Fig. 3.2. Dimensions shown are member centerline dimensions. Fig. 3.3 and Fig. 3.4 show the shear and moment diagrams respectively based on gross sectional stiffness properties. The numerical values of the forces are taken at the centre of the columns and beams. The dashed lines indicate the location of the face of column or face of beam.

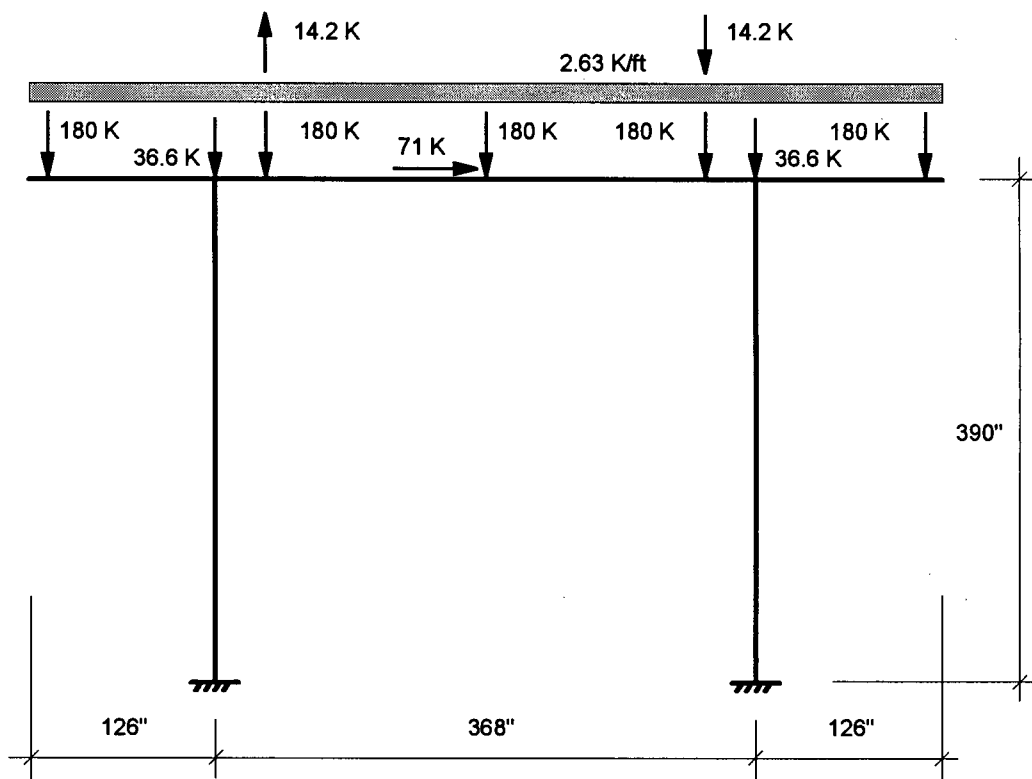


Fig. 3.2 Loading EQ + DL (AASHO 1961).

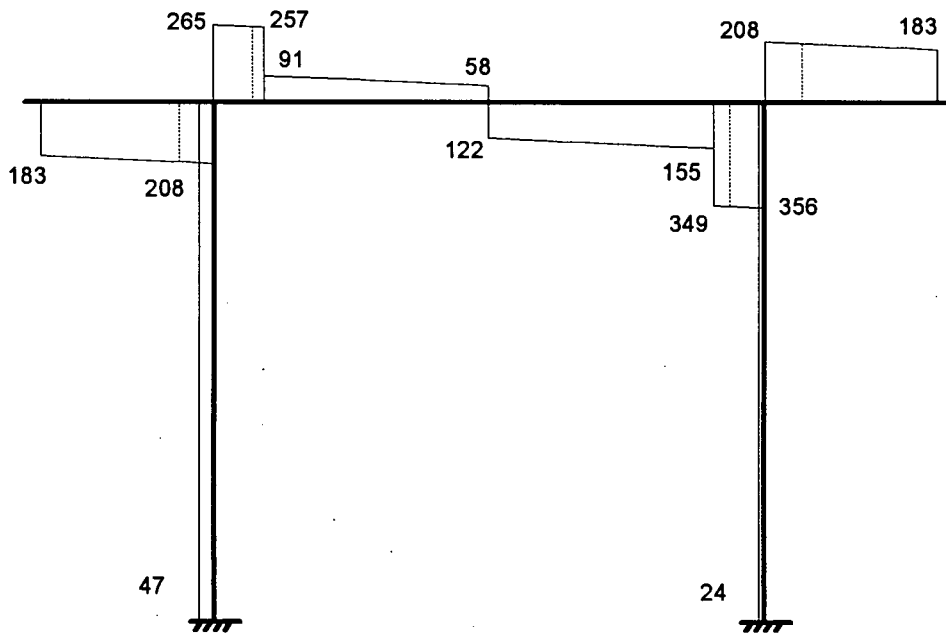
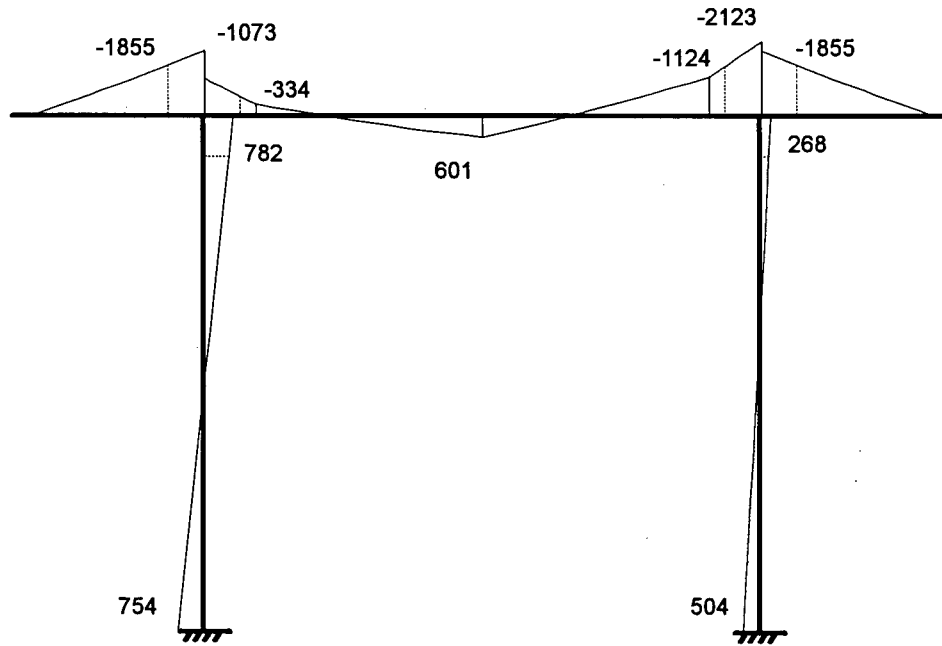


Fig. 3.3 Shear force diagram (kips) for the EQ + DL (AASHO 1961).



**Fig. 3.4** Bending moment diagram (kip-ft) for the EQ + DL (AASHO 1961).

The original dead and live loads (wind loads) were based on AASHO 1961. Calculations done in accordance with this code show that the earthquake loadings were not the governing loads for design.

### 3.4 Assessment according to ATC-6

A brief calculation using the ATC-6 approach indicates that the Oak Street Bridge does not meet current design standards. ATC-6 is not designed to assess existing and deficient structures but it lends itself nicely for a comparison. The standard ductile details are definitely not met in the Oak Street Bridge, particularly in the center of the cap beam, where there is virtually no shear reinforcement.

The analytical approach of ATC-6 is based on a single degree of freedom (SDOF) analysis. To estimate the overall stiffness of the system the column stiffness was reduced to 25% of the gross cross sectional properties and the cap beam was assumed to be rigid. The natural period is calculated to be:

$$T = 0.76 \text{ sec}$$

Assuming an Acceleration Coefficient ( $A$ ) of 0.2 (for Vancouver) and a Soil Profile Coefficient ( $S$ ) of 1.5 the equivalent lateral load is 471 kips. Application of the equivalent static load to the structure including the dead load yields the following results as depicted in Fig. 3.5 to Fig. 3.7.

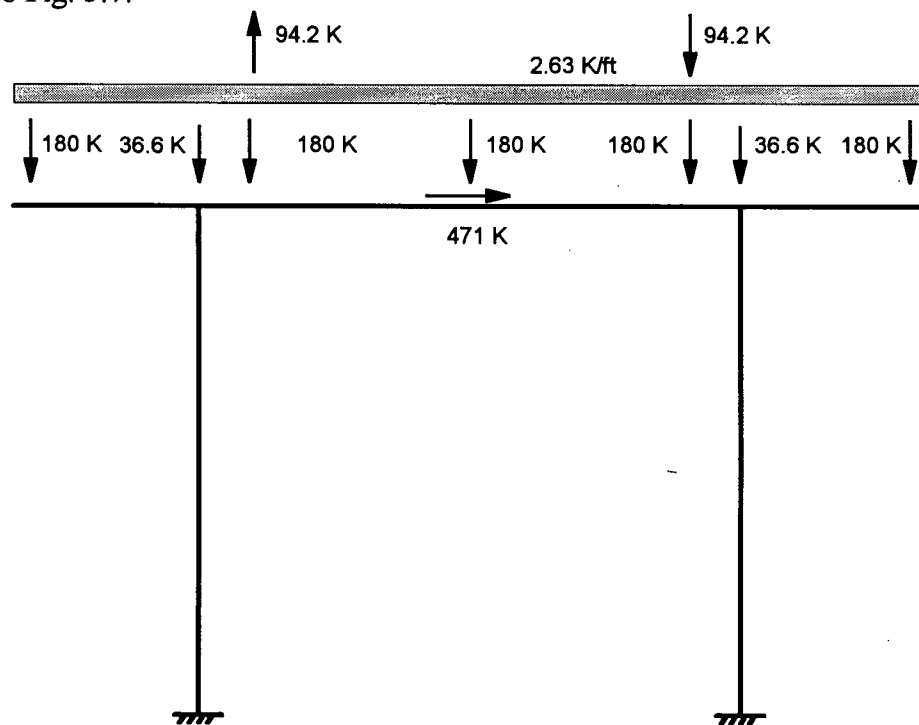


Fig. 3.5 Loading (ATC-6).

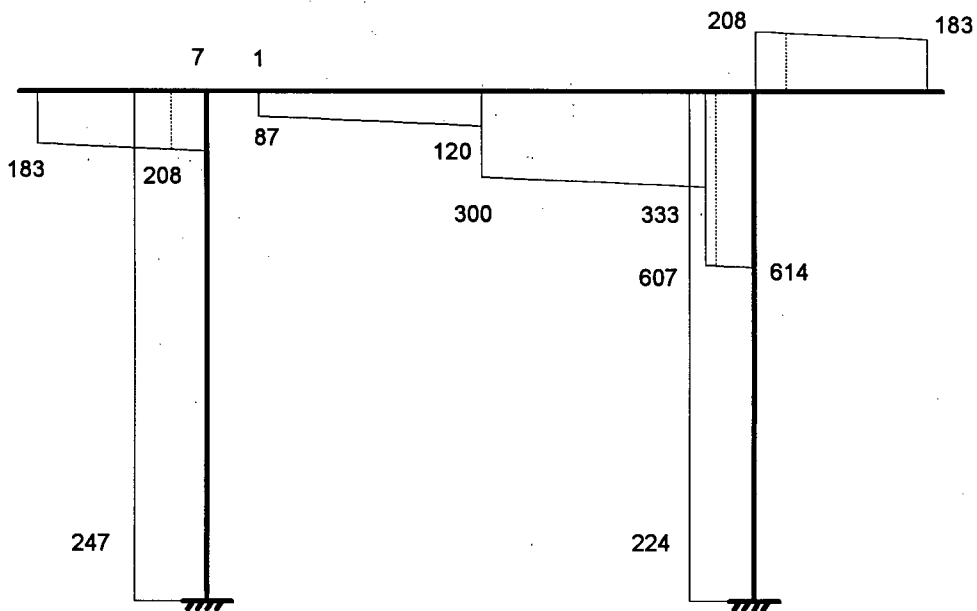


Fig. 3.6 Shear force diagram (kips) for the DL + EQ (ATC-6).

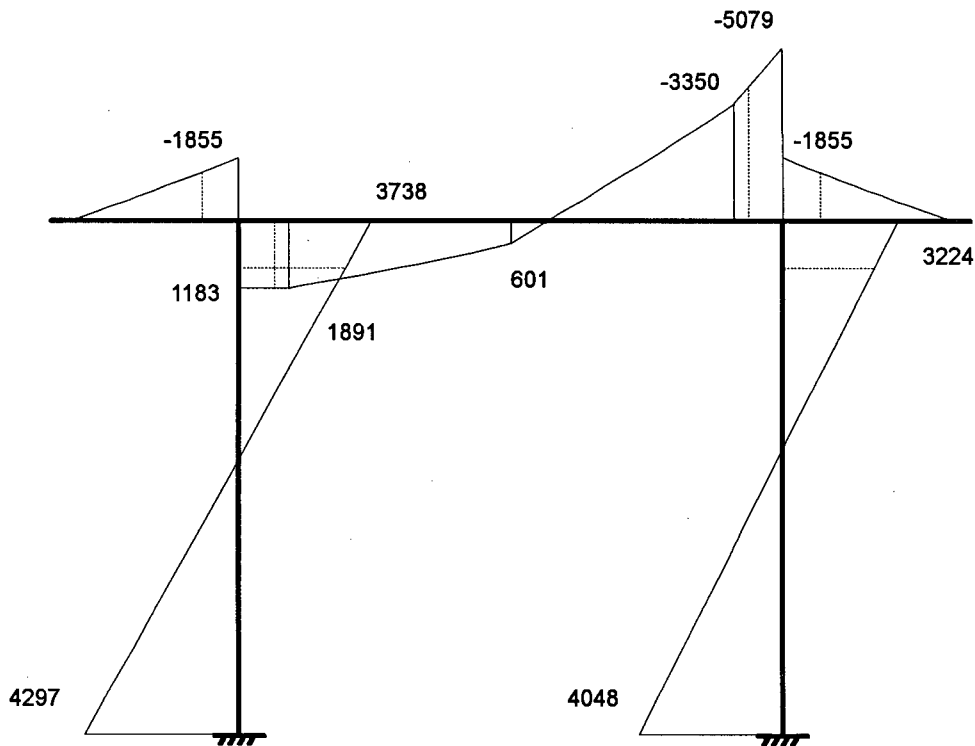


Fig. 3.7 Bending moment diagram (kip-ft) for the DL + EQ (ATC-6).

The force diagrams for the AASHO 1961 and ATC-6 are drawn to the same scale. A comparison of the two design codes is somewhat difficult, because the earlier AASHO 1961 is based on a working stress design (WSD) concept, whereas ATC-6 adheres to the limit state design (LSD) approach. A fair comparison could be made by increasing the AASHO loads by about 50%. It is apparent that the ATC force effects remain substantially greater than the increased AASHO values. In this analysis the ATC force effects are not reduced by the "R" factor, i.e. "R" is taken as 1.0.

### 3.5 Assessment of Member Capacities

The sectional capacity at a simplistic level can be separated into the flexural capacity and the shear capacity. The evaluation of the flexural capacity is done herein using a set of programs developed by CALTRANS. They are based on the Mander model for confined concrete (Mander et al. (1988)). The program finds the first yield by increasing the concrete compressive strain until the longitudinal steel yields and then terminates the iterations as soon as the maximum concrete strain is attained. Since the sections are poorly confined, the maximum concrete strain is taken as 0.005. The moment curvature response is then simplified by an elastic-perfectly plastic response that has the same area under the moment curvature curve. This leads to a slightly higher yield moment than the actual first yield moment.

The shear calculations are based on the ACI/ASCE committee 426, 1973:

$$V_n = V_c + V_s + V_p \quad (3.1)$$

$$V_c = v_c b_w d \quad (3.2)$$

$$\text{where } v_c = (0.85 + 120\rho)\sqrt{f'_c} \leq 0.2\sqrt{f'_c}$$

$$V_s = A_v f_y \frac{s}{d} \quad (3.3)$$

$$V_p = 0.2P \quad (3.4)$$

- where
- $f'_c$  = concrete compressive strength (psi).
  - $f_y$  = yield strength of stirrups (psi).
  - $v_c$  = shear strength contribution of concrete (psi).
  - $b_w$  = width of the section (in).
  - $\rho$  = ratio of tension steel  $A_s/b_w d$ .
  - $A_v$  = area of vertical reinforcement (in<sup>2</sup>).
  - $s$  = Stirrup spacing (in).
  - $d$  = distance from extreme compression fiber to centroid of the longitudinal tension reinforcement (in).
  - $P$  = axial load (lb).

Note that the  $V_p$  term in the above equation was introduced by Priestley. For simplicity this approach is called the ACI/ASCE code formula for the remainder of this thesis.

Three elements of the bridge bent were investigated, the cap beam, the columns, and the beam/column joints. The cap beam and the columns are of the main interest and were studied in flexure and shear. The joints were briefly analyzed for shear.

### 3.5.1 Cap beam

Three sections of the cap beam were investigated as depicted in Fig. 3.8. The input parameters for the various sections are listed in Table 3.1.

**Table 3.1** Sectional flexure parameters of the cap beam

<i>Section</i>	<i>Dimensions</i>	<i>Top Steel</i>	<i>top cover</i>	<i>Bot. Steel</i>	<i>bot. cover</i>
1	60"x42"	13 #11	5.70	3 #6	2.63
2	60"x42"	11 #11	5.42	4 #11	2.63
3	60"x42"	6 #11	4.25	11 #11	3.73

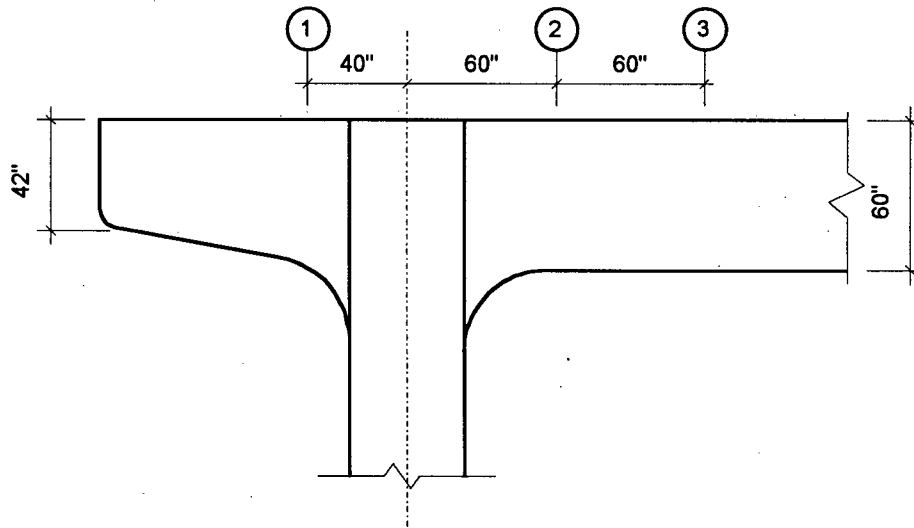


**Fig. 3.8** Cap beam sections.

The shear parameters are listed in Table 3.2. #4 rectangular ties with 135° hooks are used in the midsection outside the haunches of the cap beam and the remainder of the shear reinforcement consists of #5 ties. For section 2 only the 4-#11 bottom bars are taken into consideration for  $\rho$ , assuming the positive tension steel is more critical.

**Table 3.2** Sectional shear parameters of the cap beam.

<i>Section</i>	$\rho (+)$	$\rho (-)$	$b_w$ (in)	$d(+)$ (in)	$d(-)$ (in)	$A_v$ (in <sup>2</sup> )	$s$ (in)
1	-	0.00805	42	-	53.61	0.62	6
2	0.00248	0.00681	42	53.89	53.89	0.62	24
3	0.00681	0.00371	42	56.27	55.06	0.40	36

A brief check on the anchorage requirements into the columns of the bottom longitudinal reinforcing bar to develop full capacity indicates that with the haunch, anchorage is adequate.

The formation of a plastic hinge is expected just outside of the heavily reinforced haunch to the right of section 2 in Figure 3.8. In that region very little transverse reinforcement, #5 ties at 24 in spacing, is provided. As the development of the hinge progresses, the concrete contribution to the shear capacity diminishes (Priestley and Seible (1991)). The flexural capacities were derived using the CALTRANS program BEAM303 and the shear capacities computed herein are based on equations 3.1 to 3.4, in spite of the fact that prescribed minimum shear reinforcement is not present. The results are listed in Table 3.3.

**Table 3.3** Sectional capacities of the cap beam.

<i>Section</i>	<i>M<sub>n+</sub></i> <i>(kip-ft)</i>	<i>M<sub>n-</sub></i> <i>(kip-ft)</i>	<i>V<sub>n(+)</sub></i> <i>(kips)</i>	<i>V<sub>n(-)</sub></i> <i>(kips)</i>
1	497	4619	-	654
2	1711	4208	270	361
3	4334	2506	336	246

### 3.5.2 Columns

The column dimensions are 48" square by 30 feet tall. There are 16-#11 bars going from top to bottom of the column. The concrete cover to the main bars is 3 in. At the bottom of the column there are 4 additional #11 bars on each side of the column face parallel to the direction of the cap beam. The CALTRANS program COL604 does not allow for irregular reinforcement of the columns, therefore the section is analyzed with a regular 24 bar layout. Throughout the column there are #3 ties at a spacing of 12 in. The axial load of 554 kips for each column due to dead load is derived from the superimposed dead load of 900 kips and the self weight of the cap beam and half of the columns of 208 kips. In order to obtain a moment axial load interaction, the analysis of the top and

bottom section was carried out with zero axial load, 554 kips, and about three (3) times the dead load, 1650 kips. The results from the sectional analysis are listed in Table 3.4.

**Table 3.4** Sectional flexural capacities of the columns.

<i>Section</i>	<i>Axial Load (kips)</i>	<i>M<sub>n</sub> (kip-ft)</i>
top	0	2490
	554	3301
	1650	4850
bottom	0	3527
	554	4288
	1650	5708

The maximum axial load with no bending follows the common formula:

$$P_c = 0.85f'_c(A_g - A_s) + f_y A_s \quad (3.5)$$

Inserting the appropriate parameters into the above equation leads to a maximum axial compression capacity of 12870 kips and 13430 kips for the top section and the bottom section respectively.

For the maximum tension capacity of the column, only the steel is taken into account assuming that the concrete cracks completely and does not contribute to the axial capacity.

$$P_t = f_y A_s \quad (3.6)$$

The maximum tension capacity values are 1250 kips and 1870 kips for top and bottom column section respectively. These values are used later on in this chapter.

The parameters for the shear calculations are listed in Table 3.5. An axial load of 554 kips, which is equal to the dead load, was used for  $wf$ , since the average load on the

two columns is always the dead load value. The shear reinforcement consists of 3 legs of #3 bars.

**Table 3.5** Sectional shear parameters of the columns.

<i>Section</i>	$\rho$	$b_w$ (in)	$d$ (in)	$A_v$ (in <sup>2</sup> )	$s$ (in)
top	0.01083	48	43.94	0.33	12
bottom	0.01625	48	43.94	0.33	12

The sectional shear capacity is  $351.2 + 60.4 + 110.8 = 522.4$  kips and  $457.4 + 60.4 + 110.8 = 628.6$  kips for the top and bottom section respectively ( $V = V_c + V_s + V_p$ ).

### 3.5.3 Joint Shear Strength

The demands on the joint were determined by a simple elastic frame analysis using gross sectional properties. This analysis was used to get a critical base shear at which one of the other elements of the bridge bent start to yield. For that load level, the demands at the face of beam column joints were used to establish the joint shear demands and capacities. The joint shear strength calculations follow closely the work of Priestley and Seible (1991), which allows for an increase in the joint shear capacity for axial loads (units are in lb. and inches).

$$V_j = v_{cj} b_w h + A_j f_y \quad (3.7)$$

$$v_{cj} = \sqrt{f_t (f_t + f_a)}$$

$$f_t = 3.5 \sqrt{f_c'}$$

$$f_a = \frac{w_f}{b_w h}$$

where  $V_j$  = joint shear capacity (lb.).  
 $h$  = total depth of the section (in).

The force demands at the face of the joint is shown in Fig. 3.9 in kips for the left and right joint respectively. The bending moments were uncoupled into a force couple with a moment arm of 0.85 of the section depth. Table 3.6 lists the various joint shear demands related to the base shear  $V_{eq}$ .

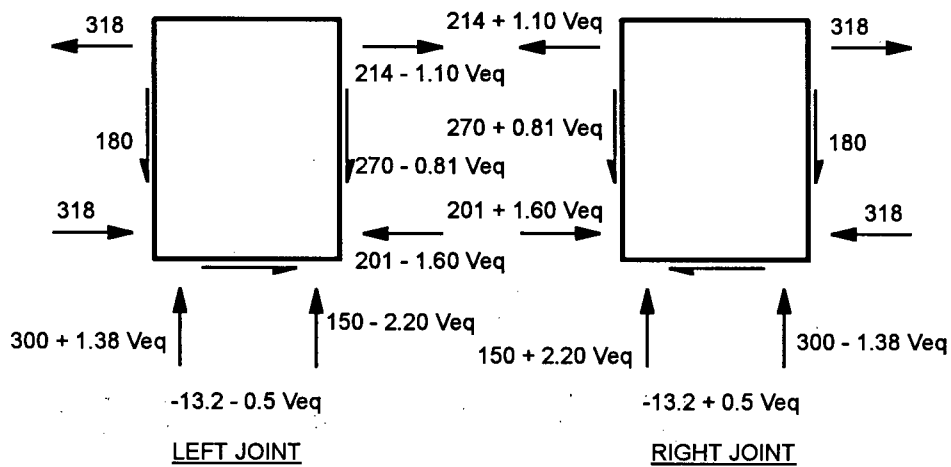


**Fig. 3.9** Force demands for the beam column joints (kips).

**Table 3.6** Joint shear demands.

<i>Shear</i>	<i>Description</i>	<i>Shear - kips</i>
$V_{LH}$	left horizontal	$104 + 1.10 V_{eq}$
$V_{LV}$	left vertical	$-120 - 1.38 V_{eq}$
$V_{RH}$	right horizontal	$104 - 1.10 V_{eq}$
$V_{RV}$	right vertical	$-120 + 1.38 V_{eq}$

From the previous frame analysis and the sectional capacities calculated earlier, a first hinge will occur at a base shear load of about 418 kips, when the cap beam reaches the positive bending moment capacity at the face of the left joint. For the horizontal joint

shear the five sets of 3 legs of stirrups plus a #5 sidebar at each face of the beam were realized for the horizontal shear reinforcement. For the vertical joint shear reinforcement the vertical column bars were neglected since they are not hooked at the top and therefore do not fully develop until about one third of the joint depth from the top. The demands and the capacities for a base shear of 418 kips are listed in Table 3.7.

**Table 3.7** Joint shears (kips).

<i>Shear</i>	<i>Demand</i>	<i>Capacity</i>	<i>Comment</i>
V <sub>LH</sub>	564	785	OK
V <sub>LV</sub>	697	728	OK
V <sub>RH</sub>	356	1030	OK
V <sub>RV</sub>	457	728	OK

The joint shear strength calculations here were based on the assumption that the highest shear demands will be imposed onto the joint before flexural hinging mechanisms occur elsewhere in the structure. Beyond that point the structure is undergoing damage at locations other than the joint and it can be inferred that the joint shear is not a critical failure mechanism in the overall response of the bridge bent.

#### 3.5.4 Conclusion

When Klohn-Crippen conducted their preliminary analysis of the bridge bent structure their calculations indicated that the joint region is not critical but that it was unclear if yielding will first occur in the cap beam or the columns. This is confirmed in this analysis. A flexural hinge is expected in positive bending in the cap beam at a base shear of 418 kips. It also should be noted that cap beam and column flexural yielding is anticipated before a joint shear failure will occur.

### 3.6 Push-Over Analysis of the Prototype (Flexural Behaviour)

The method of introduction of the lateral forces into the bridge bent has an influence on the predicted structural response. Here a study is undertaken with different deck structure models to determine the sensitivity of the lateral load application system. The influence of different loading trusses and variations of the cross sectional properties of the bent are investigated.

Two different sets of prototype member cross sectional properties have been used. One is directly adopted from the previous section (denoted MS). The other set was derived by Klohn-Crippen for their first analysis (denoted K-C). For both sets the additional stiffness due to the haunches at the beam column joints have been ignored. The differences are small and have been arrived at from different sectional analysis methods employed to get the moment curvature responses. Both sets of properties are illustrated in Table 3.8.

There is agreement between these models on the sectional areas and the effective stiffness of the cap beam and column elements. The effective stiffness is assumed to be 25% and 30% of the gross moment of inertia of the cap beam and the columns respectively. The differences in the models arise with the yield surfaces. Since the cap beam is a purely flexural element only negative and positive yield moments have to be supplied. Whereas the columns are actually beam columns and an axial load bending moment interaction relationship is required for the analysis.

In Table 3.8.,  $P_c$  is the maximum compression capacity.  $M_y$  is the moment capacity at zero axial load, and  $P_t$  is the axial tension capacity.  $P_b$ ,  $M_b$  and  $M_y$  are three parameters used to describe the conventional axial load - bending moment interaction and they may be

chosen to give the best fit for the expected range of response and therefore may not coincide with the actual balance point of the interaction (see Fig. 3.10).

**Table 3.8** Comparison of the cross sectional properties.

<i>Parameters</i>		<i>MS</i>	<i>K-C</i>
<i>E</i> (ksi)		4650	4665
<b>CAP BEAM</b>			
<i>A</i> (in <sup>2</sup> )		2520	2520
<i>I<sub>e</sub></i> (in <sup>4</sup> )		189000	188698
+ <i>M<sub>y</sub></i> (kip-ft)		1711	1450
- <i>M<sub>y</sub></i> (kip-ft)		4208	4350
<b>COLUMN</b>			
<i>A</i> (in <sup>2</sup> )		2304	2304
<i>I<sub>e</sub></i> (in <sup>4</sup> )		132710	132710
bottom	<i>P<sub>c</sub></i> (kips)	13430	13200
	<i>P<sub>b</sub></i> (kips)	1650	1980
	<i>M<sub>b</sub></i> (kip-ft)	5708	5894
	<i>M<sub>y</sub></i> (kip-ft)	3527	2918
	<i>P<sub>t</sub></i> (kips)	1870	1650
top	<i>P<sub>c</sub></i> (kips)	12870	12800
	<i>P<sub>b</sub></i> (kips)	1650	2048
	<i>M<sub>b</sub></i> (kip-ft)	4850	5264
	<i>M<sub>y</sub></i> (kip-ft)	2490	1994
	<i>P<sub>t</sub></i> (kips)	1250	1100

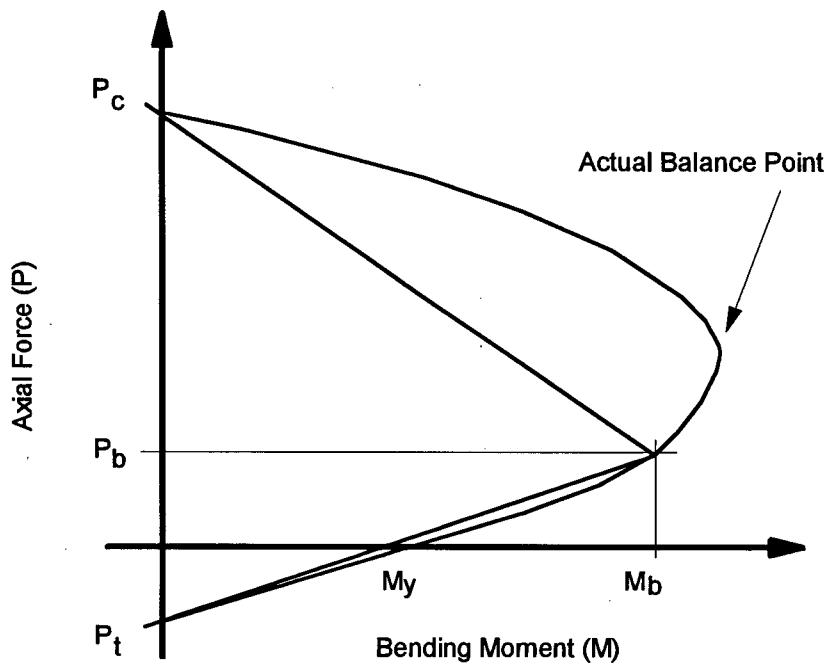


**Fig. 3.10** Model of the yield surfaces for columns (DRAIN-2DX).

Since the moment curvatures for the MS sections are idealized by an elastic-perfectly plastic response, the ideal yield moments are somewhat higher than the bending moments at first yielding of the longitudinal reinforcement. The ultimate strength of MS-V1 and MS-V2 are therefore higher than the ones of MS-V3 and K-C.

Three types of bridge deck structures are used to establish the sensitivity to the method of load application. Model MS-V1, shown in Fig. 3.11, has a racking truss to simulate the bridge deck structure as closely as possible.

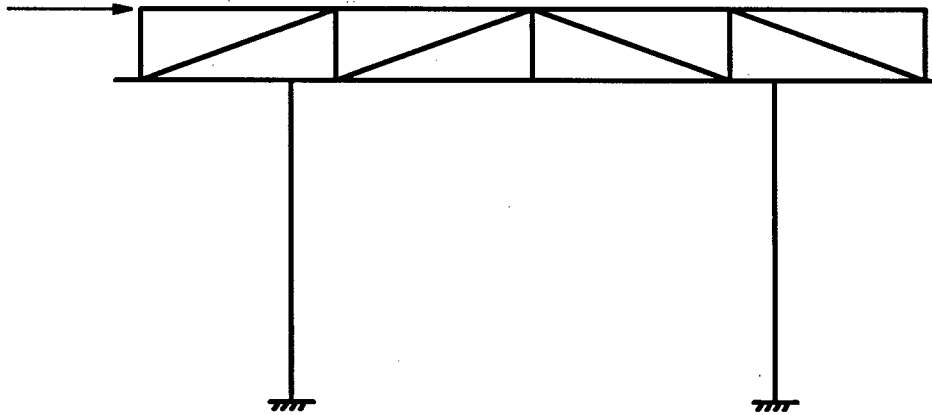


Fig. 3.11 Model for MS-V1 (racking truss).

The load application system of model MS-V2 and MS-V3 is a triangular truss connected to the beam column joint node as depicted in Fig 3.12. This system is being also used for the testing of the 45% scale model in the UBC structure labs.

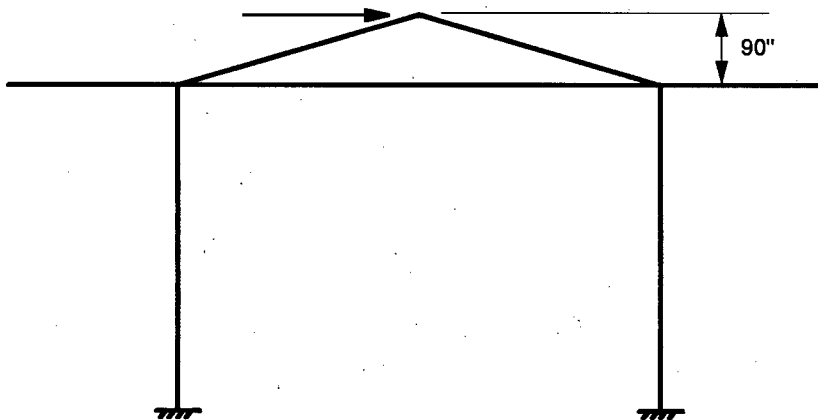


Fig. 3.12 Model for MS-V2 and MS-V3 (triangular truss).

The model independently done by Klohn-Crippen uses a different discretization of the elements of the cap beam and the columns. Also, the load application system is a series of stiff vertical cantilever elements to simulate the bridge deck (see Fig 3.13).

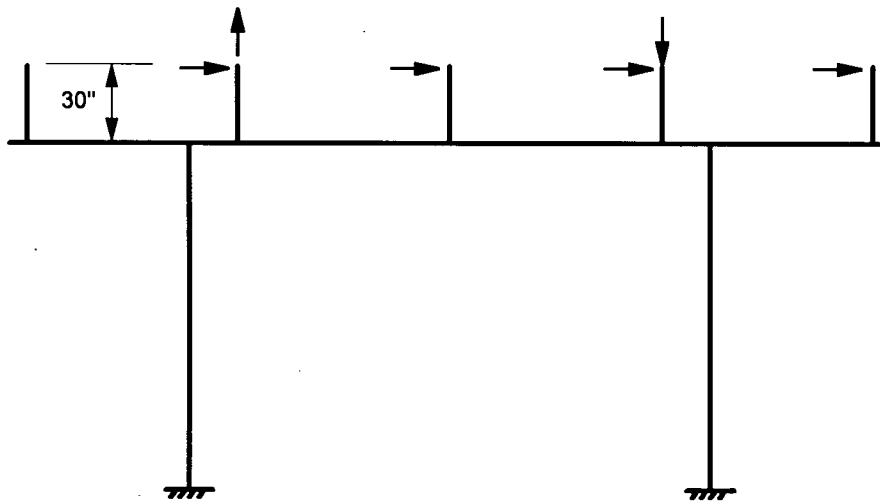


Fig. 3.13 Model for Kohn-Crippen (stiff cantilevers).

The cross sectional properties for MS-V1 and MS-V2 are the MS ones obtained earlier in this chapter, whereas the MS-V3 and K-C model use the sectional properties derived by Kohn-Crippen.

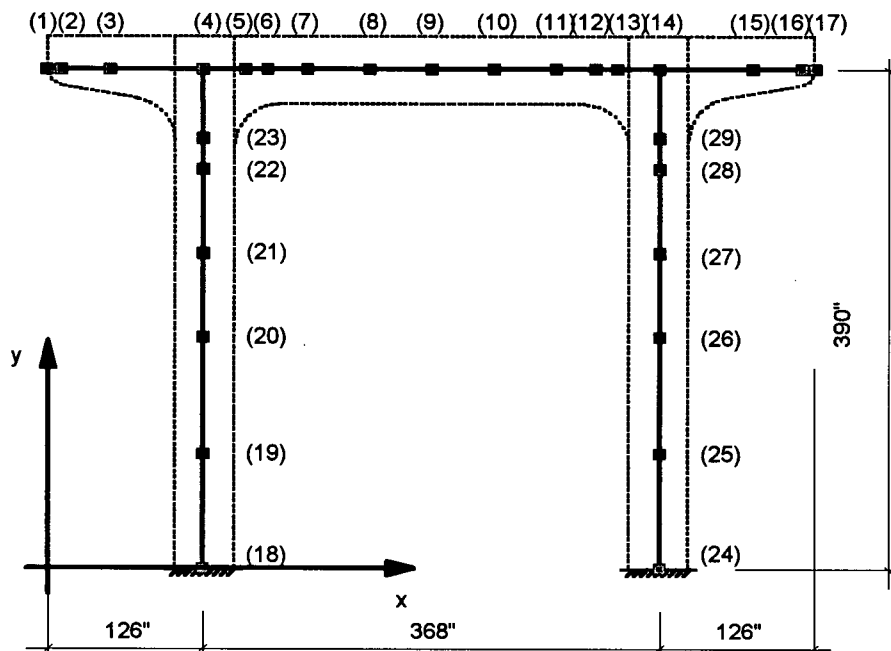


Fig. 3.14 MS-V2 Model.

MS-V2 is used as the base model against which all the other models are compared (see Fig 3.14 and Table 3.9). The joint regions are assumed to be rigid, which was accomplished by use of element offsets to the face of the columns and the cap beam to. Table 3.10 lists the hinge locations and the hinge history with corresponding total base shears ( $V_{eq}$ ).

**Table 3.9** Nodal coordinates of the computer model.

<i>Node</i>	<i>X - Coord (in)</i>	<i>Y - Coord (in)</i>	<i>Node</i>	<i>X - Coord (in)</i>	<i>Y - Coord (in)</i>
1	0.0	390.0	16	608.0	390.0
2	12.0	390.0	17	620.0	390.0
3	51.0	390.0	18	126.0	0.0
4	126.0	390.0	19	126.0	90.0
5	160.0	390.0	20	126.0	180.0
6	178.0	390.0	21	126.0	246.0
7	210.0	390.0	22	126.0	312.0
8	260.0	390.0	23	126.0	336.0
9	310.0	390.0	24	494.0	0.0
10	360.0	390.0	25	494.0	90.0
11	410.0	390.0	26	494.0	180.0
12	442.0	390.0	27	494.0	246.0
13	460.0	390.0	28	494.0	312.0
14	494.0	390.0	29	494.0	336.0
15	569.0	390.0			

**Table 3.10** Sequence of hinge formation and corresponding base shear.

<i>Model</i>	<i>MS-V1</i>	<i>MS-V2</i>	<i>MS-V3</i>	<i>K-C</i>
HINGE 1	LCT	LB	LCT	LB
$V_{eq}$ kips	386.1	377.7	325.0	327.1
HINGE 2	RB	RB	LCB	LCB
$V_{eq}$ kips	464.0	429.3	394.4	405.3
HINGE 3	LCB	LCB	RCT	RB
$V_{eq}$ kips	465.0	444.1	418.1	430.4
HINGE 4	RCB	RCB	RCB	RCB
$V_{eq}$ kips	482.3	471.1	428.4	441.6

LCT : Left Column Top

LCB : Left Column Bottom

RCT : Right Column Top

RCB : Right Column Bottom

LB : Left Beam end

RB : Right Beam end

A different load application system for the same bridge bent model does not change the order of the hinge formation but sometimes changes the location from column top to beam and has a small resulting influence on the base shear; see results for MS-V1 and MS-V2. This indicates that the beam and the column capacity/demand ratios are very close and the otherwise small influence of the load application system is important. A change in the discretization of the model but the same cross sectional properties seems to influence the hinge location and sequence in a similar way, see results for MS-V3 and KC.

The overall load deflection response as seen in Fig 3.15 are fairly similar. Model MS-V2 most closely represents the actual testing setup, and because the various models are generally in close agreement, model MS-V2 has been chosen for further investigation.

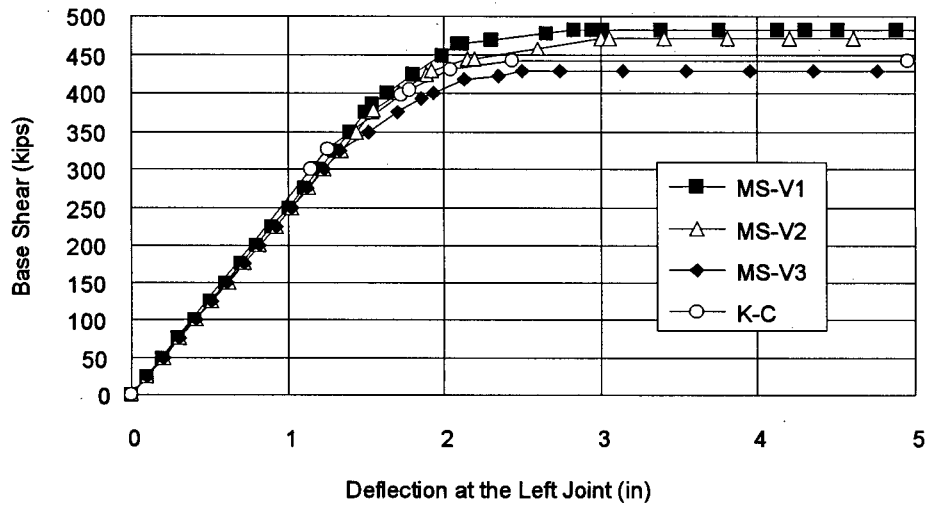


**Fig. 3.15** Comparison of base shear vs. deflection for the MS and K-C analyses.

Considering the uncertainties of the assumptions made on the physical parameters, such as the material properties and the support conditions of the footings and the bridge deck structure a maximum difference of less than 15% in the outcome of the analysis between all models for the ultimate lateral load capacity is satisfactory.

### 3.7 Modified Compression Field Theory Analysis

The push over analysis in the previous section done with DRAIN-2DX assumes flexural yielding as the predominately plastic response. This is typical for most available nonlinear analysis programs. At all stages of hinge formation a sectional shear analysis is required to determine if the shear capacity is exceeded and shear is in fact the critical failure mode.

Modern concrete theory assumes an interaction between flexure and shear. In the following program RESPONSE (Collins and Mitchell (1991)), which is based on the

modified compression field theory (Vecchio and Collins (1986)), was used to determine the sectional capacities for the analytical push over analysis model MS-V2. The program analyzes a given section by iteration of the principal strains until a convergence to the largest force state is found. It requires that the demand offset constants ( $N_o$  and  $M_o$ ) and the demand ratios ( $dN/dV$  and  $dM/dV$ ) of the axial forces and the bending moments relative to the sectional shears are provided.

$$N = N_o + dN/dV V$$

$$M = M_o + dM/dV V$$

where  $N$ ,  $M$ , and  $V$  are the sectional forces. In order to back calculate the corresponding base shear ( $V_{eq}$ ) the following relationship was used:

$$V_{eq} = V_o + dV_o/dV V$$

Sections near the joints are identified as the critical regions, one cap beam section just outside the haunch and one column section just below the haunch. The elastic demand ratios and constants are listed in Table 3.11.

**Table 3.11** Elastic demand constants and ratios.

<i>Section</i>	$N_o$ (kips)	$dN/dV$	$M_o$ (kip-ft)	$dM/dV$ (ft)	$V_o$ (kips)	$dV_o/dV$
Left Cap Beam	10.06	0	663.2	11.0	217.7	1.89
Right Cap Beam	10.06	0	663.2	-11.0	-217.7	1.89
Left Column	-532.1	1.54	56.6	11.7	-20.11	2.0
Right Column	-532.1	-1.54	-56.6	11.7	20.11	2.0

Substituting the above parameters into RESPONSE led to a yield capacity for each of the four sections (see Table 3.12).

**Table 3.12 RESPONSE Analysis Results.**

<i>Section</i>	<i>V<sub>eq</sub></i> (kips)	<i>M</i> (kip-ft)	<i>V</i> (kips)	<i>N</i> (kips)
Left Cap Beam	425	1870	110	10
Right Cap Beam	243	-2010	244	8.6
Left Column	343	2180	182	-251
Right Column	499	2750	240	-902

Here  $M$  is the sectional bending moment,  $V$  is the shear of that section,  $N$  is the axial load, all occurring at the same base shear ( $V_{eq}$ ), assuming that the distribution of forces remains the same as that given by the elastic analysis.

The first section to reach its capacity is the right cap beam at a base shear of 243 kips. The strains at the section indicate that the capacity of the section is limited by shear. The push over analysis for MS-V2 shows flexural hinging at a base shear of 378 kips for the left cap beam. A brittle failure mode is therefore expected as the overall response of the as-built bridge bent. A more detailed approach has been taken in Chapter 5 to predict the response of the testing model. An exact failure mechanism however is still difficult to identify.

In Figure 3.16 the analytical results for flexure and shear are depicted. The RESPONSE analysis is an ultimate strength analysis, but it is not entirely clear if the sections fails in a brittle manner or is able to show some ductility. The interaction of the shear and flexure is not all that well understood and more research is needed in this field.

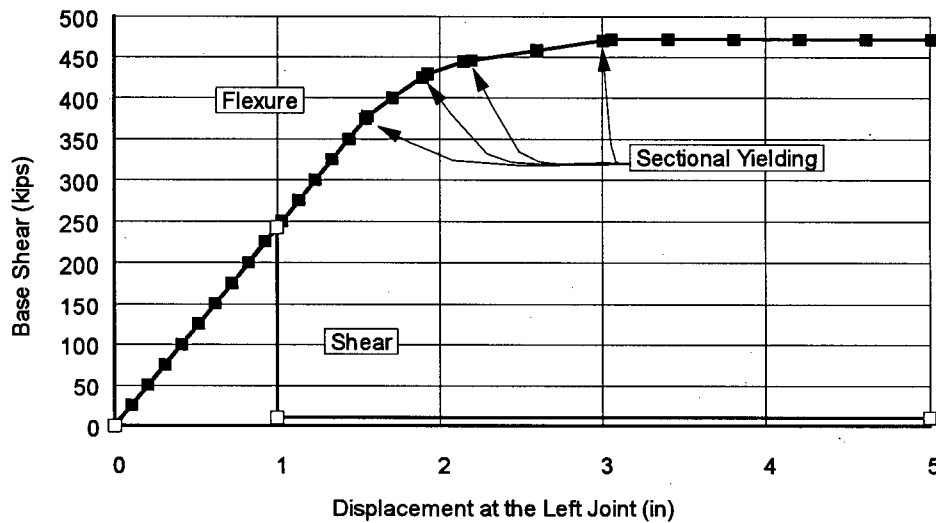


Fig. 3.16 Flexure and shear response of the bent.

### 3.8 Conclusions

The desired response for this structure is a ductile flexural mechanism that ensures sufficient ductility to withstand the anticipated seismic loadings in a favourable way. The analysis of the various elements of the bent showed that the beam column joint, as well as the columns themselves, are not the critical elements. The cap beam however is suspected to fail in shear in a possible brittle manner at a lower base shear than flexural hinging will occur in the cap beam, which is definitely an undesired response. Nonetheless entirely different failure mechanisms are conceivable, for example a stagewise flexural degradation of the moment capacity due to debonding of the reinforcement or an nominal ductile shear failure. The experimental test series sheds some light onto these matters.

## CHAPTER 4

### DYNAMIC ANALYSIS OF THE PROTOTYPE

#### 4.1 Introduction

One of the more complex problems in reinforced concrete behaviour is the analysis of plastic nonlinear response to random excitations such as earthquakes. Plastic behavior of reinforced concrete by itself is difficult to deal with; dynamic effects only add to the complexity. To make an analysis at all manageable many simplifications have to be made. The difficulty arises as to what assumptions can be made and still capture the main features of the response. Two types of analysis were performed: a linear spectral analysis and a time step analysis. The non linear time step analysis lends itself to a comparison with the pushover analysis of the previous chapter. Such an analysis is performed on the prototype using three earthquake records which were modified to fit the surface spectral accelerations of the Oak Street Bridge.

#### 4.2. DRAIN-2DX

Commercially there are several general purpose finite element programs available such as ADINA, ABACUS, ANSYS, etc. They allow the user to define their own constitutive relationships and develop new element types. Most of these software programs however have evolved from a mechanical engineering perspective and support aspects such as heat transfer, stress concentration, etc. The program used in this project was DRAIN-2DX which is geared towards structural engineering and can perform a nonlinear time step analysis as well as a spectral response analysis. It is available through the National Information Service for Earthquake Engineering (NISEE) at the Earthquake Research Center at University of California at Berkeley.

DRAIN-2DX is one of the first programs to handle nonlinear time step analysis of two dimensional frames and was first developed in 1973 by Dr. Powell at UC Berkeley. In its newest release it now incorporates modules to calculate mode shapes and spectral responses. It features a very limited number of different elements i.e. truss element, beam-column elements, a simple connection element, a structural panel element, and a link element. There are no provisions to calculate hysteretic strength or stiffness degradation.

### 4.3 Spectral Analysis of the Prototype

The Ministry of Transportation and Highways retained consultants to develop design spectra for the Oak Street Bridge. The surface spectrum applicable for bent S28 is the one for S31 depicted in Fig 4.1. 5% damping is assumed for this spectrum.

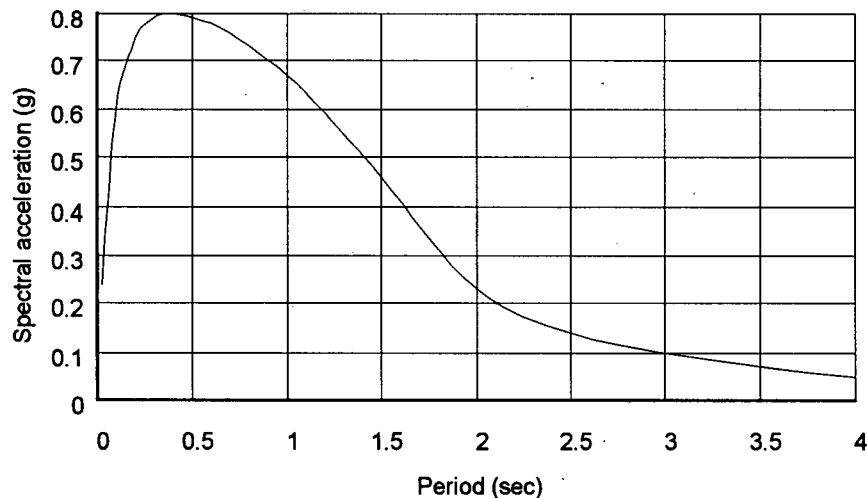
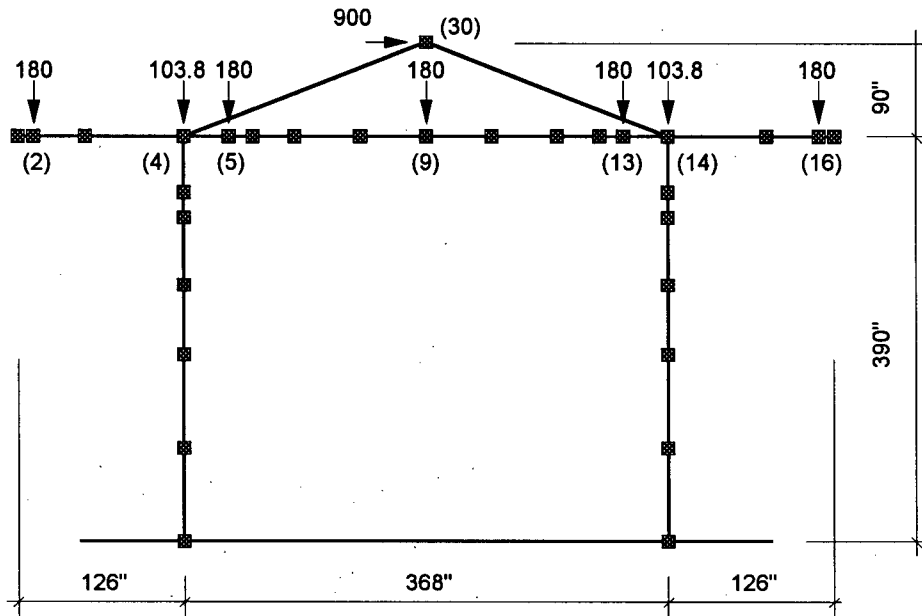


Fig. 4.1 Spectrum for Oak Street Bridge bent S31.

The spectral analysis was performed with DRAIN-2DX. The model uses a simplified system of masses (see Fig 4.2).



**Fig. 4.2** Model for the spectral analysis (weights are in kips.).

Model MS-V2 of the previous chapter is used here. The first five natural periods are listed in Table 4.1:

**Table 4.1** Natural periods for bent S28.

<i>Mode</i>	<i>Period</i>
1	0.69 sec
2	0.17 sec
3	0.12 sec
4	0.07 sec
5	0.04 sec

The combined spectral response of five modes is superimposed with the dead load forces in Fig. 4.3. The maximum bending moments in the cap beam at the face of the columns are 6550 kip-ft and 5040 kip-ft for the negative moment and positive moment respectively. The axial load from the spectral analysis is 637 kips, which when

superimposed with the axial load of the dead load of 554 kips, yields 1190 kips in compression and 83 kips in tension for uplift. The bending moment for the column in compression at the top of the column just below the joint is 5500 kip-ft and at the bottom of the column is 6730 kip-ft. in the uplift case the bending moment at the top of the column is 5960 kip-ft, and at the bottom of the column it is 6990 kip-ft. The maximum horizontal spectral displacement at the beam/column joints is 3.5".

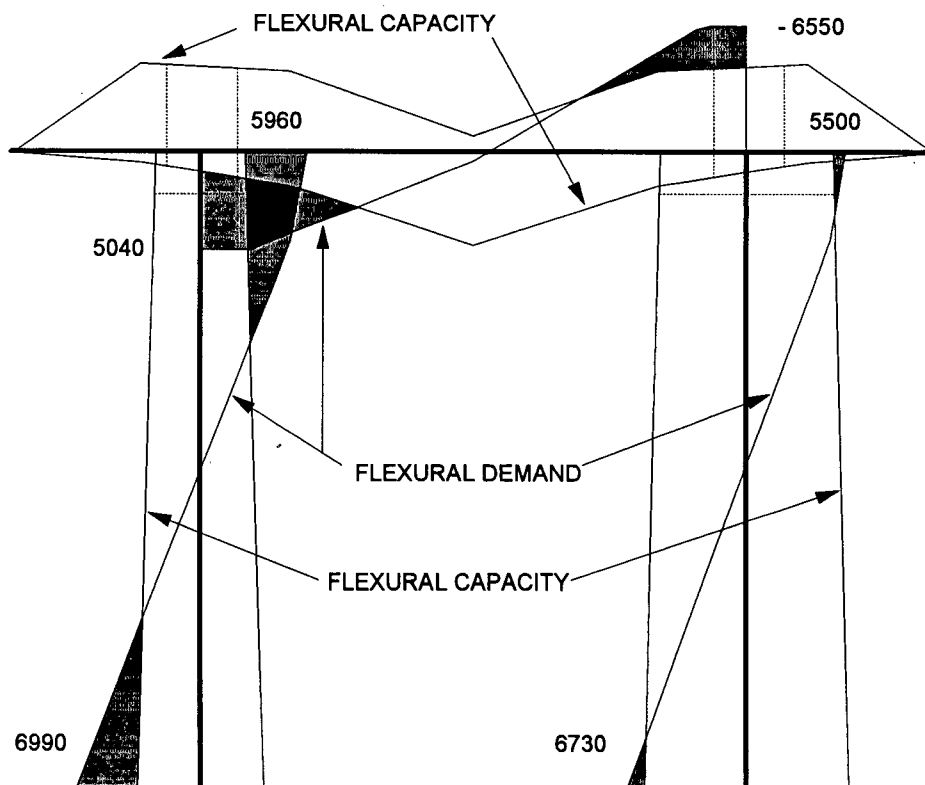


**Fig. 4.3** Spectral analysis results including the dead load and the flexural capacities (bending moments in kip-ft).

In Fig. 4.3 the demand from the spectral analysis is compared with the flexural capacities calculated in the previous chapter. The shaded areas indicate where the demand exceeds the capacity. In the left joint region the demand exceeds the capacity by the largest margin, which coincides with the location of the first hinge of the pushover

analysis. The second hinge at the right joint in the cap beam also shows a large demand/capacity ratio. The approximate yield displacement from the pushover analysis in the previous chapter is about 2". The displacement ductility demand is therefore 1.75. This is a fairly low value but not uncommon in older concrete bridge bents.

#### 4.4 Nonlinear Time Step Analysis of the Prototype

The earthquake records supplied by the soil consultants have been modified to reflect site specific soil amplifications. An attempt is made to keep the computer models for both programs as similar as possible to the models used previously. The cross sectional properties including the parameters for the yield surfaces have been adopted from the sectional analyses in chapter 3.

##### 4.4.1 Earthquake Records

The soil consultants retained by the MOTH, Dames and Moore (1991), supplied a series of earthquake records for the Oak Street Bridge listed in Table 4.2.

**Table 4.2** Earthquake records for the Oak Street Bridge.

<i>Place</i>	<i>Date</i>	<i>Site</i>	<i>PGA</i>	<i>PGV</i>
San Fernando	9-Feb-1971	Griffith Park Observatory	0.180	0.205
San Fernando	9-Feb-1971	3838 Lankershim Blvd.	0.150	0.150
San Fernando	9-Feb-1971	231 Figueroa Street	0.200	0.167

These acceleration records are rock or firm soil records. Since the foundation of the bridge is on very soft soil, significant soil amplification is to be expected. When comparing the spectra of the records with the design spectrum of Figure 4.1 it is apparent that the design spectrum has incorporated some soft soil amplification. The acceleration

as well as the time base of these firm soil earthquake records are therefore scaled to obtain a spectral response closer to the design spectrum. The scaling factors for each record are listed in Table 4.3. In Fig 4.4 the spectra for the modified earthquake records are shown in comparison with the design spectrum.

**Table 4.3** Scaling factors.

<i>Record</i>	<i>Acceleration Scale</i>	<i>Time Scale</i>
Griffith Park Observatory	1.38	1.5
3838 Lankershim Blvd.	1.07	2.5
234 Figueroa Street	1.06	2.0

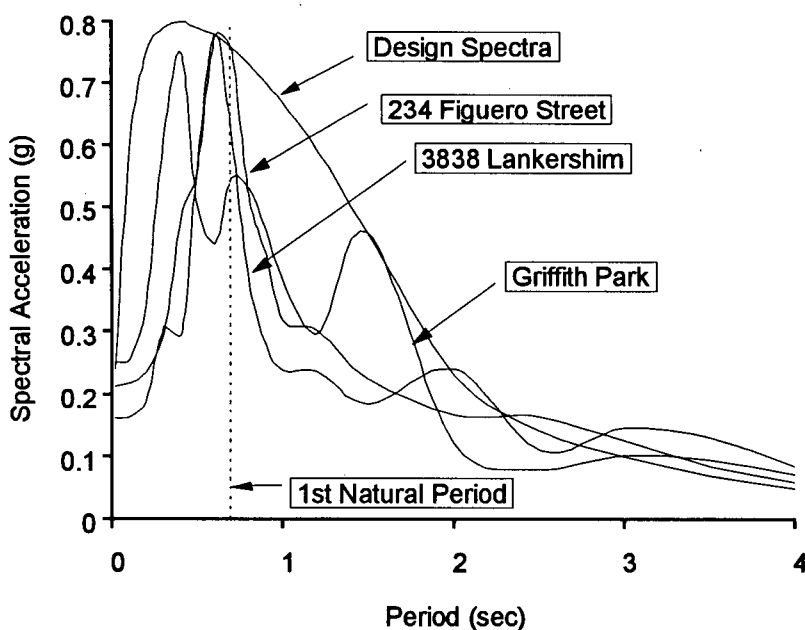


**Fig. 4.4** Modified spectra.

#### 4.4.2 DRAIN-2DX Results

The geometry and stiffness of the computer model are the same as the ones used for the spectral analysis. Minimal strain hardening is used. Also P- $\Delta$  effects were ignored in

the following analyses. The time history analyses show yielding in the beams and eventually in the columns similar to the pushover analysis. The relative displacements between the top and bottom of the bent for all three earthquake records are plotted in Fig. 4.5 to Fig. 4.7.

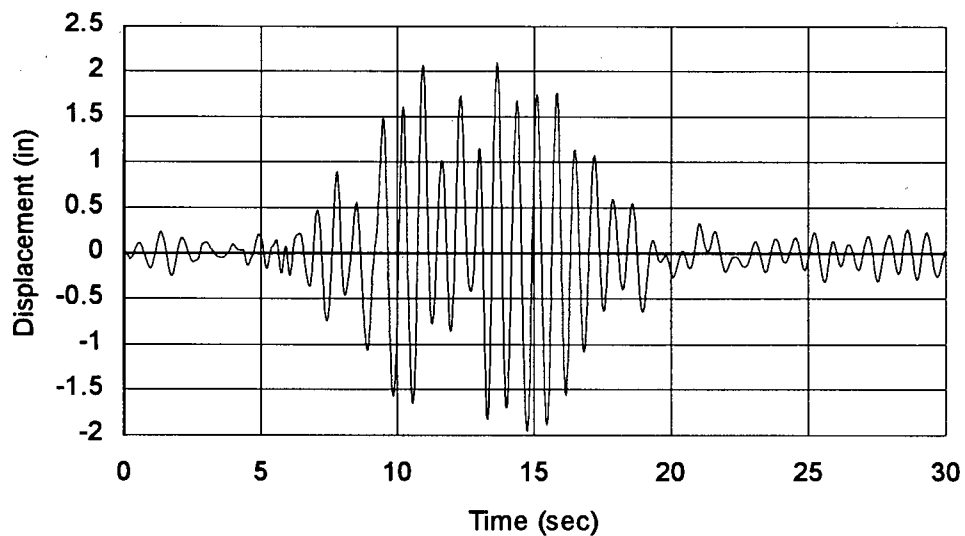


Fig. 4.5 Relative displacement history (Griffith Park Observatory record).

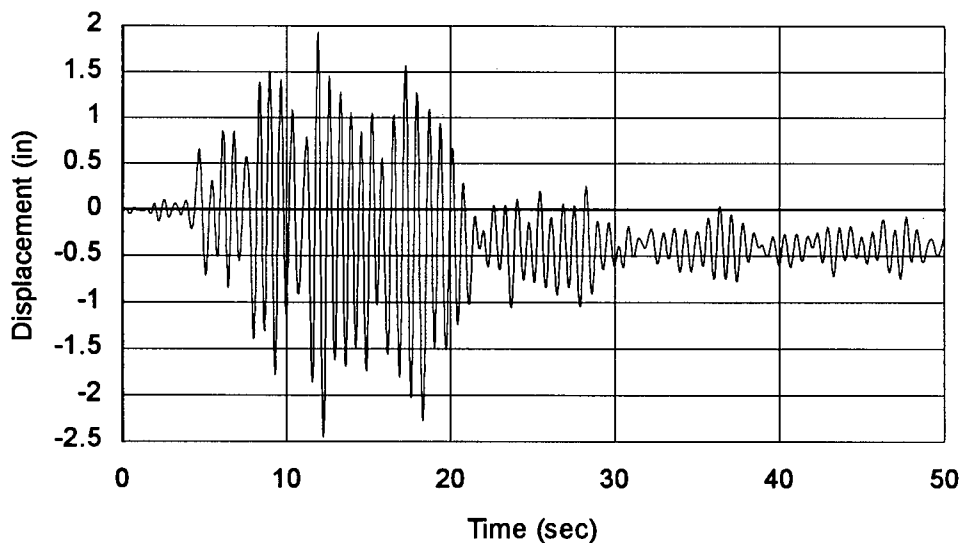
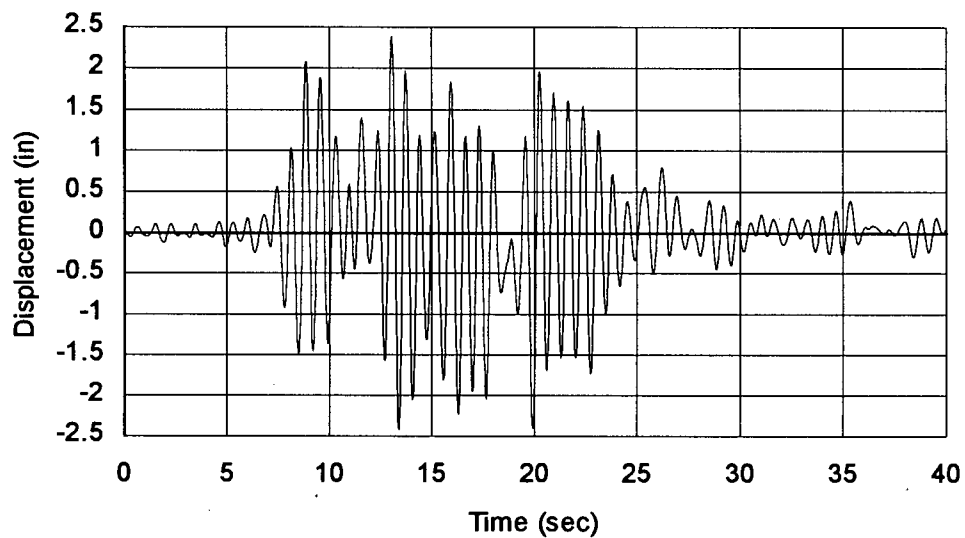


Fig. 4.6 Relative displacement history (3838 Lankershim Blvd. record).



**Fig. 4.7** Relative displacement history (234 Figueroa Street record).

The dynamic analysis of the prototype show that yielding occurs at various locations, but due to some strain hardening the computer model does not become unstable as soon as four hinges have developed and a mechanism has formed. The computer models survive the earthquake record to the end without collapsing.

The displacements of the spectral modal analysis are some what higher than the ones from the dynamic time history analyses. The response at and beyond the first natural period is the determining factor for the dynamic performance, and the spectra of the modified acceleration records are smaller than the design spectra in that range, which explains this discrepancy. Therefore it is recommended to use the displacements obtained from the spectral analysis for determining the displacement demands even though these are elastic responses.

## **CHAPTER 5**

### **PREDICTION OF THE MODEL SPECIMEN BEHAVIOUR**

#### **5.1 Introduction**

This chapter introduces the test model and an assessment of its behaviour. The choice of suitable scale is discussed, followed by a number of analyses in order to develop a basis for understanding the performance of the test specimen.

The elastic demands due to dead load and lateral load are determined in order to establish sectional forces. Flexural capacities are calculated using accepted analysis methods, with the aid of computer programs developed by CALTRANS. The effect of shear crack openings on flexural capacity is assessed, as it appears that this particular structure is rather vulnerable to this effect due to the many longitudinal bar cutoffs and low span/depth ratio. A push over analysis is performed with reduced flexural capacities induced by diagonal shear cracks. Sectional shear capacities are calculated using several design code expressions to establish the onset of shear failure. Shear combined with flexural behaviour is analyzed using the modified compression field theory. The anticipated response of the test specimen is governed by a not well understood moment shear interaction, which makes a conclusive prediction exceedingly difficult.

#### **5.2 The Test Model**

It is usually not feasible to do experiments at full scale. In this particular test a scale of 0.5 was initially selected as it results in dimensions suitable to the laboratory capabilities such as height of the available crane, and specimen weights that are manageable. Also, preliminary calculations showed that maximum loads at this scale were achievable with existing equipment. Due to height limitations of the testing facilities, the

model only represents the upper half of the columns with the cap beam. The inflection points of the prototype columns are assumed to be approximately at midheight and so the footings of the model are pinned at this location to allow rotation. The final scale factor chosen was 0.45 as this permits scaling of the prototype #11 bars to #5 bars in the model. The columns are 21.5" square and have a height to the underside of the cap beam of 81". The cap beam dimensions are 19" by 27" and the total length is 280". A drawing of the model by Klohn-Crippen is shown in Appendix A.

Loads are scaled so that stresses remain the same, thus they are scaled by the factor  $0.45^2$ . The superimposed dead load from the superstructure of the prototype is 900 kips, adding the self weight of the cap beam of 133 kips the total self weight is 1033 kips at the tops of the columns. The total dead load required to achieve the same stresses in the model columns is 209 kips. The self weight of the model cap beam and the testing frame setup is 14 kips. The additional dead load that must be applied through the dead load system is  $209 - 14 = 195$  kips. For each of the five dead load points 39 kips are required.

### 5.3 Elastic Demand Calculations

Figure 5.1 shows a diagram of a portion of the specimen, and identifies column regions, general beam regions, a haunch region, and a joint region. To account for cracking of the concrete the flexural stiffness were reduced to 30% of the gross moment of inertia ( $I_g$ ) for the cap beam general section and 25% of  $I_g$  for the column and the haunch section. The cross sectional properties are listed in Table 5.1.

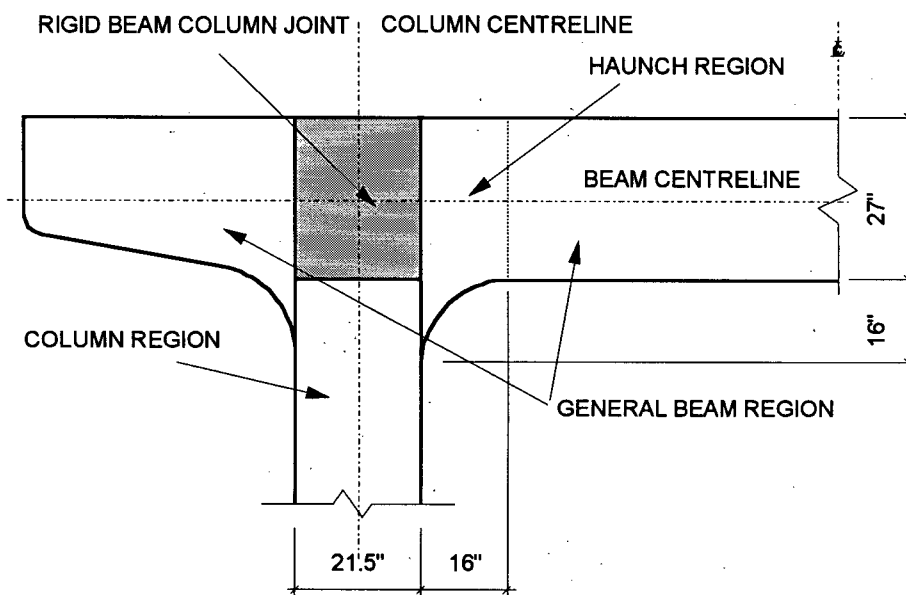


Fig. 5.1 Cap beam sections.

Table 5.1 Sectional properties.

<i>Section</i>	<i>Area (in<sup>2</sup>)</i>	<i>I<sub>e</sub> (in<sup>4</sup>)</i>	<i>% of I<sub>g</sub></i>
Cap beam - general	513	9,350	30
Cap beam - haunch	608	12,970	25
Column	462	4,450	25

The analytical model of the nodes and the elements is a scaled down version of the MS-V2 model in Chapter 3, depicted in Figure 5.2.

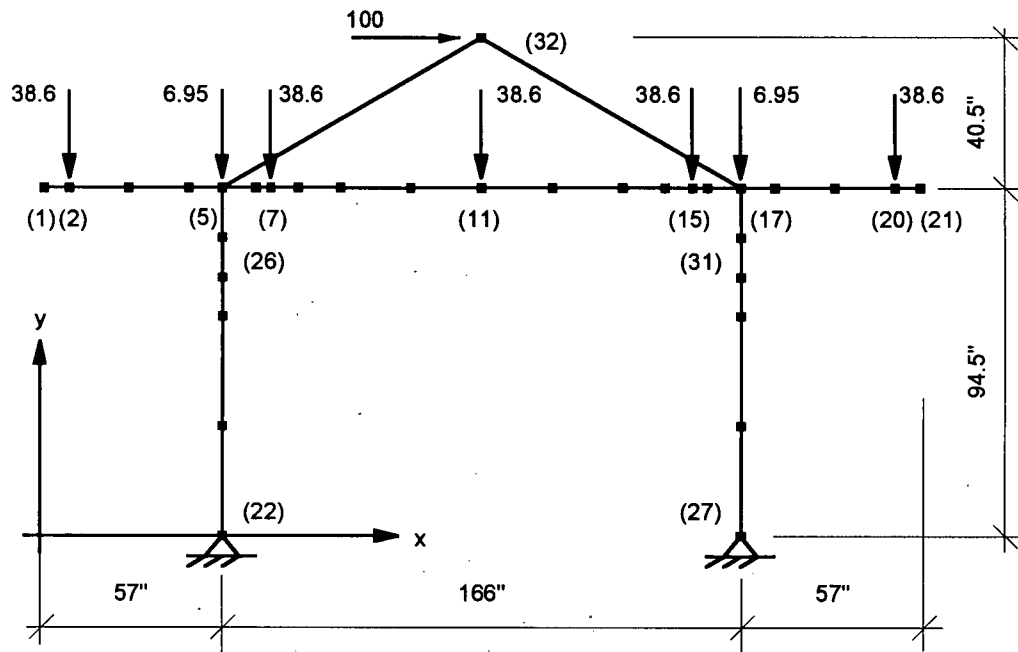
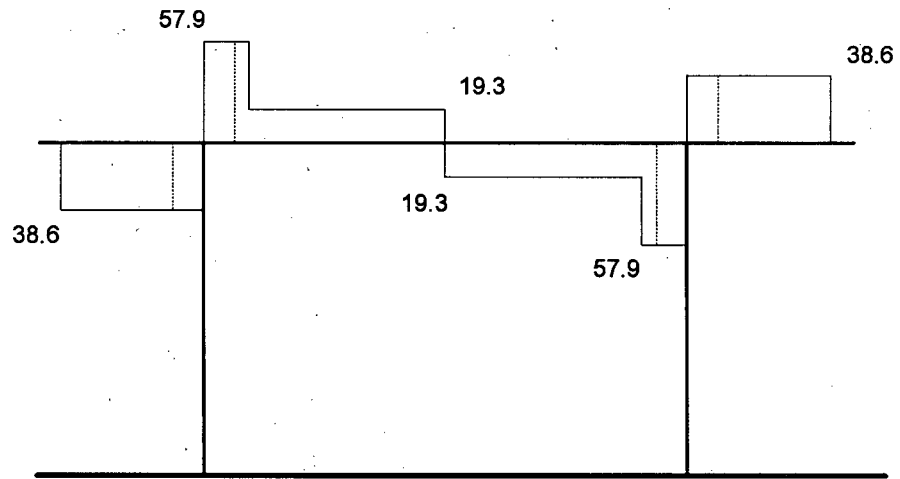


Fig. 5.2 Computer model for elastic demand calculations (forces in kips).

Table 5.2 Computer model node coordinates.

<i>Node</i>	<i>X - Coord</i>	<i>Y - Coord</i>	<i>Node</i>	<i>X - Coord</i>	<i>Y - Coord</i>
1	0.00	94.50	17	223.00	94.50
2	8.00	94.50	18	233.00	94.50
3	27.13	94.50	19	252.87	94.50
4	46.25	94.50	20	272.00	94.50
5	57.00	94.50	21	280.00	94.50
6	67.75	94.50	22	57.00	0.00
7	72.50	94.50	23	57.00	29.75
8	81.25	94.50	24	57.00	59.50
9	94.75	94.50	25	57.00	70.25
10	117.38	94.50	26	57.00	81.00
11	140.00	94.50	27	223.00	0.00
12	162.62	94.50	28	223.00	29.75
13	185.25	94.50	29	223.00	59.50
14	198.75	94.50	30	223.00	70.25
15	207.50	94.50	31	223.00	81.00
16	212.25	94.50	32	140.00	135.00

For purpose of elastic demand calculations, a loading consisting of the vertical dead loads and a lateral load of 100 kips was used. The results of an elastic analysis are shown in the Figures 5.3 to 5.6. The column shear forces and bending moments for the dead load are omitted since they are insignificant.



**Fig. 5.3** Shear force diagram for the dead load (forces in kips).

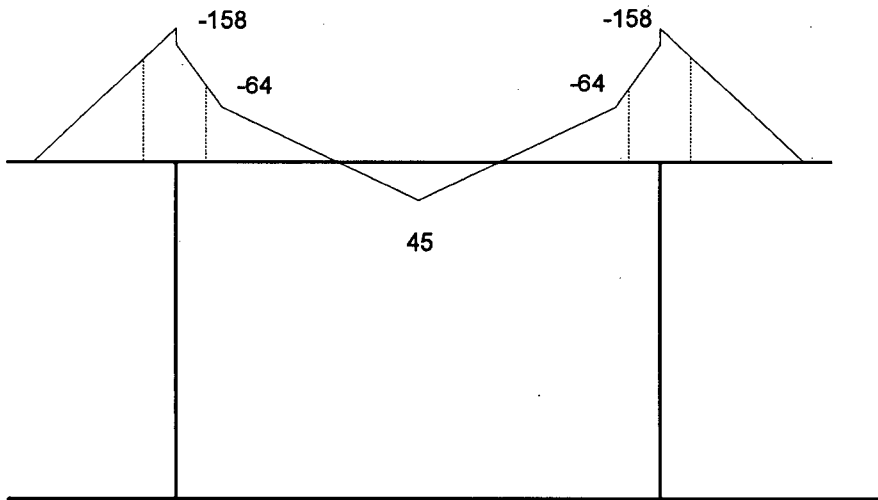


**Fig. 5.4** Bending moment diagram for dead load (moments in kip-ft).

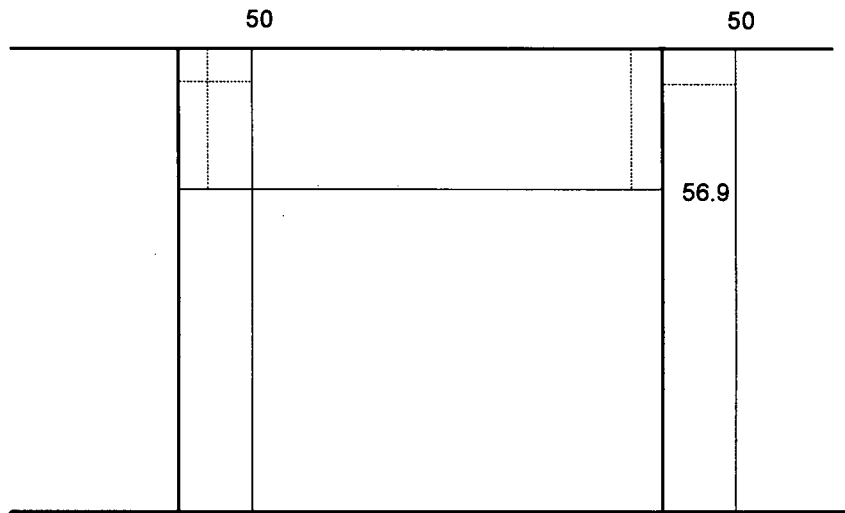


**Fig. 5.5** Shear force diagram for the lateral load of 100 kips (forces in kips).

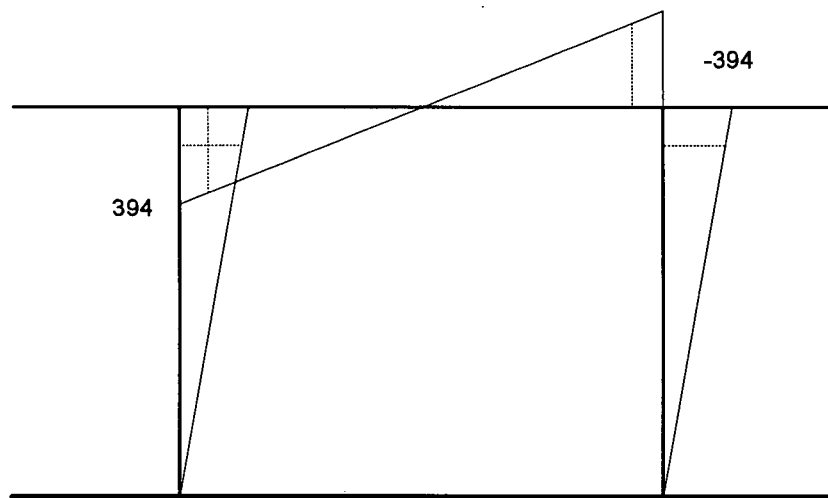


**Fig. 5.6** Bending moment diagram for a lateral load of 100 kips (moments in kip-ft).

From the geometry the shear demand in the mid portion of the cap beam for a given base shear  $V_{eq}$  is

$$V_b = 19.3 + V_{eq} \times \frac{56.9}{100} \quad (5.1)$$

and the shear in the column is

$$V_c = \frac{V_{eq}}{2} \quad (5.2)$$

#### 5.4 Flexural Analysis.

A sectional analysis was carried out using CALTRANS's programs BEAM303 and COL604R.

##### *a) Flexural Capacities of the Cap Beam:*

The longitudinal reinforcement in the cap beam curtails rapidly both at the top and bottom. The moment capacity is calculated for each section that has different reinforcement and assumed to hold up to a point where the cutoff bars are able to develop their yield strength. For #5 bars the development length is given by ACI 318-89 code as

$$\begin{aligned} l_d &= 0.042 \frac{f_y A_b}{\sqrt{f_c'}} \\ &= 8.40" \\ \text{or } l_d &= 0.00039 f_y d_b \\ &= 12.2" \end{aligned}$$

A theoretical difference between top and bottom bars is neglected here for simplification and thus the development length was taken as 12".

The results of the sectional analysis of the cap beam are listed in Table 5.3 for both positive and negative moment. The material properties were adapted from in situ tests of the existing bridge bent as mentioned in Chapter 3. The ultimate concrete strain was set to 0.005 as recommended by Paulay and Priestley (1992). The position given in Table 5.3 is the distance from the face of the column to the point where the bars are fully developed.

**Table 5.3.** Moment capacities of cap beam.

# top bars	# bot bars	top cover (in)	bot. cover (in)	+ $M_y$ (kip-ft)	position (+ $M$ ) (in)	- $M_y$ (kip-ft)	position (- $M$ ) (in)
11	4	2.08	1.0	163	1.25	391	12.25
9	6	1.90	1.0	237	31.75	344	20.25
7	7	1.63	1.0	275	42.25	279	27.25
6	9	1.63	1.28	340	46.25	237	37.25
4	11	1.63	1.43	395	60.25	160	47.25
2	13	1.63	1.92	439	66.25	88	60.25

For sections with little shear reinforcement, as soon as significant 45° shear cracks open, the negative moment capacity gets reduced to the moment capacity at a distance  $d$  (depth of the section) closer to the centre of the cap beam (see Fig 5.7). This moment capacity is shown in Fig 5.8 as the reduced moment capacity due to shear.

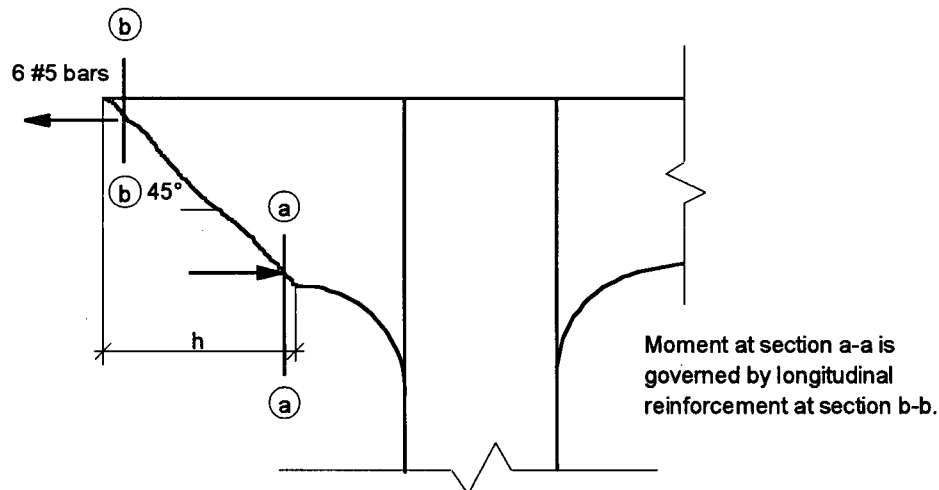


**Fig. 5.7** Bending moment reduction due to shear cracks for negative moment.

Fig 5.8 also shows the moment demand for a series of values of lateral load  $V_{eg}$ . Based on this figure, the cap beam should start to yield at a base shear a little less than 40 kips at about the quarter point of the cap beam due to the reduced moment capacity.

Somewhere above 40 kips of lateral load, enough shear cracks will develop to reduce the negative moment capacity. In positive bending, yielding would occur at about 70 kips lateral load.

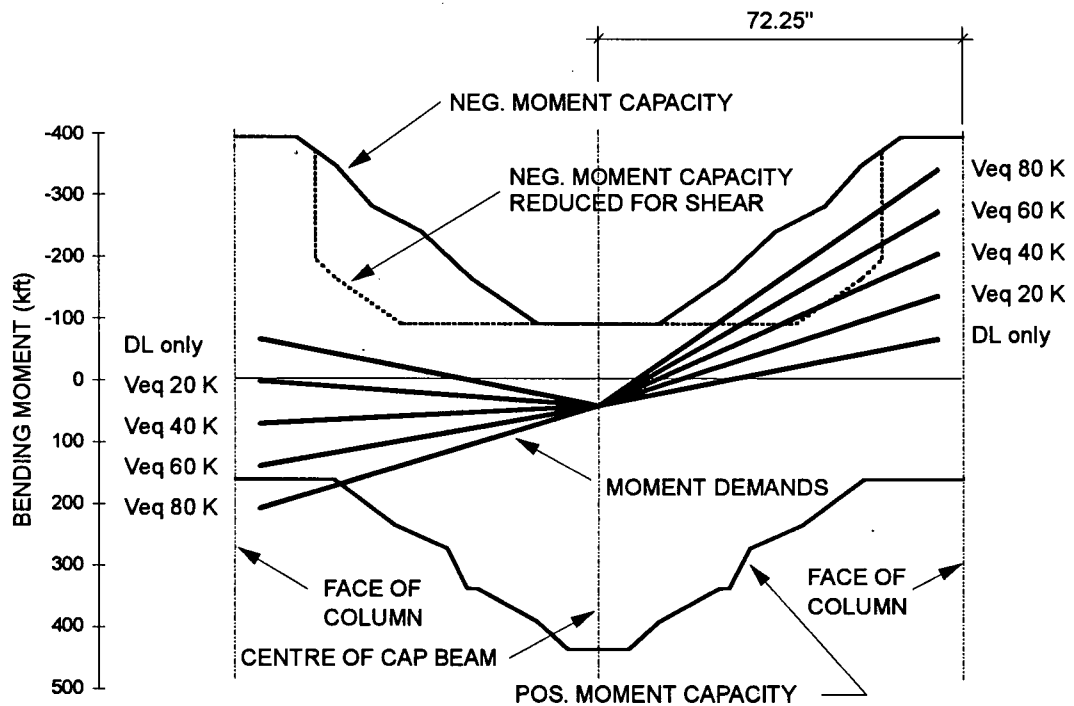


**Fig. 5.8** Flexural capacity/demand for the cap beam (push to the right).

***b) Flexural Capacity of the Column.***

The reinforcement remains the same over the height of the columns and so only one section had to be analyzed. Due to axial load effects, matching the capacity to the demand for the columns is an iterative process (see Table 5.4).

**Table 5.4** Column capacity iterations.

<i>V<sub>eq</sub></i> (kips)	<i>P</i> (kips)	<i>My-Capacity</i> (kip-ft)	<i>My-Demand</i> (kip-ft)	$\Delta$ (kip-ft)
0	103.5	284	16	+268
100	184.8	338	353	-15
95	180.7	335	338	-3
96.5	182.0	336	342	-6
94.5	180.2	335	335	0

The critical base shear for the columns in flexure is 94.5 kips. By comparison, in Section 5.4 (a) it was seen that for purely flexural behavior, the critical region was the cap beam, where yielding would occur at an approximate base shear of 40 kips.

#### 5.5. Push Over Analysis of the Test Model.

DRAIN-2DX was used to do a push over analysis of the model. The computer model is identical to the simple models used before. The negative moment yield values are the reduced yield moments at a distance  $d$  (depth of section) from the haunch towards the centre of the cap beam to account for a reduction in moment capacity due to shear cracking (see Table 5.5).

**Table 5.5** DRAIN-2DX cross sectional parameters for the test model.

<i>Parameters</i>	<i>Cap Beam - general</i>	<i>Cap Beam - haunch</i>	<i>Column</i>
E (ksi)	4650	4650	4650
A (in <sup>2</sup> )	513	608	462.5
I <sub>e</sub> (in <sup>4</sup> )	9350	12970	4450
P <sub>c</sub> (kips)	-	-	2580
P <sub>b</sub> (kips)	-	-	310
M <sub>b</sub> (kip-in)	-	-	5088
+M <sub>y</sub> (kip-in)	1870	1800	2665
-M <sub>y</sub> (kip-in)	2750	5500	2665
P <sub>t</sub> (kips)	-	-	248

The load deflection results of the pushover analysis are plotted in Fig. 5.9.

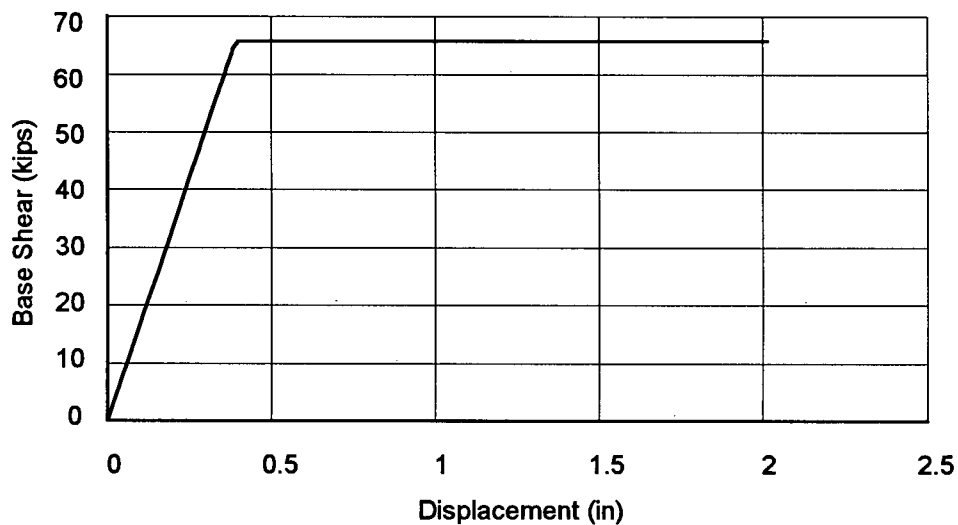


**Fig. 5.9** Push over analysis results.

The two hinges to form a mechanism in the bridge bent develop in close sequence of increasing base shears. The first hinge occurs at the right hand side of the cap beam in the region of the maximum negative moment, assuming the lateral load is applied from the left to the right. The second hinge presents itself at the left hand side in the region of maximum positive moment. An ultimate base shear of around 65 kips can be sustained by this model of the bridge bent in flexural manner. The push over analysis assumes that the critical section is just at the face of the column, but as can be seen in Fig 5.8 the critical section is closer to the quarter point of the cap beam, which has a lower sectional moment capacity than the one at the face of the column. This explains the higher ultimate base shear for the push over analysis. The aspect of shear is explored in the following section.

### 5.6 Shear Capacity.

The sectional shear capacity was computed using the ACI 318 and the ACI/ASCE shear formulae. Since the axial load of the column depends on the lateral load, which in turn determines the shear in the column, some iterations are required to find the shear capacity and the corresponding axial load; assuming the load is governed by shear.

a) ACI 318-89 : (imperial units).

$$V_n = V_s + V_c \quad (5.3)$$

$$V_s = \frac{A_v f_y d}{s} \quad (5.4)$$

$$V_c = 2 \left[ 1 + \frac{N_u}{2000 A_g} \right] \sqrt{f'_c} b_w d \quad (5.5)$$

b) ACI/ASCE : (imperial units)

$$V_r = V_s + V_c + V_p \quad (5.6)$$

$$V_s = \frac{A_v f_y d}{s} \quad (5.7)$$

$$V_c = (0.85 + 120 \rho_w) \sqrt{f'_c} b_w d \quad (5.8)$$

$$V_p = 0.2P \quad (5.9)$$

The shear calculations were done for a *typical* cap beam and a column section. The parameters are listed in Table 5.6.

**Table 5.6** Cross sectional parameters.

<i>Parameter</i>	<i>Cap Beam</i>	<i>Column</i>
Gross area $A_g$ (in <sup>2</sup> )	513	462.25
Effective height $d$ (in)	23	17.2
Width $b_w$ (in)	19	21.5
Concrete strength $f'_c$ (psi)	6000	6000
Reinforcement yield strength $f_y$ (psi)	50,000	50,000
Shear reinforcement $A_v$ (in <sup>2</sup> )	0.08	0.051
Tie spacing $s$ (in)	16	5.375
Reinforcement ratio $\rho_w$	0.00363	0.0537
Axial load $P, N_u$ (lb.)	0	varies

The two codes yielded quite different results. The ACI/ASCE approach results in a lower base shear failure load as indicated in Table 5.7.  $V_n$  is the sectional shear capacity of various sections. To normalize the results the corresponding base shears  $V_{eq}$  were calculated.

**Table 5.7** Shear capacities.

<i>Section</i>	<i>Code</i>	$V_n$	$V_{eq}$
Cap Beam	ACI 318	73.5	95.3
	ACI/ASCE	49.3	52.7
Column	ACI 318	65.3	130.6
	ACI/ASCE	54.1	108.2

It should be noted that all code shear formulae assume a minimum amount of shear reinforcement at a minimum stirrup spacing of  $d/2$ , in this case 13.5 in. The provided stirrup spacing in the middle of the cap beam is 16 in. The minimum shear reinforcement for the cap beam section at that spacing should be  $0.31 \text{ in}^2$ . The transverse reinforcement provided is  $0.08 \text{ in}^2$ . Very little research has been conducted with lightly reinforced concrete members subjected to large shears (see Pessiki et al. (1990)).

To find some bounds on the capacity of the bent the ACI/ASCE approach was chosen. In this approach the shear capacity is dependent on the amount of tension steel in the section, which accounts for the contribution of the longitudinal steel towards the shear capacity of the section. The shear capacity is then dependent on how much of the tension steel has been mobilized to withstand the negative bending of the cap beam. An increase in lateral load increases the negative moment near the centre of the beam. At exact centre,  $M_{neg}$  is zero due to lateral load. Since the negative steel curtails towards the centre of the beam, fewer and fewer bars are available to resist the longitudinal demand from the shear. Therefore the shear capacity diminishes towards the middle of the cap beam. The code formula (e.g. 5.5) is conservative in this region due to low bending moments. At a fairly low base shear of 35 kips the shear capacity exceeds the demand close to the centre of the cap beam as shown in Fig 5.10. Since Table 5.7 and Fig. 5.10 are based on the ACI/ASCE code approach the significance of the longitudinal reinforcement on the shear capacity becomes apparent.

For the columns there is no cutoff of the reinforcement. The shear capacity is to some extent dependent on the axial load, which in the ACI/ASCE formula is accounted for in the  $V_p$  term of equation (5.9). Some iterations are required to obtain the critical base shear corresponding to the minimum shear capacity. For any of the code approaches, shear in the columns is not predicted to be the critical failure mode.

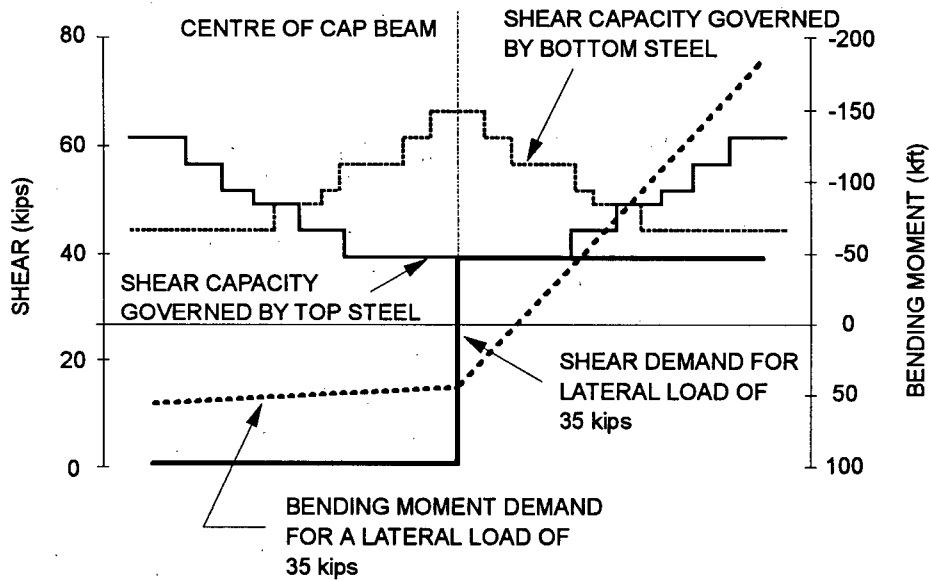


**Fig. 5.10** Shear analysis for the cap beam at a lateral load of 35 kips.

The shear formulae used by these codes are conservative in their estimation of the shear capacities. Usually the highest shear occurs near supports. For simple supported beams there is virtually no bending moment at the supports, whereas for continuous beams the highest moments occur near the supports. The ACI/ASCE code formula takes this into account to make the shear capacity dependent on the amount of longitudinal steel, which usually corresponds to the bending moment demand in the region.

### 5.7 Modified Compression Field Theory.

Here the capacities of the cap beam are analyzed based on the modified compression field theory similar to Chapter 3 using the program RESPONSE. Three sections with different steel areas were chosen for the sectional analysis. The locations of these sections are at the points of the full development of the top reinforcement and are shown in Fig. 5.11.

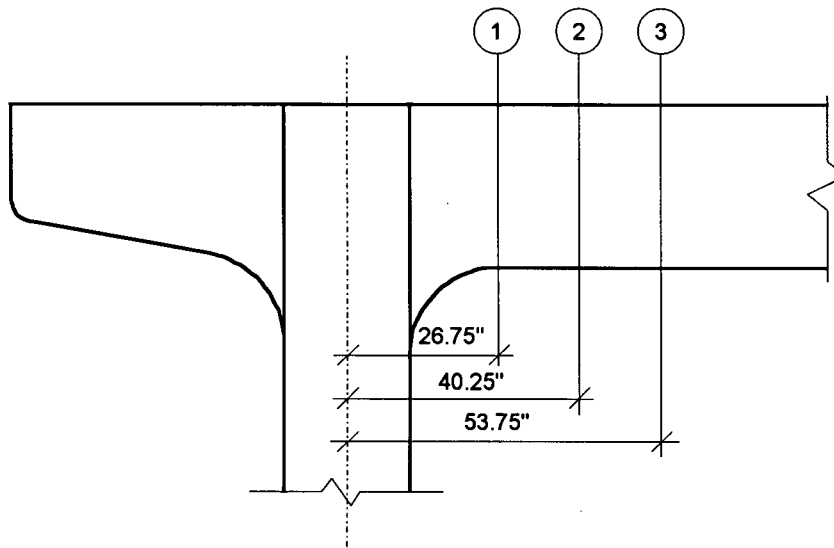


**Fig. 5.11** Sections for the RESPONSE analysis.

The reinforcement of the individual sections is listed in Table 5.8.

**Table 5.8** Reinforcement in the analysis sections.

<i>Section</i>	<i>No. of Top Bars</i>	<i>No. of Bottom Bars</i>	$A_v$ ( <i>in</i> <sup>2</sup> )	<i>s</i> ( <i>in</i> )
1	9	4	0.19	7.4
2	6	4	0.13	13.5
3	4	7	0.08	16

From the elastic force demand calculation earlier in the chapter the moment/shear ratios were determined and are used here to analyze the interaction between shear and flexure (see Table 5.9), similar to Chapter 3.

**Table 5.9** Elastic demand constants and ratios.

<i>Cap Beam Section</i>	<i>No</i>	<i>dN/dV</i>	<i>Mo</i>	<i>dM/dV</i>	<i>Vo</i>	<i>dVo/dV</i>
LEFT 1	2.4	0.0	44.6	+4.69	33.9	1.76
LEFT 2	2.4	0.0	44.5	+3.56	33.9	1.76
LEFT 3	2.4	0.0	44.5	+2.44	33.9	1.76
RIGHT 1	2.4	0.0	44.6	-4.69	-33.9	1.76
RIGHT 2	2.4	0.0	44.5	-3.56	-33.9	1.76
RIGHT 3	2.4	0.0	44.5	-2.44	-33.9	1.76

The RESPONSE results are listed in Table 5.10.

**Table 5.10** RESPONSE results.

<i>Cap Beam Section</i>	<i>Ve<sub>q</sub></i> <i>kips</i>	<i>M</i> <i>kip-ft</i>	<i>V</i> <i>kips</i>	<i>N</i> <i>kips</i>
LEFT 1	81.1	170.2	26.8	2.2
LEFT 2	91.8	161.8	32.9	2.4
LEFT 3	141.6	193.7	61.2	2.4
RIGHT 1	80.3	-259.8	64.9	2.3
RIGHT 2	71.9	-169.4	60.1	2.4
RIGHT 3	69.2	-98.4	58.6	2.9

The critical base shear of 69.2 kips is governed by the RIGHT 3 section and is significantly higher than the 35 kips obtained from the ACI/ASCE approach and the 40 kips obtained by the modified sectional capacity analysis also at the quarter point of the cap beam. The negative flexural capacity of 98 kip-ft for the RESPONSE analysis is only slightly higher than the critical moment capacity of 88 kip-ft from the CALTRANS's program BEAM303. RESPONSE however gives an ultimate force state at which the section fails, whereas BEAM303 provides an idealized yielding response.

It is difficult to estimate to what degree the bending moment capacity is reduced due to shear. Some of the shear is resisted by the longitudinal steel, partly as a tension tie in the traditional shear truss model, and partly as a simple dowel action. A rather crude estimate of the onset of nonlinear behavior is 40 Kips of base shear and the maximum expected base shear is about 70 kips. Nevertheless considering all the uncertainties the testing program is very much justified.

## **CHAPTER 6**

### **TEST SETUP**

#### **6.1 Introduction**

The test set up was specifically designed to carry out the experiment on the Oak Street Bridge Bent Test at the UBC Structures Laboratories. The scale of 45% and the outside expected performance envelopes were established by Klohn-Cripppen. The fabrication of the specimens was tendered out to a local contractor and was done off-site. The contractor had to meet some stringent material specifications to ensure reasonable representation of the existing structure. The test frame was designed as part of this thesis and was contracted out to a local steel fabricator. The data acquisition system relies upon the available system in the structures labs at UBC.

#### **6.2 Material Properties of the Test Specimen**

The contractor was given a window for the concrete strengths of 4.8 to 5.5 ksi. Obtaining reinforcement steel at a yield strength of 50 ksi was more difficult. The contractor had to get the main reinforcing steel in the United States. The ties and stirrups are standard wire sizes and could be procured in Canada. The wires had to be annealed to reach the required yield strengths. This proved to be more complicated than anticipated, since the original yield strengths of the material and the consequent cold working was not exactly known. Some experimenting was required. However in one of the batches the yield strength was very close to the desired values.

### 6.3 The Loading Frame

The test setup, shown in Fig 6.1, was designed specifically to test the specimens representing a typical two column bent of the Oak Street Bridge at a scale of 0.45. Klohn-Crippen set the maximum lateral design load to 150 kips and the maximum displacement to  $\pm 3$ " for all the specimens, including the retrofitted ones. A hydraulic jack with a stroke of 12" and a capacity of 225 kips was available. The reaction frame was designed for the full jack capacity; the remainder of the test setup was designed for the 150 kips. Since the test program is particularly interested in the cap beam and the beam column joint response, an important concern was the lateral load application into the cap beam. A triangular load truss was devised to introduce the lateral loads. The vertical dead loads were introduced at five bearing points. Since the bearings at the footings simulated the inflection points of the columns, they had to provide freedom of rotation, but withstand uplift.

#### 6.3.1 Reaction Frame.

The reaction frame system consists of two A-frames connected at the top by a spreader beam onto which the actuator is attached. Some lateral bracing perpendicular to the main axis of the test setup provides lateral stability and enough strength to temporarily brace the specimen for erection. Both supports and the reaction frame are tied together at the floor level; the A frames are therefore self equilibrating for the lateral loads, but rely on the strong floor for vertical reactions to resist overturning.

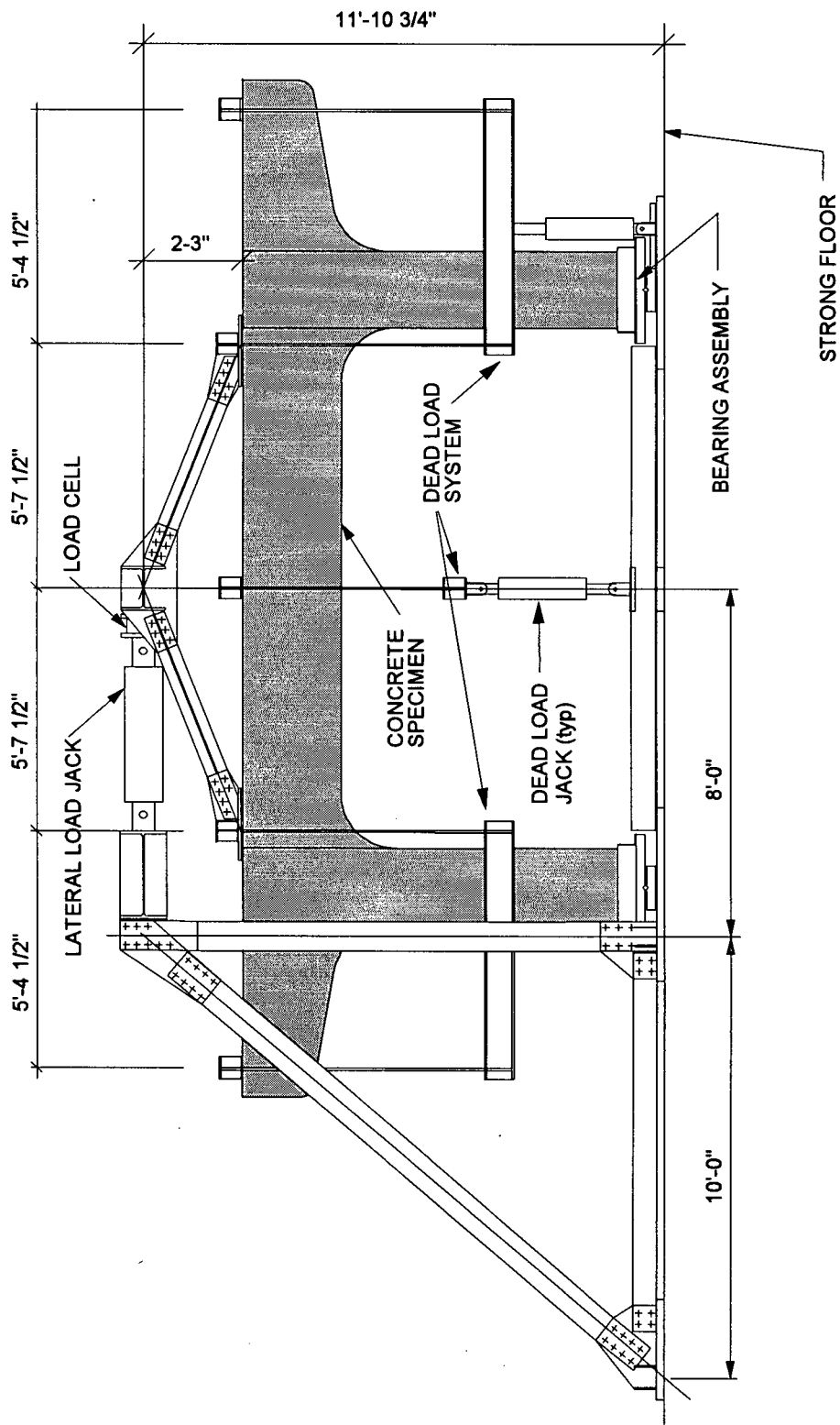


Fig. 6.1 Test setup.

### 6.3.2 Dead Load System.

The vertical dead load was applied at all five superstructure bearing points. The outer two loads on both ends of the specimen were applied using a spreader beam system on each side of the specimen and the center load was applied by a single actuator. All jacks were fed in series through one hydraulic loop and the pressure was controlled with one manual hydraulic reducing valve. To attain the required load of 39 kips, the hydraulic pressure in the jacks was set at 2412 psi.

### 6.3.3 Load Distribution System

The consultants on the project assumed that only the two first interior supports of the bridge bent closest to the columns will transfer the lateral load of the bridge deck into the bent. For this reason, a triangular truss was chosen to carry actuator lateral load to the test specimen. Since some concrete dilation was expected, the load application system was designed as a determinate triangular truss. The connections of the truss elements were not pinned, but the flexibility of the members was assumed sufficient to allow for expansion of the cap beam. Oversized holes in the gusset plates make it possible to readjust the position of the truss after several load cycles. The truss was designed to withstand the maximum expected lateral load of 150 kips.

### 6.3.4 Bearing Assembly.

The supports of columns were to simulate inflection points and therefore allow for rotational freedom, but restrain vertical and horizontal movement. Since the system is statically determinate vertically, only the horizontal reactions had to be measured. Refer to Figure 6.2 for the details of the bearing assembly. The whole bearing assembly rested on a lubricated Teflon pad, which allowed for horizontal movement, but the assembly was held in place by a thick reaction plate, which was strain gauged. It was essentially a load cell. The friction load on the Teflon pads increases with an increase of vertical load.

Before the first test, some calibration runs were conducted to find the correlation. The friction on the Teflon pads was very sensitive to the vertical load and it was unfortunately not very linear. At the time of the calibration, only the dead load was available to impose some vertical load; therefore the bearings could be calibrated for only a small range of vertical loads.

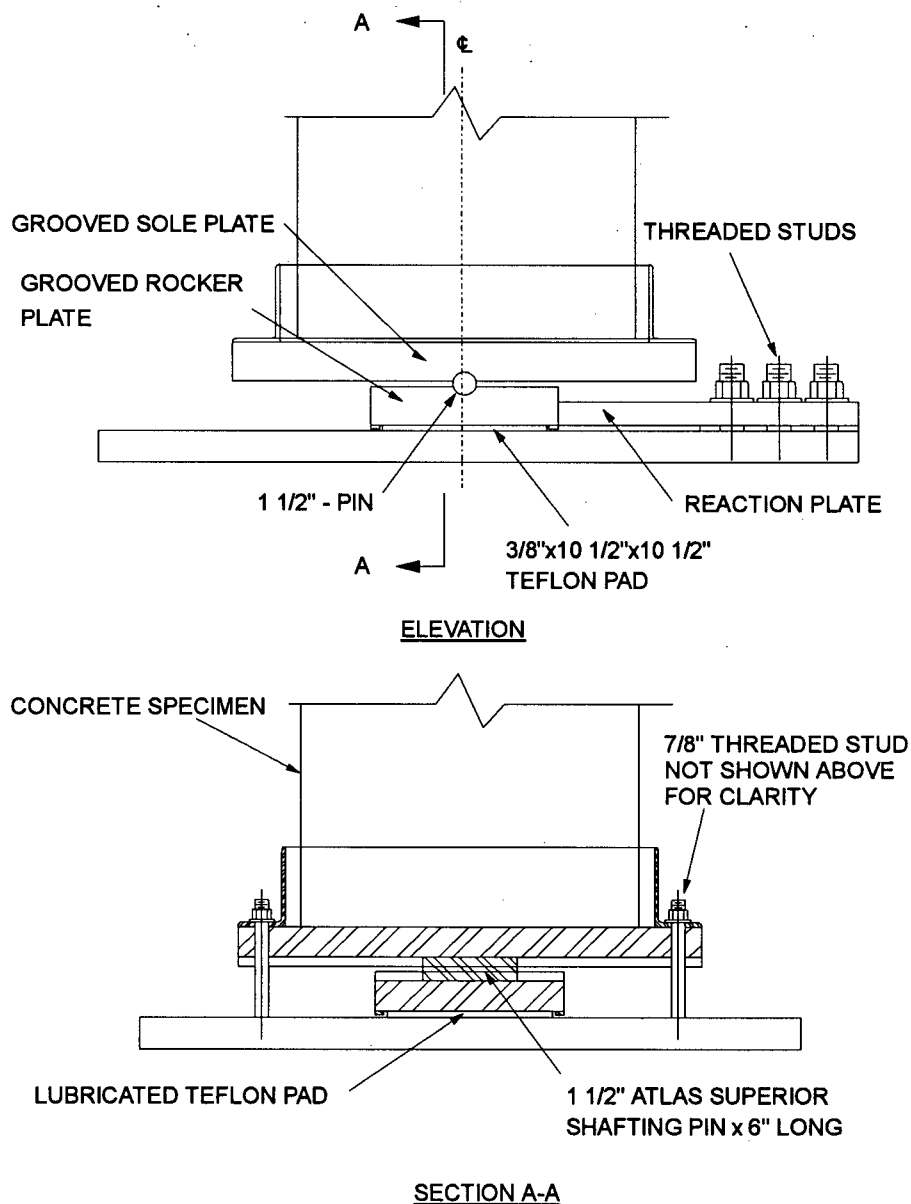


**Fig. 6.2** Bearing assembly.

## **6.4 Data Acquisition**

The data acquisition system collects and measures the signals from physical sensors mounted on the specimen. The signals are conditioned, converted from analog to digital, and then stored.

### **6.4.1 Data Acquisition System Components**

Physically the system consists of five main components, a personal computer with a large hard drive, software, a signal conditioning unit including an analog to digital converter, a data acquisition board, and a large number of transducers and strain gauges, which are the actual sensors.

The personal computer controls the data acquisition board driven by the software and stores the data as a ASCII file on the hard drive. In this experimental setup the computer has a 486DX 66 MHz CPU and local buses with a 210 MB hard disk.

The software is a commercial data acquisition software, LabVIEW (Laboratory Virtual Instrumentation Workbench). This program allows the user to customize his/her requirements by using virtual instruments. Instead of a written program code the program is discretized in fundamental tasks and put together with icons symbolizing the virtual instruments to one data acquisition program.

The data acquisition board is mounted in the personal computer and is a multifunctional I/O board (AT-M10-16X) with an analog to digital converter and timing I/O functions.

The signal conditioning unit converts and feeds the collected signals from the various data acquisition devices as an analog signal to the data acquisition board. The basic conversion in signal conditioning is amplification and filtering of the signal. The

system used here is called SCXI (Signal Conditioning eXtensions for Instrumentation) and is a high performance, multi channel system for the PC-based data acquisition board.

The transducers of the physical data acquisition devices sense any applicable physical stimulus. In this particular case there were about seventy strain gauges which were mounted to the reinforcing steel, about ten displacement transducers, and three load cells.

#### 6.4.2 External Instrumentation

Six LVDT's (Linear Variable Differential Transducers) and four LMP's (Linear Motion Potentiometers) were used to measure external displacements of the specimen during the test.

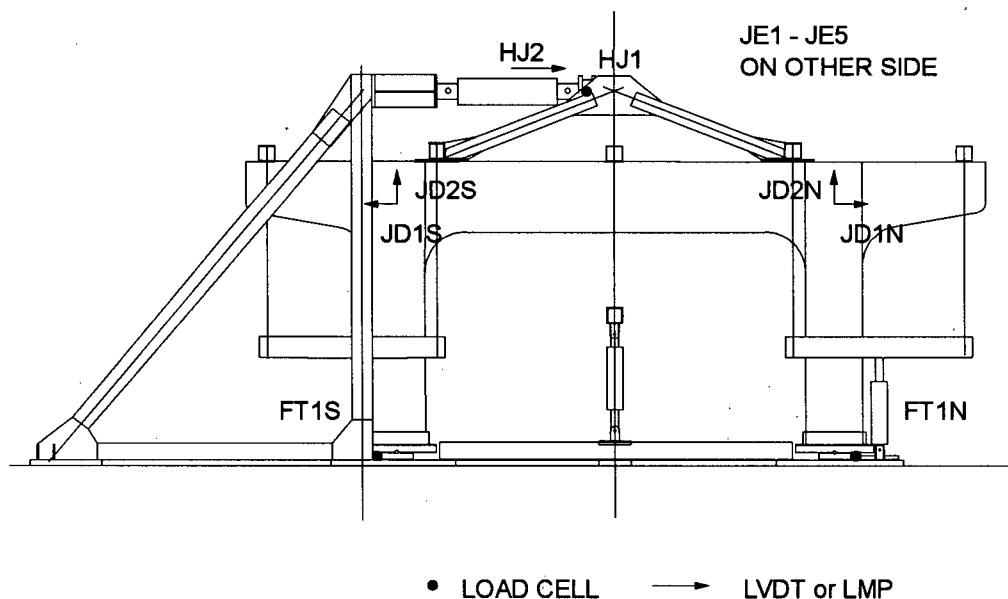


**Fig. 6.3** External instrumentation locations.

The location of the LVDT's and LMP's is depicted in Fig 6.3. Four LMP's are located at the center of the joints to measure the vertical and horizontal displacement of the two joints. An LVDT was mounted to the jack and used in the loading system to control the jack movements during displacement control. Five LVDT's were placed at the north joint to read joint distortions.

A load cell was placed between the jack and the loading truss to measure the load applied by the horizontal jack and was used for the actuator control under load control. For the first test this load cell did not function. Two pressure transducers were placed into the hydraulic system of the loading jack. Unfortunately this system did not compensate for the friction in the jack, which had to be removed at a later stage from the recorded data.

Since the system was statically determinate vertically but indeterminate horizontally it was desirable to measure the shear in the columns by measuring the horizontal reactions through the instrumented bearings. Unfortunately the signals from these strain gauges turned out to be very noisy.

#### 6.4.3 Internal Instrumentation

About seventy strain gauges were mounted on reinforcing steel throughout the specimen as depicted on Klohn-Crippen drawing Q117-SK2 (see Appendix A).

In addition, six strain gauges were placed on two aluminum strips as shown on Fig. 6.4. These aluminum strips measure internal deformations in the joint and provided a correlation with the measured external joint distortions, and were installed as shown in Fig. 6.5 in an attempt to determine joint cracking stresses, and draw conclusions on external crack patterns.

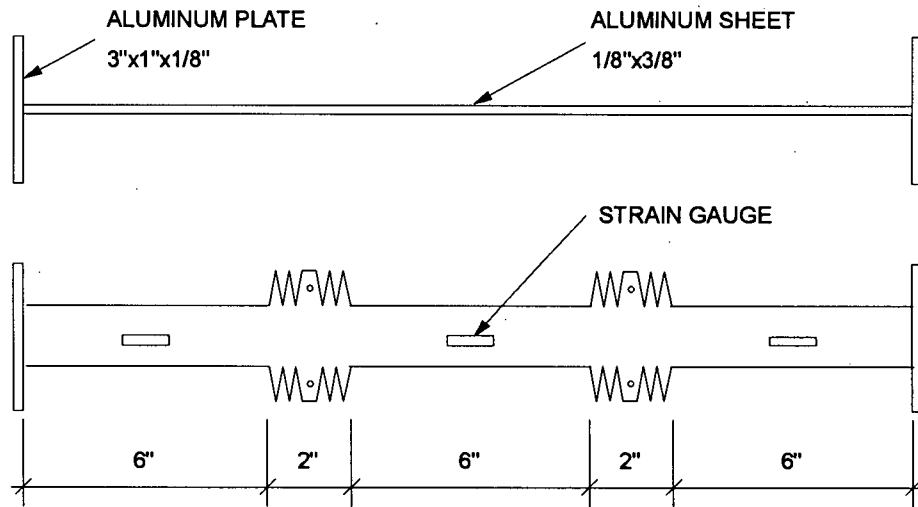


**Fig. 6.4** Internal deformation measurement.

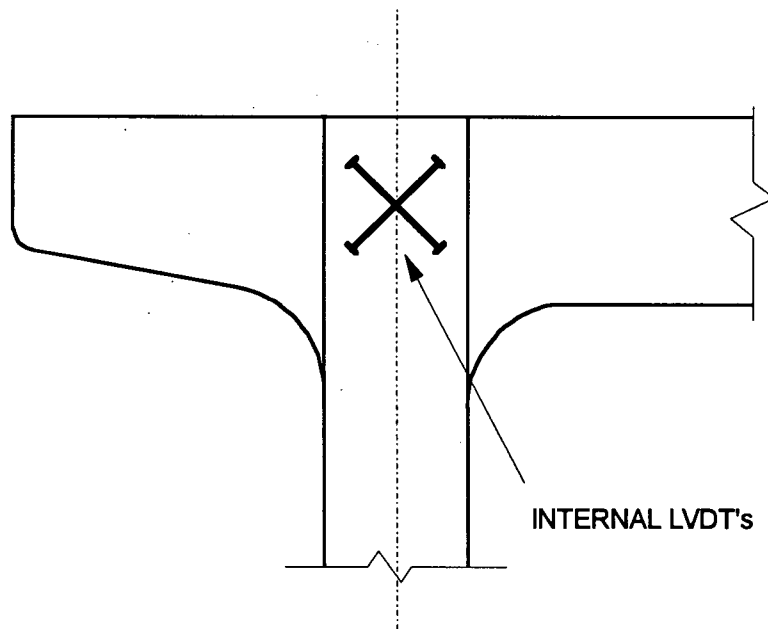


**Fig. 6.5** Arrangement of internal gauges.

## 6.5 Data Processing

The data acquisition program was recently purchased by the Department of Civil Engineering at the University of British Columbia. At this time the collection of about 90 data channels is possible. The output is a simple ASCII file with all the channels readings in separate columns. The readings are all voltages between -10 Volts and +10 Volts. The standard 60 Hz analog filter, which filters the noise from the power supplies, caused a tracking problem; i.e. certain channels would overshadow adjacent channels, and therefore the filter could not be used. This resulted in considerable noise in the records.

Because of the large amount of data a FORTRAN program called DP (*Data Processing*) was written by the author to filter the original data and to reduce the amount of data by eliminating close data points (see Appendix C). The filtering routines were adapted from Press et al. (1989). The program first reads the raw data into a large array, each channel in a separate column, which is then run through a smoothing subroutine channel by channel. The subroutine initially removes any linear trend in the data. Then it uses a Fast Fourier Transform to low-pass filter the data, and the linear trend is reinserted at the end. The user specifies a smoothing constant, which specifies the number of points over which the data is smoothed. After some experimenting, the smoothing constant was set to 15, which gives, in the opinion of the author, a reasonable fit. After the data is smoothed the voltage readings are converted to physical units, i.e. strains, displacements, and forces. Finally the data is reduced by deleting data points that lie close together. For this routine up to 20 control channels with associated different limits for the tolerance can be chosen. The result is then stored as an ASCII file. Fig. 6.6 demonstrates the effects of the filtering processes; the noisy raw data is converted to smooth filtered data.

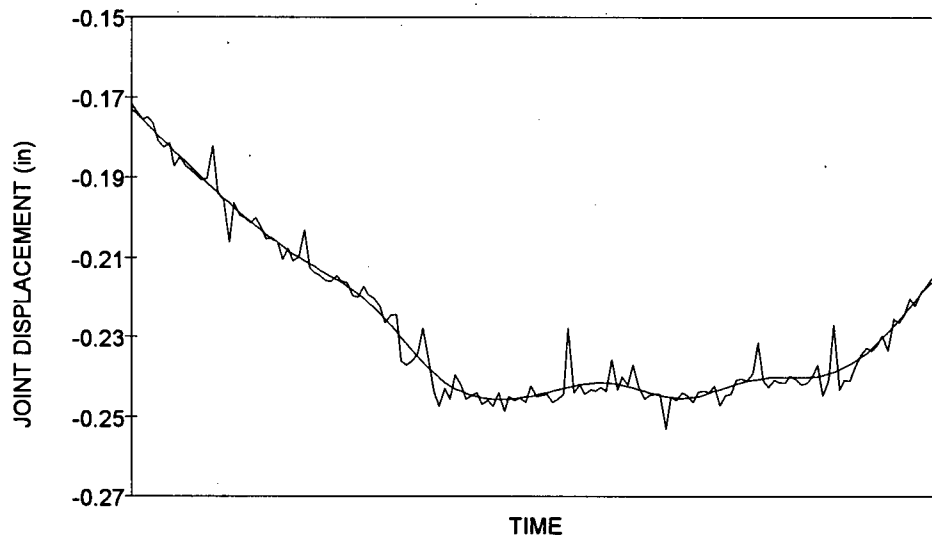


**Fig. 6.6** Filtering on a sample of data.

### **6.6 Load Application (Load History)**

The testing procedure was in essence to load the test specimen to sequences of three cycles of lateral load or displacement at increasing predetermined levels until the specimen failed. The separate steps of the conduct of the test are discussed in more detail in Chapter 7.

For this first test the load cell, which was used to control the actuator under load control, was not functional and the entire test had to be done under displacement control. The LVDT used for displacement control was on the loading jack and so the elastic deflection of the frame had to be taken into consideration in calculating the specimen displacement required for the various loading stages.

The general philosophy was to have a few load sequences in the elastic range in order to calibrate the system and establish the reliability of the data acquisition system, before proceeding to the first yield level. Usually one can estimate the yield forces quite easily, but yield displacements are more difficult to predict, due to the uncertainties of the

actual stiffness degradation caused by the cracking of the concrete. A common approach is to load to 75% of the estimated yield load under load control, measure the displacement, and extrapolate this to the yield displacement (see Fig. 6.7). The remainder of the testing is conducted under displacement control with sequences at multiples of the yield displacement leading to a history of displacement ductility levels.

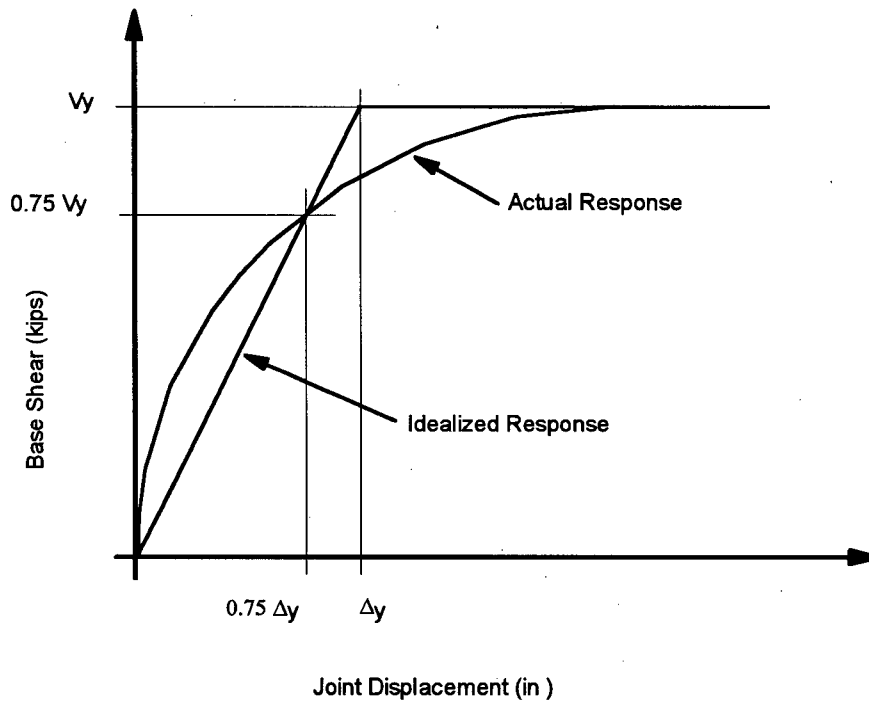


**Fig. 6.7** General test responses.

Table 6.1 shows the target loading history of the first test. A more detailed account of the actual test loads and displacements are given in Chapter 7. One should note that since the first test was conducted entirely under displacement control, only a very crude estimate of the 75% of yield could be made and consequently an exact yield point was not clearly established.

**Table 6.1** Target loading sequence for the first test.

<i>SEQ</i>	<i><math>\Delta</math> (in)</i>	<i>Comments</i>
C	0.04	
D	0.08	
E	0.12	40 kips
F	0.20	50 kips
G	0.25	65 kips 1.0 $\Delta y$
H	0.45	1.5 $\Delta y$
I	0.65	2.0 $\Delta y$
J	0.90	3.0 $\Delta y$
K	1.25	4.0 $\Delta y$

## CHAPTER 7

### INTERPRETATION OF TEST RESULTS

#### 7.1 Introduction

The discussion is restricted to the first test of the series, the as-built model of Oak Street Bridge Bent S28. Some of the data acquisition devices responded quite well, notably the LVDTs (Linear Variable Displacement Transducer) and the LMPs (Linear Motion Potentiometer) on the joints and the actuator, as well as the pressure transducers in the hydraulic system of the lateral load actuator. Most of the other devices however gave fairly noisy responses. The LVDTs arranged at the joint at the North end registered very little joint distortions. The two internal LVDTs placed in the same joint also showed very small signatures. Also, no visual cracks were observed at the joints, which indicates that the beam/column joints did not undergo any significant deformations. The column shear load cell readings were noisy but a trend could be detected. Most of the strain gauges mounted on the reinforcement gave recordings throughout the test; only a very few did not function from the start.

The detailed observations of the test are listed in Table 7.1, which references a few photographs taken during the test. The load deflection curves were developed as a primary record of the response of the test specimen. To ascertain the working condition of the strain gauges a closer examination was made of the strain gauges on the top of the cap beam. The measured maximum strains for a particular sequence in the elastic range at various locations along the cap beam were compared to the analytical values at the same base shear. Finally an explanation of the failure of the specimen is attempted.

## 7.2 Event Table

The test was broken up into sequences denoted by ascending letters as described in Table 7.1. Each sequence represents two to three cycles at one load level. Cycle A pushes to the North (right) and cycle B pulls to the South (left). At the beginning of all the sequences, all the load control devices were balanced and zeroed, i.e. the load cell, the pressure transducers and the LVDT on the lateral jack. The scan rate for the data acquisition system was set to 2 scans per second. When first switched on, about 50 scans of the whole system were recorded and the dead load was slowly applied. Another 50 scans are taken with only the dead load in place before the lateral load is applied. The load was manipulated by a load controller which in turn controls a servo valve in the hydraulic loop of the lateral load actuator. The load application follows a preset loading function generated by a separate unit. Usually a sinusoidal wave form is used so that the load application slows down at its peaks allowing observation of the specimen at the critical instances. The load was held at the peak of each cycle to mark the cracks on the specimen with felt pens and to take pictures. The data acquisition system was turned off at the end of each sequence and a preliminary data analysis was done to ensure that the data had been properly recorded. This process was repeated for each sequence.

A detailed account of all the observations during the test is given in Table 7.1. A series of photographs were taken throughout the test. A few of them are compiled in Appendix B.

Table 7.1 The Event Table.

SEQ	CYC	$\Delta$ (in)	LD (kips)	$\mu$	Comments	Photo
A					low level loading sequence	
B					low level loading sequence	
C		0.04	20		low level loading sequence	
D		0.08	30		few flexural cracks developed on the top of the cap beam	
E	1A	0.12	40		development of 45deg shear cracks at the top of the north end of the cap beam and flexural cracks on the bottom of the south end of the cap beam	
	1B				more cracks developing opposite and symmetrical to cycle 1A	
	3A				no more additional cracks	
	3B				no more additional cracks	B.1
F	1A	0.20	50		few more shear cracks	
	1B				only a few more cracks	
G	1A	0.25	65	1.0	more cracks. the load seemed to be dropping off when holding at the max	
	1B				same as above	
	3B				the shear cracks in the cap beam were widening to 0.9 mm (one major crack on the north end of the beam); some of the shear cracks were now horizontal at the top of the cap beam and indicating debonding of the top reinforcement close to the centre of the beam	B.2
H	1A	0.45		1.5	major shear crack at the back of the specimen	
	1B				major shear crack opening on the top and the side, crack widths 4.0 mm	
	3A				shear cracks at the north end 2.0 mm	
	3B				shear crack width 4.0 mm	
I	1A	0.65		2.0	shear crack widths 7.0 mm	B.3
	1B				shear crack widths 7.0 mm	B.4

*SEQ* : Sequence*CYC* : Cycle $\Delta$  : Joint Displacement in inches.*LD* : Target Load in kips $\mu$  : Ductility Level

Table 7.1 The Event Table (continued).

SEQ	CYC	$\Delta$ (in)	LD (kips)	$\mu$	Comments	Photo
J		0.90		3.0	before starting the loading the top A-frame was readjusted by undoing the 12 bolts on the north side; some release was observed; the concrete dilated a little and the frame put some constraint onto the beam	
	1A				shear crack width 12.0 mm; some of the wiring on the reinforcing became visible in the cracks; the load was slowly decreasing while holding at the max. displacement; spalling on the back side	
	1B				the load was still decreasing while the displacement is on hold; severe bulging and debonding on the top of the beam at the south end. the shear cracks reach 13.0 mm; after removal of loose concrete, rebar became exposed	
	2A				more spalling	
	2B				a large piece of concrete fell off at the middle of the cap beam and exposed reinforcing steel	
	3A				more spalling	B.5
	3B				more spalling, rubble was falling into the cracks	B.6
K	1A	1.25		4.0	severe cracking. the specimen started to fall apart; debonding at the top of the beam. shear failure occurred and the load dropped to zero	B.7
	1B				dramatic damage, but the load could still be held in this direction	B.8/B.9

*SEQ* : Sequence*CYC* : Cycle $\Delta$  : Joint Displacement in inches.*LD* : Target Load in kips $\mu$  : Ductility Level

### 7.3 Load - Deflection Curves

The overall response of the bent is best represented by load deflection curves, which plot the total lateral loads against the average horizontal joint displacements.

Since the lateral load was measured by the pressure transducers in the hydraulic loop of the loading jack, the load readings include the friction in the hydraulic system. The friction acts against the direction of the jack movement and therefore leads to higher load readings than actually applied onto the specimen. Comparing loading and unloading sequences in the purely elastic range an average friction component of 5 kips was detected, which was manually removed from the jack load readings. The base shears given in the following discussions are corrected for the friction.

**Table 7. 2** Loading history.

<i>SEQ</i>	<i>Base Shear expected (kips)</i>	<i>Base Shear measured (kips)</i>	<i>jack disp. (LVDT) expected (in)</i>	<i>jack disp. (LVDT) measured (in)</i>	<i>expected joint disp. (in)</i>	<i>measured joint disp. (in)</i>	$\mu$
C	20		0.14		0.10		
D	30	29	0.21	0.18	0.15	0.08	
E	40	33	0.28	0.22	0.20	0.12	
F	50	43	0.35	0.34	0.25	0.19	
G	65	48	0.46	0.43	0.33	0.25	1
H		57	0.63	0.67	0.50	0.46	1.5
I		55	0.80	0.85	0.67	0.63	2
J		45	1.06	1.16	0.93	0.90	3
K		14	1.36		1.24	1.25	4

Since the load cell on the main actuator was not functional, the entire test had to be performed under displacement control. The displacement is controlled by the feed back from the LVDT mounted on the lateral load actuator. These jack displacements also

include a component from the elastic deflection of the reaction frame which was analytically determined to be 0.02" per 10 kips. Later on it was discovered however that the elastic deformation of the frame is closer to 0.03" per 10 kips. A first yield was anticipated at 65 kips at a joint displacement of 0.33". The expected and the actual load history is listed in Table. 7.2.

Several shear cracks in the cap beam started to form at a relatively low level, sequence E, at a base shear of 33 kips (see photo B.1 and Fig. 7.1). This coincides with an anticipated shear failure from the analysis. From that point on there is a slight stiffness degradation up to sequence G, the estimated yield displacement based on flexural yielding. Large cracks started to form on the top of the specimen indicating debonding of the top reinforcement (see photo B.2). The little vertical reinforcement provided was not sufficient to confine the longitudinal steel. At ductility level 1.5, sequence H, the hysteresis loops start to open up showing plastic deformation. Strength was still increasing and the maximum base shear of about 60 kips was reached at that point. The first cycle of sequence I ( $\mu=2.0$ ), see Fig. 7.2, shows little strength degradation, however the following cycles show severe strength degradation. The debonding of the top reinforcement progressed with each load cycle. Degradation continued with each cycle of sequence J and then on the first cycle of sequence K the beam failed completely at the negative moment (south) end. At this stage the bent continued to carry the dead load and could still resist a small amount of lateral load as the north end of the beam had not yet failed. At the failed south end the shear was being carried by tension in the bottom bars, see Photo B.8 and B.9. At the ultimate load stage virtually complete strength loss was observed in a brittle shear failure of the cap beam.

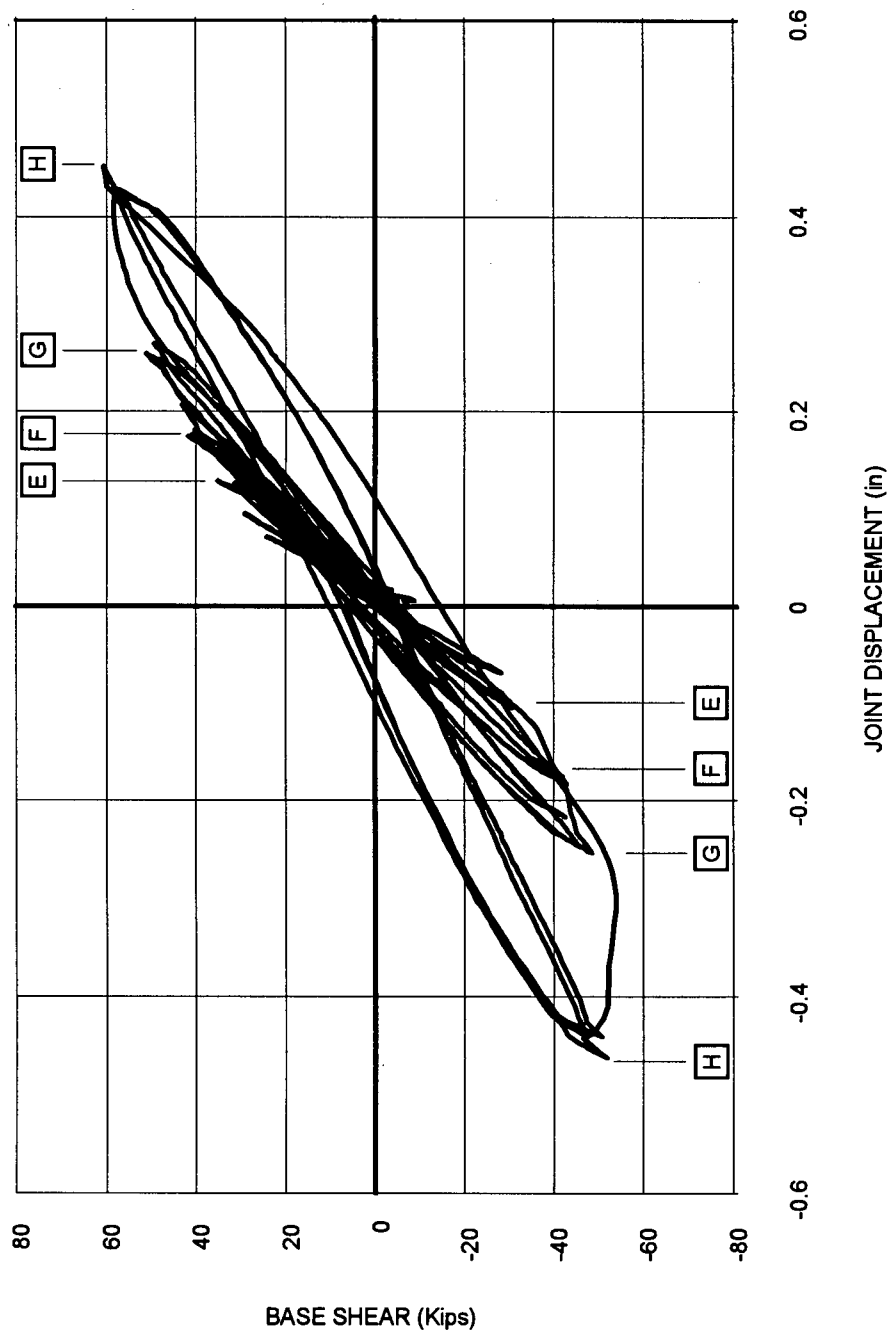


Fig. 7.1 Load deflection curve up to sequence H.

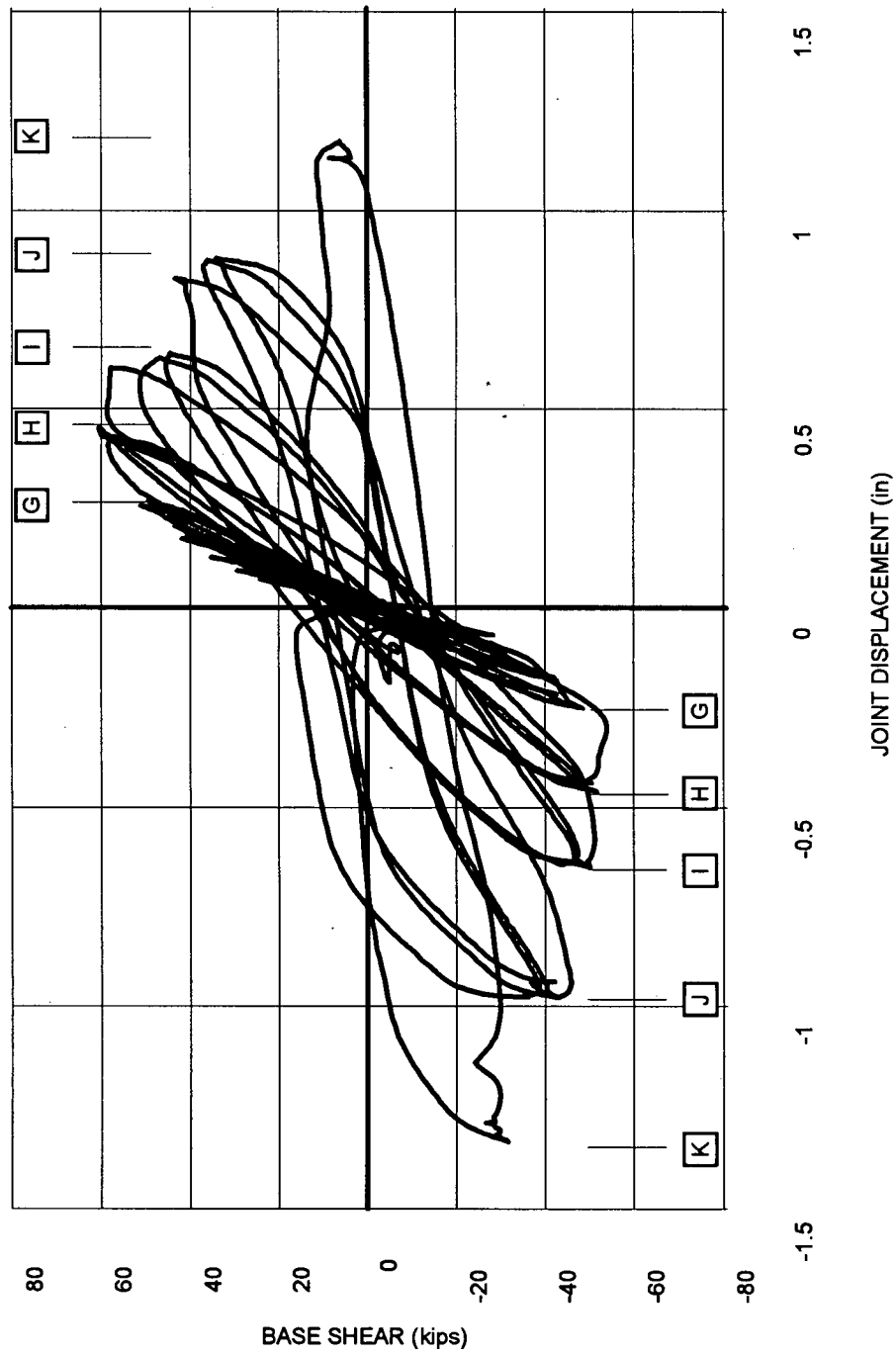


Fig. 7.2 Load deflection for OSB1.

An envelope of the load deflection plots is shown in Fig 7.3 and compared to the results of the monotonic push over analysis of the model. It is seen that the actual maximum lateral load is somewhat lower than the calculated one.

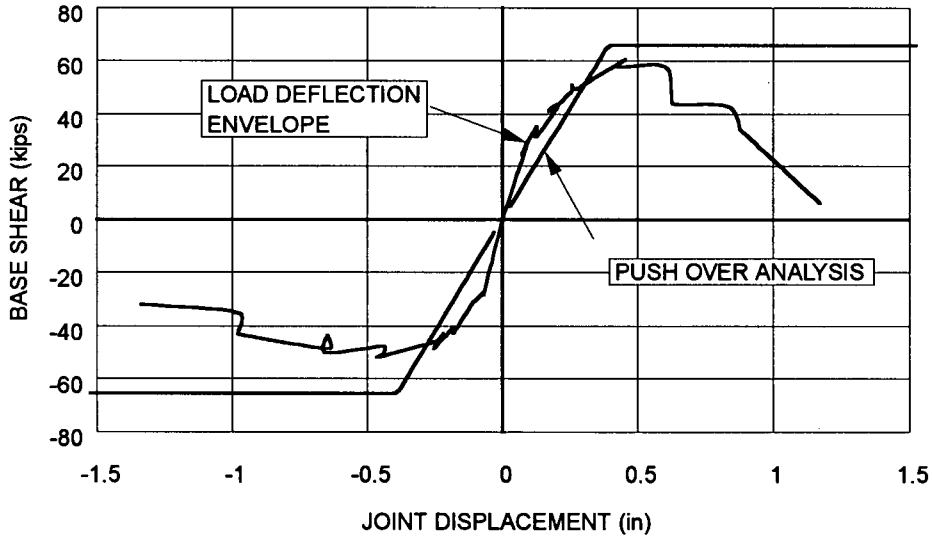


Fig. 7.3 Load deflection envelope for OSB1.

From the above Fig. 7.3 it can be seen that the initial stiffness of test specimen was somewhat higher than the assumed cracked one of the computer models. This is due to the effects of crack development and the associated stiffness degradation. On average however the predicted stiffness of the model is a fair representation up to the yield level. Realistically the structure failed as soon as the strength started to degrade in sequence H. The test specimen hence reached a displacement ductility of about 1.5, which is comparable to analytical displacement ductility of 1.75. At ductilities over 2 serious strength degradation was observed. This indicates adverse hysteretic behaviour, which the computer programs used herein are not able to model. Others have made attempts to capture this response pattern with some success (Kunnath et al. (1992), and Stone and

Taylor(1993)). The hysteresis loops indicate that the as-built bridge bent shows little energy absorption and very poor ductile behaviour.

#### 7.4 Strain gauge results

Most of the strain gauges were functional throughout the test and only a few saturated when their capacity was exceeded. From the visual observations during the test, two regions of the cap beam experienced serious damage. One is the region of shear failure just outside the haunches and the other is at the top of the cap beam, where the top reinforcement debonded at the final stages of the test. The shear failure region has very little shear reinforcement and the data from the few strain gauges is inconclusive. The strains along the top show consistent readings through most of the test until the final stages when the gauges saturated. The maximum tension strain readings are depicted in Fig. 7.4 and Fig. 7.5 up to the sequence when one of the strain gauges reached saturation. For the exact strain gauge location refer to Klohn-Crippen's Drwg Q117-SK2 in Appendix A.

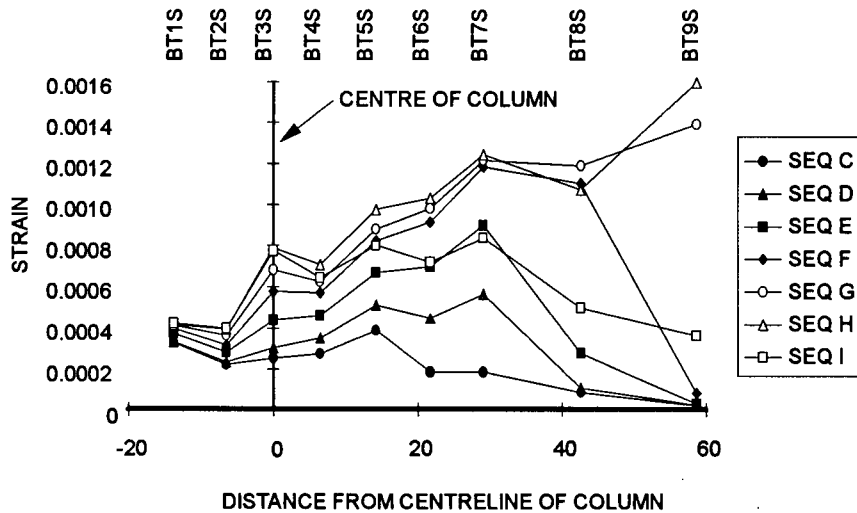


Fig. 7.4 Strain gauge reading, top reinforcement at south end, negative moment.

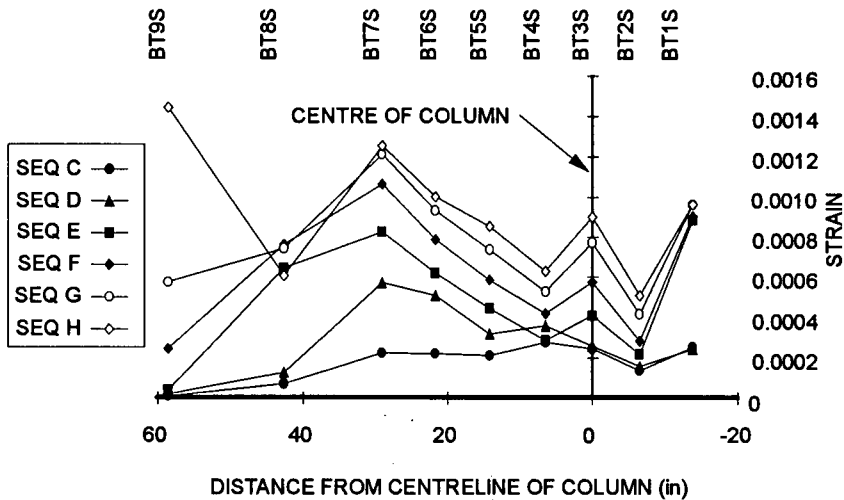


Fig. 7.5 Strain gauge reading, top reinforcement at north end, negative moment.

The maximum strains nearly reached the yield strain 0.0017. From these strains the actual forces in the reinforcing bars can be calculated. Assuming an effective sectional depth of  $0.8h$ , the bending moments in the section can be estimated as shown in Fig. 7.6 and Fig. 7.7.

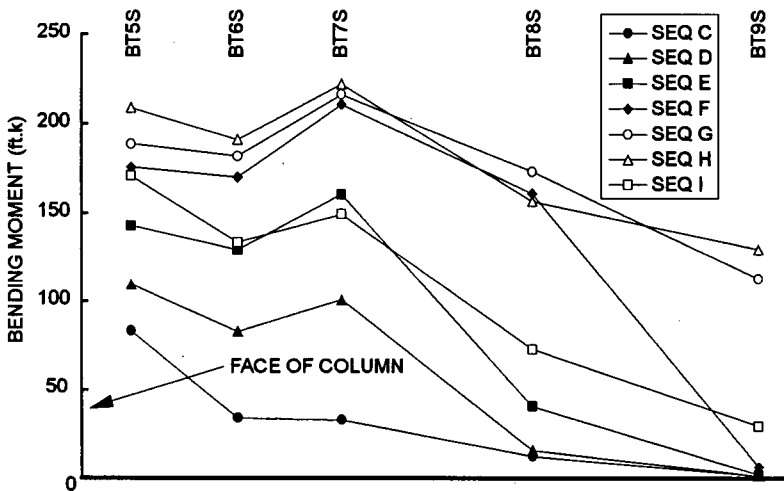


Fig 7.6 Bending moments in the cap beam at the south end of specimen.

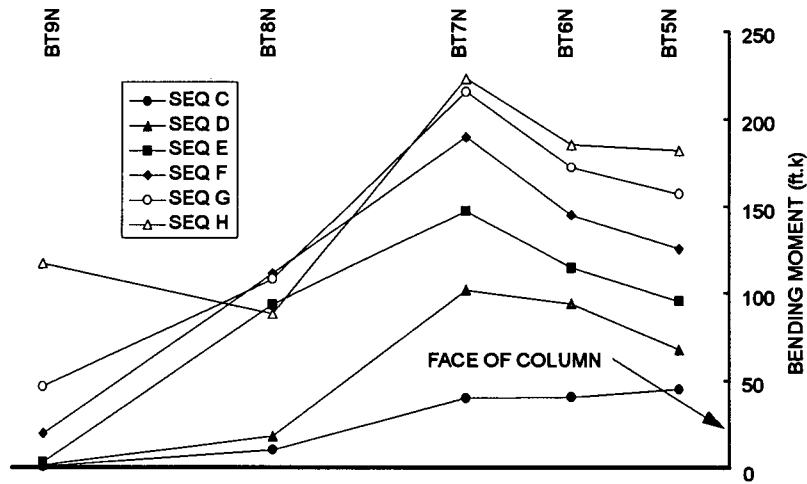


Fig. 7.7 Bending moments in the cap beam at the north end of specimen.

One would expect the largest moments to be at the face of the column, but the measured bending moments seem to dip in haunch region, even though the larger effective depth in this region has been taken into account. In Fig 7.8 the measured bending moments in the cap beam at a base shear of 33 kips (sequence E) are compared against the bending moments obtained from a elastic push over analysis at the same base shear. This low ductility level was chosen to demonstrate the working conditions of the strain gauges in the mostly elastic range of the test, since the analytical responses are more accurately defined.

As can be seen there is reasonable agreement between the experimentally determined moments and the calculated moments, although at one point there is up to a 100% difference between the north end and the south end. Since during the entire test the 60 Hz analog filters were turned off and the sampling rate was only 2 Hz, the small signatures of the strain gauges were severely corrupted. Therefore the strain gauges for

this test are not a very reliable data acquisition device and at best can only indicate a trend, but by no means give an exact account of the strains they measure. Notable is the slight reduction in the measured bending moments just at the face of the column in the haunch region.

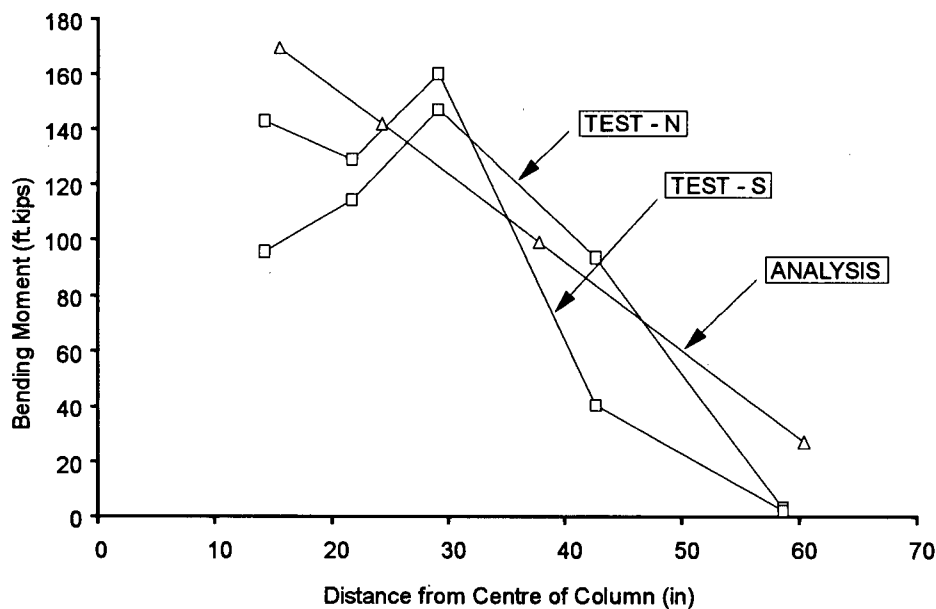


Fig 7.8 Bending moments in the cap beam at base shear 33 kips.

### 7.5 Comments on the Response of the Test Specimen

The largest axial strains in the top rebar of the cap beam are at about the quarter point of the cap beam. This is also where most of the cracking occurred and near to a cutoff point. Initial flexural cracks developed into diagonal shear cracks in the later sequences of the test. The strain gauges attached to the stirrups in this area never seemed to register any strains vertically. The diameter of these stirrups is very small and there were no gauges right at the main diagonal crack; local yielding was the main effect on these bars. Inasmuch as neither the concrete alone provides enough capacity nor the

insufficient contribution of the vertical shear reinforcement, the longitudinal reinforcement added significantly to the shear capacity of the section. The failure at ultimate load was a brittle shear failure of the cap beam. The shear reinforcement at that stage was ruptured. After failure, the specimen was held together by tension in the highly deformed lower reinforcing bars.

Very little cracking occurred in the beam column joints indicating that the weak element in the existing structure is definitely the cap beam. Strength retrofits of the beam and columns will put higher forces into the joints. At this stage the ductile performance of the joints is questionable due to just nominal shear reinforcement and the difficulty to strengthen the haunch region adequately. Locally the columns might still show some undesirable debonding of the main reinforcement due to the nominal confinement of the column reinforcing steel.

## **CHAPTER 8**

### **CONCLUSIONS**

#### **8.1 Introduction**

This work represents the first part of a large scale testing program at UBC on the as-built and retrofitted concrete bridge bents of the Oak Street Bridge. The objective of this phase of the project was to determine the performance parameters of the intended test series, to design and implement the test setup, and to test and analyze the first test specimen, an as-built specimen. The preliminary findings indicate severe ductile deficiencies and a brittle failure mechanism at ultimate loads, which confirms initial assessments and emphasizes the need for seismic upgrading of the existing structure.

When the Ministry of Transportation and Highways of British Columbia decided to pursue testing as part of the upgrading efforts of the Oak Street Bridge, the structural consultants Klohn-Crippen and representatives from UBC's structural engineering group in Civil Engineering had to decide on the scope and design parameters of the test series. Testing was deemed to be cost effective due to the large number of similar structural elements not only found in the Oak Street Bridge, but also in the Queensborough Bridge. The test specimens were to model the cap beam and parts of the columns to the first inflection point of a typical prototype bridge bent.

#### **8.2 Analytical Predictions**

The analysis considered a typical prototype bent and the scaled experimental test model. Preliminary assessment and dynamic analysis was conducted on the prototype. The test model was analyzed to find the response parameters for the design of the test set up and for later comparison to the test results.

A general seismic assessment of the prototype using the 1961 AASHO design guidelines and the 1983 ATC-6 bridge design code shows a dramatic increase in seismic lateral load demand over that time period. For the original design seismic loadings were preempted by wind loadings. ATC-6 puts a lateral load demand of 470 kips on the structure, for which it was clearly not designed. Deficiencies were identified in the cap beam and the columns of the bridge bent for loads much less than the ATC-6 values.

A member capacity assessment of the beam, column, and the beam/column joint indicates flexural hinging in the cap beam at a lower base shear demand than from ATC-6. The predicted hinge region in the cap beam is very poorly reinforced for shear and was suspected to have a very poor ductile response. The push over analysis using cracked sectional properties taking only flexure into account shows a first yield at 378 kips and an ultimate load of 475 kips. A shear strength analysis based on the compression field theory unveiled a much lower critical base shear of 243 kips. The nonlinear dynamic analysis using three modified earthquake records gives similar ultimate loads to the push over analysis and yields a displacement ductility of 1.75, which is very low but not uncommon in older concrete structures.

It was realized that this concrete structure does not meet modern minimum requirements for longitudinal and transverse reinforcement and therefore the imaginable failure mechanisms are some what dubious. In order to conduct the test yield levels and estimates of the ultimate loads and displacements had to be determined to establish a load application history. Investigating various assessment approaches a first flexural yielding the cap beam for the test model was estimated around 40 kips. The compression field theory gives an ultimate base shear of 69 kips. It is difficult to predict to what extent the longitudinal reinforcement contributes to the shear capacity and thus the interaction of flexure and shear in a poorly reinforced regions in the cap beam. The experimental tests

series was therefore very much justified to determine the actual response of the bridge bent.

### **8.3 Test Setup**

As part of this research various retrofit schemes were to be investigated. The maximum estimated responses were based on an assumed full retrofit using overstrength material properties. The design criteria of the test setup for strength and deflection were derived from these conservative predictions.

At the time of the completion of this thesis all the test specimens have been tested and the test setup has performed to its specifications. The only defect was an eccentricity in the loading A-frame mounted to the specimen, due to inherent construction tolerances of the connection points on the test specimen itself. The loading frame started to deform laterally due to this secondary effects and had to be strengthened with a diagonal brace. In hindsight, a much greater lateral stiffness in the loading frame would have been better.

A large data acquisition program was installed to record the displacement, force, and strain gauge measurements. The analysis of all the data will take quite some time and is currently being undertaken by other graduate students at UBC. A first and brief look at the readings indicate that most of the devices were functional through out the test. Since the test setup is indeterminate in the horizontal direction, some effort was put into measuring the lateral forces at the bottom column supports and still provide a rotational degree of freedom. The device provided pinned supports, and was instrumented to establish lateral reaction at each pin. Unfortunately the calibration for lateral load was crude to be of use.

#### 8.4 Test Results

The definition of yielding in this test is some what ambiguous. There is no distinct hinging pattern apparent. The specimen gradually developed severe cracks in the cap beam just outside the haunches. Based on the load displacement curves, the best way to define yielding is a significant deviation from the linear response, which occurred at sequence 'G' at a measured base shear of 48 kips and a joint displacement of 0.25 in. The ultimate load was attained at sequence 'H' at 57 kips and a displacement of 0.47 in. The following sequences showed rapid deterioration and strength degradation until the specimen failed at a base shear of 14 kips and a displacement of 1.25 in. Assuming failure as soon as strength degradation sets in a displacement ductility of 1.88 was found, which compares well with the predicted one of 1.75. Scaling the ultimate capacity to the actual bridge bent gives a base shear capacity of 281 kips, which is very much below modern lateral load demands of 470 kips. The hysteresis loops are pinched and the severe strength degradation clearly indicates the poor ductile response and the ineffective energy absorption of the as built bridge bent. Considering this very low ductility of the structure one has to assume that the lateral load demands have to be resisted essentially in the elastic region to provide a satisfactory seismic performance, which is clearly not the case here. Seismic upgrades of some sort are therefore necessary.

Preliminary investigation of all the strain gauges show that most of the gauges were functional through out the test. A closer look at the gauges at the top of the cap beam revealed quite large discrepancies of up to 100% for symmetrical placed gauges, which should read similar strains. The data obtained from these gauges are to be considered with some reservation and only a trend at best in the response can be derived from these readings.

## 8.5 Conclusions

The Oak Street Bridge, built in the 1950's, was recognized by the British Columbia Ministry of Transportation and Highways as being seismically deficient by today's standards. The deficiencies are in the lateral load carrying capacity, the lack of control over failure mode, and in many of the details of the steel reinforcement.

The details of the reinforcing steel and the corresponding lack of ductility make a prediction of the response very difficult. This is further complicated by the fact that there are no readily accepted standards for retrofit design of bridges for improved seismic behaviour. For these reasons, the Ministry of Transportation and Highways, upon the advice of their consultants, decided that a program of experimental testing would be an effective way to determine the actual performance of the concrete bridge bents of the approach spans. The undertaking here is twofold; first to find a reasonable approach to predict the response analytically, and secondly to carry out an experimental test program to establish the actual capacity and ductility of a scaled model of the bridge bent.

Various analytical examinations of the prototype and model bridge bent uncovered serious deficiencies in the cap beam. A push over analysis based on a purely flexural response shows an ultimate base shear capacity slightly below elastic (unit force reduction factor;  $R = 1$ ) demands to current standards (ATC-6). However a simple shear analysis predicts a failure at a much lower base shear level and a non ductile brittle response can therefore be expected. Since there is so little transverse shear reinforcement in the cap beam, much less than the modern design guidelines require, conventional shear analyses are not quite applicable. A more refined approach based on the compression field theory indicates an interaction between shear and flexure and hence a reduction in flexural capacity due to demands on the longitudinal reinforcing bars from the shear. Yet a concise prediction of the failure mechanism in the cap beam still remains quite difficult. A

dynamic analysis using various modified earthquake records reveals fairly small displacement ductilities of less than two ( $< 2$ ), which is not uncommon for older concrete structures. All the above analyses point at a very poor ductile response to lateral loads.

The experimental test program was initiated to determine the actual response parameters and secondly to proof test a few retrofit schemes based on findings of the as built specimen. The first test, an as built one, confirmed the predicted low ductility and also the brittle response of the cap beam with little energy absorption. Also found was a significant strength degradation due to debonding of the longitudinal, which is credited to the poor confinement of the main rebars. The uncertainties to predict a response of older structures in particular to seismic attack invariable makes experimental testing the only satisfying approach to obtain their seismic response. The aspect of retrofitting these deficient structures is an even less understood issue and inspires ongoing research all over the world.

## BIBLIOGRAPHY

1. AASHO 1961, *Standard Specification for Highway Bridges*, Washington, DC, American Association of State Highway Officials, 1961. Ed. 8,
2. ACI/ASCE Committee 426, *Suggested Revisions to Shear Provisions for Building Codes*, American Concrete Institute, Detroit, 1978, pp. 88.
3. ATC-6, Applied Technology Council "Seismic Design Guidelines for Highway Bridges," *Report ATC-6*, Washington DC, Federal Highway Administration, 1981.
4. Byrne, P.M., "Seismic Loading, Soil Modeling and Analysis," *Proceedings of the Seismic Soil/Structure Interaction Seminar (CSCE)*, Vancouver, May 29, 1993.
5. Chai, Y.H., Priestley, M.J.N. and Seible, F., "Seismic Retrofit of Circular Bridge Columns for Enhanced Flexural Performance," *ACI Structural Journal*, v 88 n 5, 1991, pp. 572-584.
6. Choi, C.-K. and Kwak, H.-G., "The Effect of Finite Element Mesh Size in Nonlinear Analysis of Reinforced Concrete Structures," *Computers and Structures*, v 36 n 5, 1990, pp. 807-815.
7. Clough, R.W. and Penzien, J., *Dynamics of Structures*, New York, McGraw-Hill, 1975.
8. Collins, M.P. and Mitchell D., *Prestressed Concrete Structures*, New Jersey, Prentice Hall, 1991.
9. Collins, M.P., "Towards a Rational Theory of RC Members in Shear," *Journal of the Structural Division, ASCE*, v 104 n ST4, 1978, pp. 649-666.
10. Commentary J : Effects of Earthquakes, *Supplement to the National Building Code of Canada 1990*, Ottawa, National Research Council of Canada, 1990. pp. 202-220.

11. Crippen International Ltd., "Oak Street Bridge No. 1380 - Two-Column Bent Test Program - Comparison of Five Major Bridges," Report prepared for the Ministry of Transportation and Highways of British Columbia, 1993.
12. Dames and Moore, "Geotechnical Study and Seismic Evaluation - Oak Street Bridge," *Final Report to the Ministry of Transportation and Highways of British Columbia*, 1991.
13. Filippou, F.C. and Fences, G.L., "Nonlinear Static and Dynamic Analysis of Reinforced Concrete Members, Subassemblages and Structures," *Seismic Workshop in San Diego 1990*, pp. 195-202.
14. Filippou, F.C., "Models of Nonlinear Static and Dynamic Analysis of Concrete Freeway Structures," *Seismic Design and Retrofit of Bridges, Seminar Proceedings*, Berkeley, 1992.
15. Hu, H.-T. and Schnobrich, W.C., "Nonlinear Analysis of Cracked Reinforced Concrete," *ACI Structural Journal*, v 87 n 2, 1990, pp. 199-207.
16. Kunnath, S.K.; Reinhorn, A.M. and Lobo, R.F., *IDARC Version 3.0 : A Program for the Inelastic Damage Analysis of Reinforced Concrete Structures* (NCEER 92-0022), Buffalo, N.Y., National Centre for Earthquake Engineering Research, 1992.
17. Mander, J.B., Priestley, M.J.N. and Park, R., "Theoretical Stress-Strain Model for Confined Concrete," *ASCE Journal of Structural Engineering*, v 114 n 8, 1988, pp. 1804-1826.
18. Mitchell, D., Tinawi, R. and Sexsmith, R.G., "Performance of Bridges in the 1989 Loma Prieta Earthquake. Lessons of Canadian Designers," *Canadian Journal of Civil Engineering*, v 18 n 4, 1991, pp. 711-734.
19. Paulay, T. and Priestley, M.J.N., *Seismic Design of Reinforced Concrete and Masonry Buildings*, New York, John Wiley & Sons, 1992.

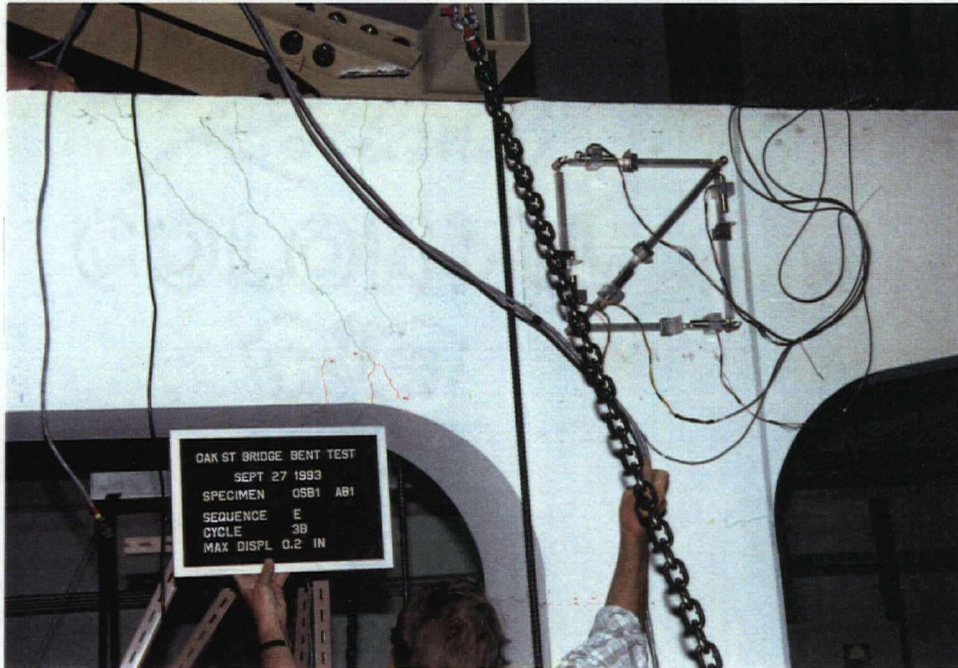
20. Paulay, T., Park, R. and Priestley, M.J.N., "Reinforced Concrete Beam-Column Joints under Seismic Actions," *ACI Journal Proceedings*, v 75 n 11, 1978, pp. 585-593.
21. Pessiki, S.P.; Conley, C.H.; Gergely, P. and White, R.N., *Seismic Behavior of Lightly-Reinforced Concrete Column and Beam-Column Joint Details (NCEER 90-0014)*, Buffalo, N.Y., National Center for Earthquake Engineering Research, 1990.
22. Powell, G., "Observations on the Practical Application of Nonlinear Analysis," *Seismic Design and Retrofit of Bridges, Seminar Proceedings*, Berkeley, 1992.
23. Powell, G.H., *DRAIN-2D user's guide*, Berkeley, CA, Earthquake Engineering Research Center, University of California, 1973.
24. Press, William H.; Teukolsky, Saul A.; Flannery, Brian P. and Vetterling, William T., *Numerical Recipes, The Art of Scientific Computing (FORTRAN Version)*, Cambridge, Cambridge University Press, 1989.
25. Priestley, M.J.N. and Calvi, G.M., "Towards a Capacity-Design Assessment Procedure for Reinforced Concrete Frames," *Earthquake Spectra*, v 7 n 3, 1991, pp. 413-437.
26. Priestley, M.J.N. and Seible, F., "Design of Seismic Retrofit Measures for Concrete Bridges," *Seminar on Seismic Assessment and Retrofit of Bridges*, Report SSRP - 91/03, San Diego (UCSD), 1991, pp. 197-250.
27. Priestley, M.J.N., "Seismic Assessment of Existing Concrete Bridges," *Seminar on Seismic Assessment and Retrofit of Bridges*, Report SSRP -91/03, San Diego (UCSD), 1991, pp. 82-149.
28. Schultz, A., "Experiments on Seismic Performance of RC Frames with Hinging Columns," *ASCE Journal of Structural Engineering*, v 116 n 1, 1990, pp. 125-145.
29. Seed, R.B. and Dickenson, S.E., "Site-Dependent Seismic Site Response," *Proceedings of the Second Annual Seismic Research Workshop (CALTRANS)*, Sacramento, March 16 - 18, 1993.

30. Seible, F. and Priestley, M.J.N., "Damage and Performance Assessment of Existing Concrete Bridges under Seismic Loads," *Proc. U.S.-Japan Seismic Retrofit Workshop*, 1990, pp. 203-222.
31. Stevens, N.J., Uzumeri, S.M., Collins, M.P. and Will, G.T., "Constitutive Model for Reinforced Concrete Finite Element Analysis," *ACI Structural Journal*, v 88 n 1, 1991, pp. 49-59.
32. Stone, W.C. and Taylor, A.W., *Seismic Performance of Circular Bridge Columns Designed in Accordance With AASHTO/CALTRANS Standards*, Gaithersburg, MD, National Institute of Standards and Technology, 1993.
33. Vecchio, F.J. and Collins M.P., "Modified Compression-Field Theory for Reinforced Concrete Elements Subjected to Shear," *ACI Journal, Proceedings*, v 83 n 2, 1986, p. 219-231.
34. Vecchio, F.J. and Selby, R.G., "Toward Compression-Field Analysis of Reinforced Concrete Solids," *ASCE Journal of Structural Engineering*, v 117 n 6, 1991, pp. 1740-1758.

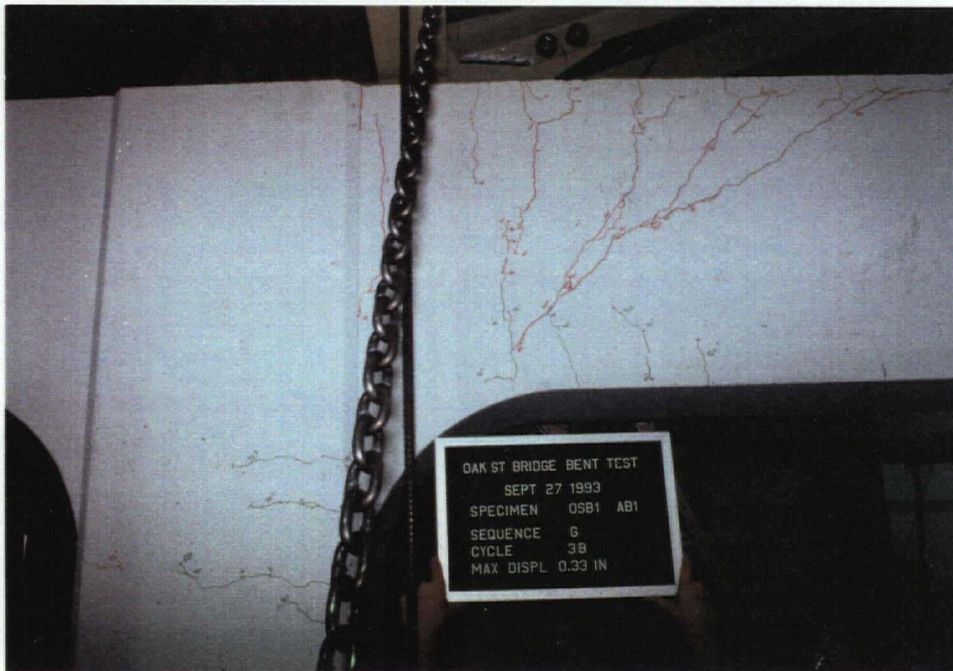
**APPENDIX A**  
**STRUCTURAL DRAWINGS**

Structural drawings Q117-01 and Q117-11 from KLOHN-CRIPPEN.

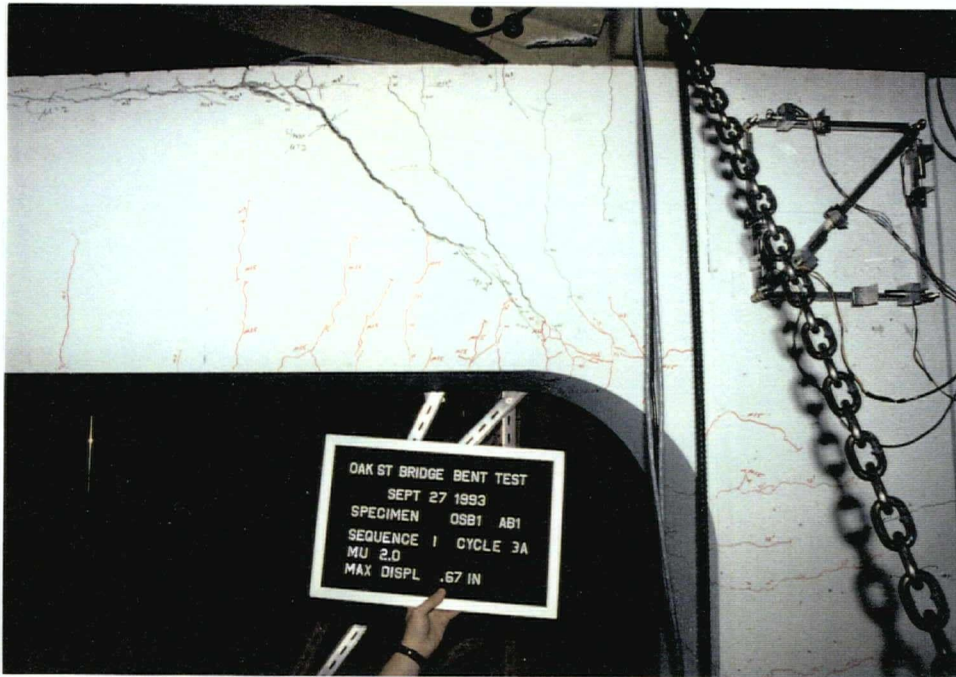
**APPENDIX B**  
**PHOTOGRAPHS OF THE FIRST TEST**



Photograph B.1 Sequence E - Cycle 3B



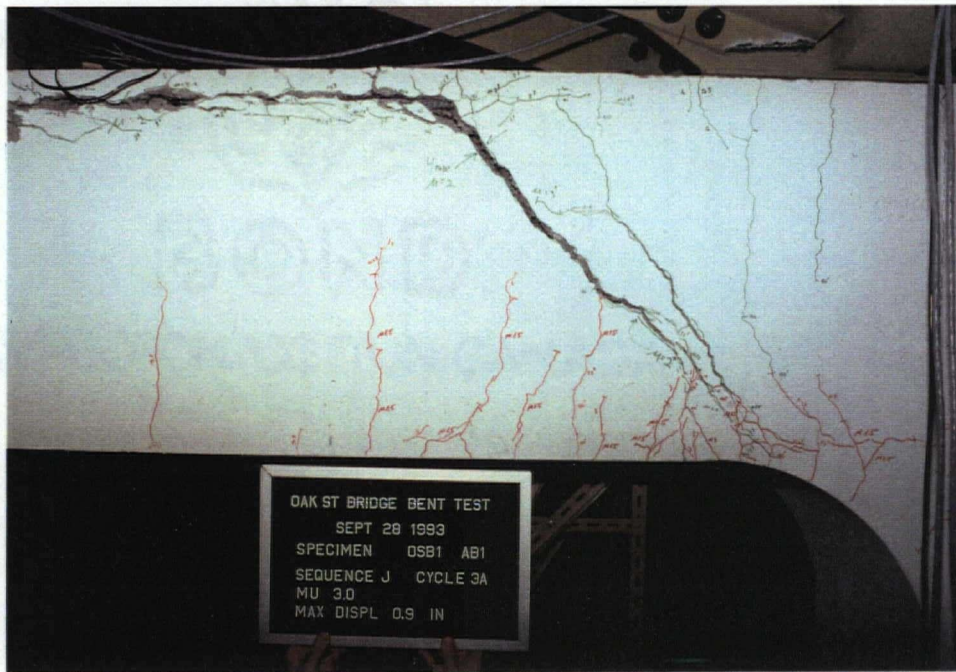
Photograph B.2 Sequence G - Cycle 3B



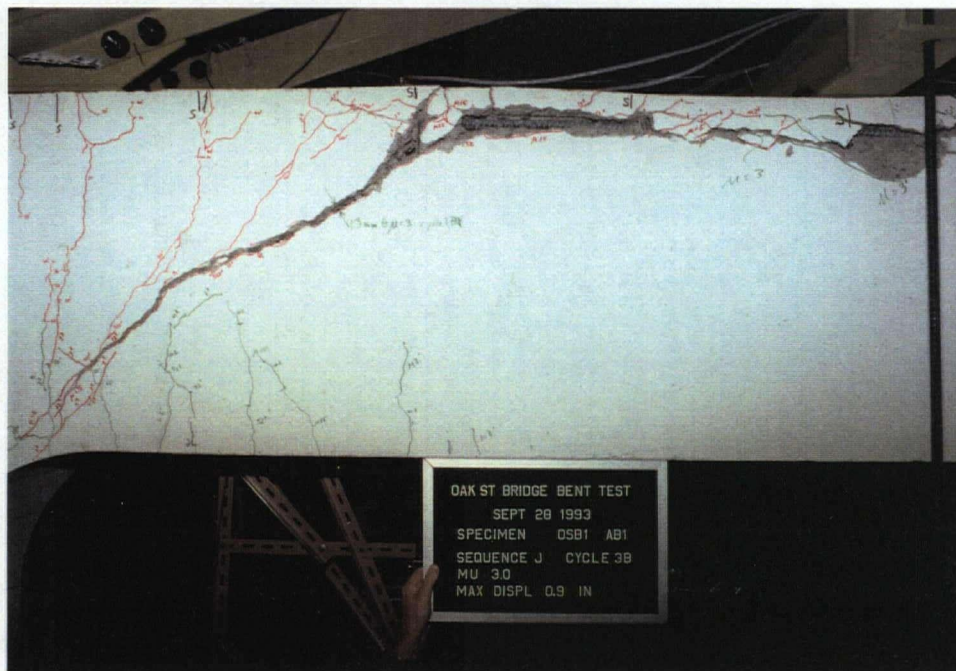
Photograph B.3 Sequence I - Cycle 3A



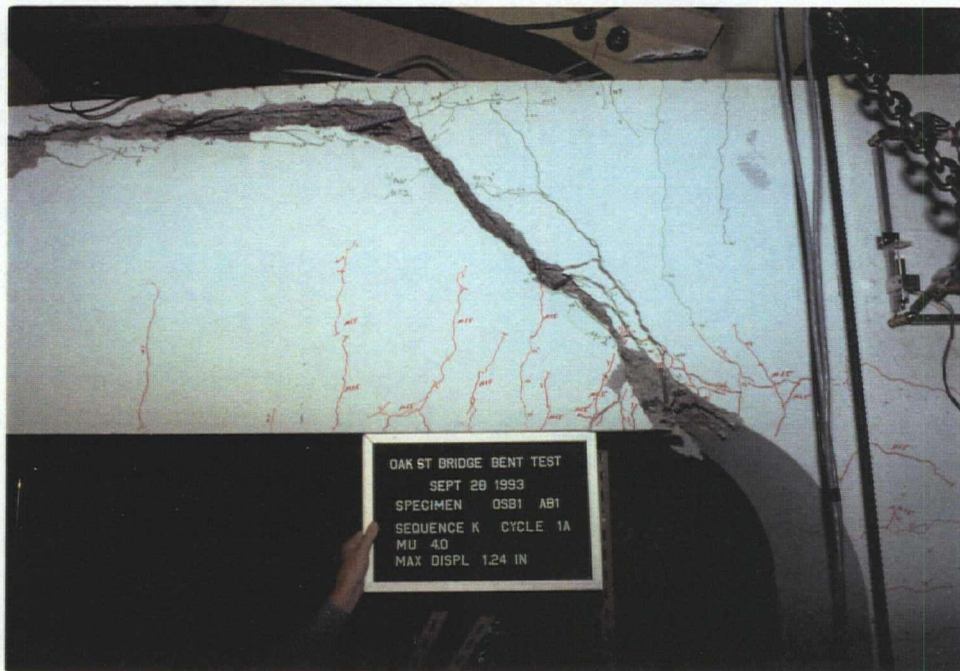
Photograph B.4 Sequence I - Cycle 3B



Photograph B.5 Sequence J - Cycle 3A



Photograph B.6 Sequence J - Cycle 3B



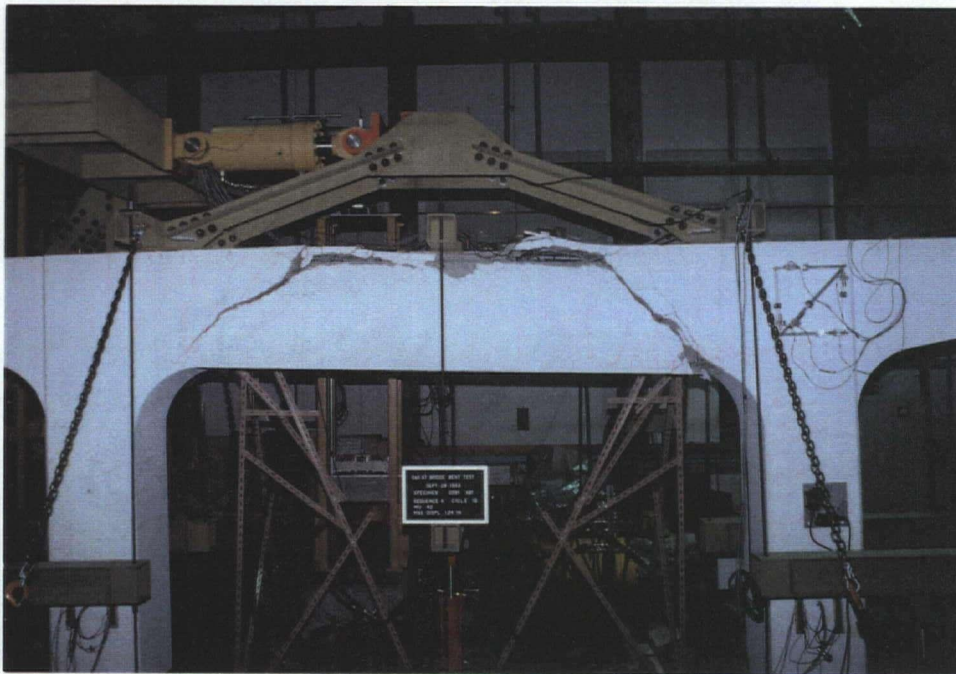
Photograph B.7 Sequence K - Cycle 1A



Photograph B.8 Sequence K - Cycle 1B



Photograph B.9 Sequence K - Cycle 1B



Photograph B.10 Completed Test.

## APPENDIX C DP - PROGRAM

### C.1 The DP Program

```
C *****
C   DATA PROCESSING PROGRAM
C   VERSION 4.1
C   27. OCTOBER 1993
C *****

C   This program tries to smooth the data with an weighted average
C   and conversion to actual units. Add the data reduction routine.
C   Try to compile it with the Lahey compiler

PROGRAM DATAFAB
C *** VARIBALE DEFINITION
INTEGER NCH, NCHCH, TYPE(100), I, J, K, N, NMAX
REAL F(3,100), DATA(2048,100), DLTCH(20), TOL(20), CHCH(20,3)
REAL STRG, LDCELL, LVDT, LMPS, FOOTING, LINPOT, AVG, DIFF
REAL PTS, DELTA, VALUE
C   REAL ZERO
CHARACTER TITLE*40, FCNT*12, FIN*12, FOUT*12, DATE*10
CHARACTER DES(100)*8
LOGICAL SAVE

C -----

C *** READ COMMAND LINES

WRITE (*,*) ' THIS IS A DATA FABRICATION PROGRAM'
WRITE (*,*) ' BY MARKUS SEETHALER'
WRITE (*,*) ' '
WRITE (*,*) ' ENTER THE CONTROL DATA FILE NAME : '
READ (*,*) FCNT
WRITE (*,*) ' ENTER THE INPUT FILE NAME : '
READ (*,*) FIN
WRITE (*,*) ' ENTER THE OUTPUT FILE NAME : '
READ (*,*) FOUT

C -----

C *** READ CONTROL DATA FILE
OPEN(UNIT=5, FILE=FCNT, STATUS='OLD')
WRITE(*,*) ' READING THE CONTROL DATA FILE'

READ(5, '(A40)') TITLE
WRITE(*,*) ' ', TITLE
READ(5, '(A10)') DATE
```

```

      READ(5,*) NCH
      READ(5,*) PTS

      DO 10 I=1,NCH
        READ(5,1000) DES(I)
1000  FORMAT (A8)
10    CONTINUE

      DO 20 I=1,NCH
        READ(5,*) TYPE(I), (F(J,I),J=1,3)
20    CONTINUE

      READ(5,*) NCHCH
      DO 25 I=1,NCHCH
        READ(5,1500) (CHCH(I,J),J=1,3),TOL(I)
1500  FORMAT (3I3,4X,F8.3)
25    CONTINUE

      CLOSE(UNIT=5)

C -----
C *** OPEN THE DATA FILES
      WRITE (*,*) ' OPENING THE FILES '
      OPEN(UNIT=6,FILE=FIN,STATUS='OLD')
      OPEN(UNIT=7,FILE=FOUT,STATUS='UNKNOWN')

C -----
C *** PROCESS THE DATA FILE

C **  READING THE DATA IN

      WRITE (*,*) ' READING THE DATA '
      N = 1
30    CONTINUE
        READ(6,*,END=40) (DATA(N,J),J=1,NCH)
        N = N +1
        GOTO 30
40    CONTINUE
      NMAX = N - 1

C -----
C *** RUN THE SMOOTH ROUTINE ON ONE COLUMN

      WRITE (*,*) ' SMOOTHING THE DATA '
      DO 50 J = 1,NCH

        CALL SMOOFT(DATA(1,J),NMAX,PTS)

```

50 CONTINUE

C -----

C \*\*\* DATA CONVERSION TO ACTUAL UNITS

```

WRITE (*,*) ' CONVERSION OF THE DATA TO REAL UNITS'
DO 90 J=1,NCH
  IF (TYPE(J) .EQ. 1) THEN
    DO 100 K = 1,NMAX
      DATA(K,J) = STRG(DATA(K,J),F(1,J))
100    CONTINUE
  ELSE IF (TYPE(J) .EQ. 2) THEN
    DO 110 K = 1,NMAX
      DATA(K,J) = LDCELL(DATA(K,J),F(1,J))
110    CONTINUE
  ELSE IF (TYPE(J) .EQ. 3) THEN
    DO 120 K = 1,NMAX
      DATA(K,J) = LVDT(DATA(K,J),F(1,J))
120    CONTINUE
  ELSE IF (TYPE(J) .EQ. 4) THEN
    DO 130 K = 1,NMAX
      DATA(K,J) = LMPS(DATA(K,J),F(1,J))
130    CONTINUE
  ELSE IF (TYPE(J) .EQ. 5) THEN
    DO 140 K = 1,NMAX
      DATA(K,J) = FOOTING(DATA(K,J),F(1,J))
140    CONTINUE
  ELSE IF (TYPE(J) .EQ. 6) THEN
    DO 150 K = 1,NMAX
      DATA(K,J) = LINPOT(DATA(K,J),F(1,J))
150    CONTINUE
  ELSE
    WRITE (*,*) 'WE HAVE A PROBLEM!!!'
    STOP
  END IF
90  CONTINUE

```

C -----

C \*\*\* DATA OUTPUT

```

WRITE (*,*) ' DATA OUTPUT'

WRITE(7,1100) TITLE
1100 FORMAT (A40)
WRITE(7,1200) DATE
1200 FORMAT (A10)
WRITE(7,1300) 'SCAN', (DES(J),J=1,NCH)
1300 FORMAT (A7,100(' ',A8))

```

```

SAVE = .TRUE.
DO 160 K = 1, NMAX

  DO 170 I=1,NCHCH
    IF (CHCH(I,2) .EQ. 1) THEN
      VALUE = DATA(K,CHCH(I,1))
    ELSE IF (CHCH(I,2) .EQ. 2) THEN
      VALUE = AVG(DATA(K,CHCH(I,1)),DATA(K,CHCH(I,3)))
    ELSE IF (CHCH(I,2) .EQ. 3) THEN
      VALUE = DIFF(DATA(K,CHCH(I,1)),DATA(K,CHCH(I,3)))
    END IF

    DELTA = ABS(VALUE - DLTCH(I))

    IF (DELTA .GE. TOL(I)) THEN
      SAVE = .TRUE.
      DLTCH(I) = VALUE
    ENDIF
170   CONTINUE

    IF (SAVE) THEN
      WRITE (7,1400) K, (DATA(K,J),J=1,NCH)
1400   FORMAT(' ',I5,100(' ',F11.6))
      WRITE(*,*) 'SCAN : ',K
      SAVE = .FALSE.
    END IF

160   CONTINUE

C -----
C *** CLOSING UP SHOP

WRITE(*,*) ' THIS IS THE END OF STORY, SO FAR'

CLOSE (UNIT=6)
CLOSE (UNIT=7)

STOP
END

C -----

SUBROUTINE SMOOFT(Y,N,PTS)

C *** Smooths an array Y of length n, with a window of full width of
order
C   PTS neighboring points, a user supplied value, Y is modified.

PARAMETER(MMAX=2048)
DIMENSION Y(MMAX)

```

```

M=2
NMIN=N+2.*PTS
1  IF (M.LT.NMIN) THEN
    M=2*M
    GO TO 1
ENDIF
IF (M.GT.MMAX) PAUSE 'MMAX too small'
CONST=(PTS/M)**2
Y1=Y(1)
YN=Y(N)
RN1=1./(N-1.)
DO 11 J=1,N
    Y(J)=Y(J)-RN1*(Y1*(N-J)+YN*(J-1))
11 CONTINUE
IF (N+1.LE.M) THEN
    DO 12 J=N+1,M
        Y(J)=0.
12 CONTINUE
ENDIF
MO2=M/2
CALL REALFT(Y,MO2,1)
Y(1)=Y(1)/MO2
FAC=1.
DO 13 J=1,MO2-1
    K=2*J+1
    IF (FAC.NE.0.) THEN
        FAC=AMAX1(0.,(1.-CONST*J**2)/MO2)
        Y(K)=FAC*Y(K)
        Y(K+1)=FAC*Y(K+1)
    ELSE
        Y(K)=0.
        Y(K+1)=0.
    ENDIF
13 CONTINUE
FAC=AMAX1(0.,(1.-0.25*PTS**2)/MO2)
Y(2)=FAC*Y(2)
CALL REALFT(Y,MO2,-1)
DO 14 J=1,N
    Y(J)=RN1*(Y1*(N-J)+YN*(J-1))+Y(J)
14 CONTINUE
RETURN
END

```

C -----

```

SUBROUTINE REALFT(DATA,N,ISIGN)
C *** Fourier transform w/ real numbers.

```

```

REAL*8 WR,WI,WPR,WPI,WTEMP,THETA
DIMENSION DATA(*)
THETA=6.28318530717959D0/2.0D0/DBLE(N)

```

```

C1=0.5
IF (ISIGN.EQ.1) THEN
  C2=-0.5
  CALL FOUR1 (DATA, N, +1)
ELSE
  C2=0.5
  THETA=-THETA
ENDIF
WPR=-2.0D0*DSIN(0.5D0*THETA)**2
WPI=DSIN(THETA)
WR=1.0D0+WPR
WI=WPI
N2P3=2*N+3
DO 11 I=2, N/2+1
  I1=2*I-1
  I2=I1+1
  I3=N2P3-I2
  I4=I3+1
  WRS=SNGL(WR)
  WIS=SNGL(WI)
  H1R=C1*(DATA(I1)+DATA(I3))
  H1I=C1*(DATA(I2)-DATA(I4))
  H2R=-C2*(DATA(I2)+DATA(I4))
  H2I=C2*(DATA(I1)-DATA(I3))
  DATA(I1)=H1R+WRS*H2R-WIS*H2I
  DATA(I2)=H1I+WRS*H2I+WIS*H2R
  DATA(I3)=H1R-WRS*H2R+WIS*H2I
  DATA(I4)=-H1I+WRS*H2I+WIS*H2R
  WTEMP=WR
  WR=WR*WPR-WI*WPI+WR
  WI=WI*WPR+WTEMP*WPI+WI
11 CONTINUE
IF (ISIGN.EQ.1) THEN
  H1R=DATA(1)
  DATA(1)=H1R+DATA(2)
  DATA(2)=H1R-DATA(2)
ELSE
  H1R=DATA(1)
  DATA(1)=C1*(H1R+DATA(2))
  DATA(2)=C1*(H1R-DATA(2))
  CALL FOUR1 (DATA, N, -1)
ENDIF
RETURN
END

```

C

```

-----
SUBROUTINE FOUR1 (DATA, NN, ISIGN)
REAL*8 WR, WI, WPR, WPI, WTEMP, THETA
DIMENSION DATA (*)
N=2*NN

```

```

J=1
DO 11 I=1,N,2
  IF (J.GT.I) THEN
    TEMPR=DATA (J)
    TEMPI=DATA (J+1)
    DATA (J)=DATA (I)
    DATA (J+1)=DATA (I+1)
    DATA (I)=TEMPR
    DATA (I+1)=TEMPI
  ENDIF
  M=N/2
1  IF ((M.GE.2).AND.(J.GT.M)) THEN
    J=J-M
    M=M/2
    GO TO 1
  ENDIF
  J=J+M
11 CONTINUE
MMAX=2
2  IF (N.GT.MMAX) THEN
  ISTEP=2*MMAX
  THETA=6.28318530717959D0/(ISIGN*MMAX)
  WPR=-2.D0*DSIN(0.5D0*THETA)**2
  WPI=DSIN(THETA)
  WR=1.D0
  WI=0.D0
  DO 13 M=1,MMAX,2
    DO 12 I=M,N,ISTEP
      J=I+MMAX
      TEMPR=SNGL(WR)*DATA(J)-SNGL(WI)*DATA(J+1)
      TEMPI=SNGL(WR)*DATA(J+1)+SNGL(WI)*DATA(J)
      DATA(J)=DATA(I)-TEMPR
      DATA(J+1)=DATA(I+1)-TEMPI
      DATA(I)=DATA(I)+TEMPR
      DATA(I+1)=DATA(I+1)+TEMPI
12    CONTINUE
      WTEMP=WR
      WR=WR*WPR-WI*WPI+WR
      WI=WI*WPR+WTEMP*WPI+WI
13    CONTINUE
      MMAX=ISTEP
    GO TO 2
  ENDIF
  RETURN
  END

```

C -----

```

REAL FUNCTION STRG (D,F)
C *** COMPUTES THE STRAIN READING FOR STRAIN GAUGES

```

C ARGUMENT DECLARATIONS

REAL D, F(5)

STRG = (D-F(3))/F(2)\*4/F(1)

RETURN

END

C -----

REAL FUNCTION LDCELL (D, F)

C \*\*\* COMPUTES THE LOAD CELL READING

C ARGUMENT DECLARATIONS

REAL D, F(5)

LDCELL = (D+F(2))\*F(1)

RETURN

END

C -----

REAL FUNCTION LVDT (D, F)

C \*\*\* COMPUTES THE LVDT READING

C ARGUMENT DECLARATIONS

REAL D, F(5)

LVDT = D\*F(1)

RETURN

END

C -----

REAL FUNCTION LMPS (D, F)

C \*\*\* COMPUTES THE LMPS READING

C ARGUMENT DECLARATIONS

REAL D, F(1)

LMPS = D\*F(1)

RETURN

END

C -----

REAL FUNCTION FOOTING (D, F)

C \*\*\* COMPUTES THE FOOTING READING

C ARGUMENT DECLARATIONS

REAL D, F(5)

FOOTING = D\*F(1)

RETURN

END

C -----

REAL FUNCTION LINPOT (D, F)

C \*\*\* COMPUTES THE STRING LINEAR POT READING

C ARGUMENT DECLARATIONS

REAL D, F(5)

LINPOT = D\*F(1)

RETURN

END

C -----

REAL FUNCTION AVG (A, B)

C \*\*\* COMPUTES THE AVERAGE BETWEEN TO CHANNELS

C ARGUMENT DECLARATIONS

REAL A, B

AVG = (A + B)/2

RETURN

END

C -----

REAL FUNCTION DIFF (A, B)

C \*\*\* COMPUTES THE DIFFERENCE BETWEEN TWO CHANNELS

C ARGUMENT DECLARATIONS

REAL A, B

DIFF = A - B

RETURN

END

## C.2 User Guide

The programs asks interactively for the filenames of the control data file, the data file and the output file. A free format is used to read the data files. The output file has commas as delimiters. All files are ASCII files.

### THE CONTROL DATA FILE

#### GENERAL INFORMATION

TITLE	Alpha-numeric upto 40 character
DATE	Alpha-numeric upto 10 character
NCH	No. of data channels
PTS	Smoothing constant

#### DATA CHANNEL DESIGNATION

DES(1)	Designation of the data channels, Alpha-numeric upto 8 character
--------	--

DES(NCH)

#### DATA CONVERSION

TYPE (1),F(1..3,1)	TYPE: Data Acquisition Device
--------------------	-------------------------------

F: Factors

TYPE (NCH),F(NCH..3,1)	TYPE = 1 ; Strain Gauge
------------------------	-------------------------

F(1,\*) ; Gauge Factor

F(2,\*) ; Excitation Voltage

F(3,\*) ; Offset

TYPE = 2 ; Load Cell

F(1,\*) ; Scale Factor

F(2,\*) ; Offset

F(3,\*) ; N/A

TYPE = 3 ; LVDT

F(1,\*) ; Scale Factor

F(2,\*) ; N/A

F(3,\*) ; N/A

TYPE = 4 ; LVDT

F(1,\*) ; Scale Factor

F(2,\*) ; N/A

F(3,\*) ; N/A

TYPE = 5 ; LMPS

F(1,\*) ; Scale Factor

F(2,\*) ; N/A

F(3,\*) ; N/A

TYPE = 6 ; Footing

F(1,\*) ; Scale Factor

F(2,\*) ; N/A

F(3,\*) ; N/A

OUTPUT CONTROL

NCHCH

No. of output checking controls

CHCH(1,1..3),TOL(1)

CHCH(NCHCH,1..3),TOL(NCHCH)

CHCH(\*,1) : First control channel No.

CHCH(\*,2) : Checking type

= 1; just check first control channel

= 2; average between first and second control ch.

= 3; difference between first and second cntrl ch.

TOL(\*) : Tolerance of the output control.